

**Evaluating the impacts of climate change
on flooding and socio-economic risk using a
large ensemble dataset in the Lower Chao
Phraya River Basin, Thailand**

Aakanchya Budhathoki

2024

**Evaluating the impacts of climate change
on flooding and socio-economic risk using a
large ensemble dataset in the Lower Chao
Phraya River Basin, Thailand**

by

Aakanchya Budhathoki

**A dissertation submitted in partial fulfillment of the
requirement for the degree of Doctor of Philosophy**

Department of Civil and Earth Resources Engineering

Kyoto University, Japan

2024

Declaration of Authorship

I affirm this thesis, entitled “Evaluating the impacts of climate change on flooding and socio-economic risk using a large ensemble dataset in the Lower Chao Phraya River Basin, Thailand” and the content presented in it is my own investigation, with any external contributions explicitly acknowledged within the text. I also confirm that I have not previously submitted this work for any academic degree or qualification at Kyoto University or any other educational institution.

Aakanchya Budhathoki

Acknowledgements

The completion of the dissertation marks the fulfillment of a dedicated effort during a full-time PhD program in the Hydrology and Water Resources Research (HYWR) Laboratory at Kyoto University. This accomplishment was facilitated by the invaluable support and thoughtful contributions of numerous individuals.

This research owes its formative success to Prof. Yasuto Tachikawa and Asst. Prof. Tomohiro Tanaka, the two indispensable individuals without whom its realization would not have been achievable. Firstly, my sincere thanks to Prof. Yasuto Tachikawa for his immense support and supervision. His guidance has consistently motivated me to delve deeper into my work. Subsequently, my deepest appreciation to Asst. Prof. Tomohiro Tanaka, around whom most of my discussions centered. His constant support, guidance, and continuous motivation to freely express my ideas are aspects for which I am profoundly grateful. He has always been patient, flexible, and encouraging, and he has allowed me to think critically, which has significantly contributed to my development as a researcher.

Sincere appreciation goes to Prof. Yutaka Ichikawa and Assoc. Prof. Sunmin Kim for their invaluable comments and suggestions that have shaped my research over the past three years. Despite Assoc. Prof. Yorozu moving out of the HYWR Laboratory, I am grateful for his insightful reflections during lab seminars that remain invaluable. Many thanks to Asst. Prof. Aulia Febianda Anwar Tinumbang for her bits of advice and suggestions.

I want to heartily acknowledge Ms. Mayumi Iwasa for her comprehensive support in every aspect that made my stay in Japan smoother and truly priceless. I cannot thank her enough, and my debt of gratitude remains everlasting. I also extend my thanks to all my fellow labmates, especially Feng Shi and Chang Juiche whose presence was

indispensable in making this Ph.D. journey complete. Furthermore, I express my gratitude to the Ministry of Education, Culture, Sports, Science, and Technology (MEXT), Japan, for providing financial support while conducting this research.

Gratitude to the colleagues at NCE Bangkok Regional Hub, UNDP, Thailand, for providing me with a unique perspective on applying scientific principles in practice during my internship. In addition, acknowledgement to Asst. Prof. Anurak Sriariyawat, Asst. Prof. Piyatida Ruangrassamee, Asst. Prof. Pongsak Suttinon, the faculties of Chulalongkorn University, for providing guidance and assistance with data, offering valuable suggestions to enhance my research. Also, huge appreciation to Dr. Teerawat Ram-Indra and Dr. Thatkiat Meema for supporting with data and Thai translation whenever required.

Thanks a bunch to my all my friends especially, Triambak Baghel, Prabiti Kaphle, Ashrika Sharma, and Bhavin Pradhan for supporting me in every possible way. And wholeheartedly thanks to Manoj Khaniya for being part of my chosen family.

Words cannot fully convey my gratitude to my parents, Usha Pandey, and Krishna Raj B.C., who have been exemplars in my life. Thank you Mamu and Papa for your limitless support, love, sacrifices, and for being the bedrock during my journey. This achievement is as much yours as it is mine. Big thanks to my younger sister, Aatmika Budhathoki, for taking care of Mamu and Papa while I was away. Thanks to all the members of the Shah family, especially my mother-in-law, Meena Shah, who has showered me with immense love. Last but, most importantly, all my love and appreciation to my husband, Abhishek Bahadur Shah, who has consistently uplifted me in all my decisions. Thank you for your love, encouragement, patience, and belief in my abilities; your unwavering support has been invaluable, making this achievement possible. I owe the success of this research to each and every one of you.

Abstract

Large basins are highly susceptible to the risk of flooding that occurs due to changes in climate parameters, such as temperature and precipitation patterns. Serious repercussions are likely to occur in basins with densely populated areas and farming communities. This is due to the prolonged and intense effects of floods, which significantly impact the lower valleys and deltas of large river basins. To better forecast floods in huge river basins, a probabilistic dataset that helps address the lack of data on heavy rainfall is required by developing several climate simulations. Hence, the high-resolution atmospheric model known as the “Database for Policy Decision-Making for Future Climate Change” (d4PDF) has been widely used in predicting historical and future climate simulations. This dataset aims to provide an understanding of climate change projections for different temperature rise scenarios that help in decision-making in national and global climate change policies. Moreover, there is confidence in the d4PDF dataset to have improved estimation of infrequent weather events with long-term return periods. Thus, to analyze the impact of climate change on flooding and its consequences on population and agriculture and estimate the economic damage assessment in the Chao Phraya River Basin (CPRB), this study uses the d4PDF dataset with thousands of years of climate data.

First of all, a 1K-FRM river flow-routing simulation with 6000 years of past and 5400 years of future data is carried out to evaluate the impact on extreme streamflow at a 10-km resolution in the CPRB. The projection of future climate parameters corresponds to a +4K warming scenario in this study. The Bhumibol and Sirikit dams, which are the two primary upstream dams, are the focus of a dam operating module included in this model. Additionally, it uses a validated linear reservoir model to depict overflow in the middle stream in a simplified manner. The results of dam inflow are bias-corrected using quantile-quantile mapping (QQM) to eliminate any biases that they inherit. The

bias-corrected dam inflows are then reintroduced into 1K-FRM to obtain discharge at the Nakhon Sawan (C2) station. At this stage, the upstream bias is eliminated while the middle-stream bias is retained. These results are compared with observed discharges at the C2 station and corrected with the hydrograph flood volume (i.e., discharge capacity greater than $2000 \text{ m}^3/\text{s}$). This spatial approach to bias correction is opted to achieve robust bias removal, even when the biases between upstream and mid-stream catchments are in different directions. The findings from the extreme streamflow assessment indicate an increase in hydrograph flood volumes, earlier onset of floods, and prolonged flood duration, suggesting that future floods are likely to be more severe compared to past climate conditions.

Following the estimation of extreme discharge in CPRB, this study undertakes the assessment of flood inundation and exposure in the CPRB's delta, specifically the Lower Chao Phraya River Basin (LCPRB), which begins from C2 station. The analysis hereinafter is carried out for 2700 years of past and 2430 years of future climate data out of 6000 and 5400 years, respectively, which is sorted based on the hydrograph flood volume. This study employs the Inundation Model Coupling Rainfall-runoff (IMCR) model for the inundation simulation, which assesses the climate change impact on flood inundation with parameters such as flood extent and depth. The assessment is carried out for various flood levels at a 2-km resolution. The flood levels are greater than 0 m, which is the usual case, along with the typical and critical depths of 0.45 m and 3 m, respectively. Future flooding events with different return periods are expected to be more intense in both the inundation area and maximum volume when compared to the past climate across all analyzed depth scenarios.

Due to the numerous facilities and opportunities in the capital city of Thailand, a considerable number of populations reside in Bangkok and its nearby provinces. In addition, since the river flooding brings a lot of river nutrients, the region is also highly favorable for agriculture cultivation. Therefore, utilizing the inundation simulation outputs, the consequences of climate change on demographics and agriculture cultivation is explored in the future in this study. The impact of climate change on population exposure is anticipated to decrease due to the projected population, which is likely to decline towards the end of the century. Although the combined effects of decreasing population and climate change are not expected to increase overall population exposure, events with higher return periods are likely to impact a larger population than those with lower return periods across all depths, like the inundation simulation. Con-

versely, keeping the population constant as in the past climate, it is anticipated that the effect of climate change on the exposed population is likely to increase. Similar to this, climate change impacts on exposed areas and the average duration of rice maturity are likely to rise in various frequency events in the future for depths greater than 0.5 m. This could be the effect of longer floods with high flood levels. In addition, an increase in the exposed rice area in the future surpasses the increase in the average duration. This could be due to the fact that the rice area that is exposed lies near the river channel, facilitating faster drainage of water through the channel.

In the final part, this study utilizes d4PDF datasets to estimate the flood risk curve for agricultural damage in the LCPRB. Similar to the exposure assessment of rice, a depth greater than 0.5 m is considered for the damage estimate. The analysis is carried out for different fragility data for rice cultivation based on spatial locations. It is noteworthy that in calculations based on yield loss data from the Philippines, Myanmar, and Japan, the economic damage seen in the 2011 flood surpasses the damage recorded in all past climate dataset of d4PDF. The findings suggest that climate change's effect on future frequent flooding events could have higher potential economic damage. Both high- and low-frequency events in the future are likely to significantly impact major agricultural cultivation, leading to massive economic losses. This indicates that future climates are likely to have a higher impact on extreme floods and resulting damages, particularly since the 2011 flood stands out as one of the events with the highest economic damage.

Table of Contents

Abstract	i
List of Figures	v
List of Tables	xi
1 Introduction	1
1.1 Background	1
1.2 Overall objective	4
1.2.1 Specific objectives	4
1.3 Outline of the thesis	5
2 Study area and d4PDF	7
2.1 Description of study area	7
2.1.1 The Chao Phraya River Basin	7
2.1.2 The Lower Chao Phraya River Basin	8
2.1.3 Overview of the 2011 Great Thailand Flood	11
2.2 Multi-ensemble climate change scenario dataset, d4PDF	12
3 Climate change impact assessment on extreme river discharge using 1K-FRM in the CPRB	15
3.1 Introduction	16

3.2	Framework for bias correction and river-routing simulation	18
3.3	Hydrological observation data	19
3.4	River routing model 1K-FRM and its application	20
3.5	Spatial bias correction at upstream and downstream	22
3.6	Results and discussion	23
3.6.1	d4PDF past and future extreme river flow impact assessment	23
3.6.2	Future extreme river flow characteristics	30
3.7	Conclusions	33
4	Climate change impact assessment on flood inundation using IMCR in the LCPRB	37
4.1	Introduction	38
4.2	Framework for flood-inundation simulation	40
4.3	Streamflow and topography data	40
4.4	Inundation Model Coupling Rainfall-runoff model (IMCR) and its application	41
4.5	Results and discussion	43
4.5.1	2011 inundation simulation	44
4.5.2	d4PDF past and future inundation simulation	45
4.6	Conclusions	53
5	Demographic and agriculture exposure assessment in the LCPRB	55
5.1	Introduction	56
5.2	Framework for exposure assessment	58
5.3	Exposure data	59
5.3.1	Population data	59
5.3.2	Agricultural data	60
5.4	Methodology for exposure assessment	62

Table of Contents

5.4.1	Population exposure	62
5.4.2	Agricultural exposure	62
5.5	Results and discussion	62
5.5.1	Population exposure assessment	63
5.5.2	Agricultural exposure assessment	71
5.6	Conclusions	78
6	Agricultural damage assessment in the LCPRB	81
6.1	Introduction	82
6.1.1	Framework for agricultural economic damage assessment	83
6.2	Fragility curve, cropping calender and rice data	85
6.3	Methodology for agricultural economic damage assessment	86
6.4	Results and discussion	87
6.4.1	2011 agricultural economic damage assessment	88
6.4.2	d4PDF past and future agricultural economic damage assessment	89
6.5	Conclusions	95
7	Conclusions	97
	References	101
A	Supplementary materials	119
A.1	Appendix for Chapter 4	120
A.2	Appendix for Chapter 5	124
A.3	Appendix for Chapter 6	126

List of Figures

1.1	Overall outline of the thesis.	5
2.1	Location map of the Chao Phraya River Basin, Thailand (Lower Chao Phraya River Basin, highlighted in the red square).	9
3.1	Overall methodological framework opted in this chapter. The light gray oval box represents the data used; dark gray rectangular box represents the method opted; light gray box represents the model outputs; and black box represents the outcome and arrow represents the respective method flowlines.	19
3.2	Cumulative probability plot of observed (black dots), raw (light-gray lines), and corrected (light-blue lines) ensemble for wet season volume at (a) Bhumibol, (b) Sirikit, and (c) for hydrograph flood volume at C2. The gray dots show the median of raw ensembles as a baseline of bias correction. The median of corrected ensembles (blue dots) perfectly matches observation data.	24
3.3	Scatter plot between bias of wet-season volume in the (a) Bhumibol and (b) Sirikit dams and (c) their total with respect to that at C2.	25

3.4	Cumulative probability plot of observed (black dots), raw (light-gray lines), corrected (light-blue lines), and projected future (light-red lines) ensemble for wet season volume at (a) Bhumibol, (b) Sirikit. The gray dots show the median of raw ensembles as a baseline of bias correction. The median of corrected ensembles (blue dots) perfectly matches observation data. The median of the future ensembles (red dots) shows an increasing trend.	27
3.5	Cumulative probability plots of observed (black dots), raw (light-gray lines), corrected (light-blue lines), projected future (light-red lines) ensemble and 2011 flood volume (yellow dotted lines) for hydrograph flood volume at C2 (a) SSC, (b) TSC. The gray dots show the median of raw ensembles as a baseline of bias correction. The median of corrected ensembles (blue dots) perfectly matches observation data. The median of the future ensembles (red dots) shows an increasing trend.	29
3.6	(a) Peak discharge and (b) hydrograph flood volume at each return period for wet season in past climate and six SST ensembles of 4-degree rise experiments at C2.	31
3.7	Starting period of the flood in the past and six SST future members in the CPRB (the blue dashed line shows the past climate experiment; light dashed lines show each SST ensemble; the red solid line shows the median for the 4-degree rise experiment) at C2.	32
3.8	Duration of floods in past and six future SST members in the CPRB (blue: past climate experiment; red: 4-degree rise experiments) at C2.	33
4.1	The overall methodological framework opted for the inundation simulation (a) 2011 flood for model validation and (b) d4PDF past and future climate.	40
4.2	Inundation Model Coupling Rainfall-runoff model (IMCR).	41
4.3	Simulated maximum inundation area for the 2011 flood in comparison to satellite remote sensing data from TFMS flood map for 2011. The red cross in the figure represents the C2 station and orange box represents the King's Dyke in the LCPRB.	44

4.4	Comparison between past and future (six SST GCMs) d4PDF (a) inundation area and (b) inundation maximum volume.	45
4.5	Comparison plots of peak discharge with inundation (a) area (b) maximum volume; and hydrograph flood volume with inundation (c) area and (d) maximum volume for the past and future (GF) climate.	46
4.6	Simulated past flood inundation extent and depth for the d4PDF (a) 5-year, (b) 10-year, (c) 50-year and (d) 100-year return period with respect to depth > 0 m (the color bar represents the inundation depth in meters and the red cross represents the C2 station).	49
4.7	Simulated future flood inundation extent and depth for six SST GCMs (a) CC, (b) GF, (c) HA, (d) MI, (e) MP and (f) MR with respect to the d4PDF 10-year return period and depth > 0 m (the color bar represents the inundation depth in meters and the red cross represents the C2 station).	51
4.8	Simulated future flood inundation extent and depth for six SST GCMs (a) CC, (b) GF, (c) HA, (d) MI, (e) MP and (f) MR with respect to the d4PDF 100-year return period and depth > 0 m (the color bar represents the inundation depth in meters and the red cross represents the C2 station).	52
5.1	Methodological framework opted in this chapter for the demographic and agriculture exposure assessment for (a) 2011 flood and (b) d4PDF past and future climate in the LCPRB.	58
5.2	Spatial population distribution in the LCPRB based on the GWP SEDAC dataset for (a) 2010 and (b) 2100 (SSP5) (the red cross in both (a) and (b) represents the C2 station).	59
5.3	Landuse map modified based on LDD data for 2015 in the LCPRB (the red cross represents the C2 station).	60
5.4	Percentage rice cultivation area based on GISTDA data for 2023 in the LCPRB (the red cross represents the C2 station).	61
5.5	Population exposure map of 2011 flood (the red cross represents the C2 station).	63

5.6	Cumulative frequency distribution plots for d4PDF past and future climate with respect to the exposed population for (a) SSP5 projected population and (b) constant population as d4PDF past climate.	64
5.7	Population exposure to past floods for the d4PDF (a) 5-year, (b) 10-year, (c) 50-year and (d) 100-year return period with respect to depth > 0 m (the color bar represents the population in nos. and the red cross represents the C2 station).	67
5.8	Population exposure to future floods for six SST GCMs (a) CC, (b) GF, (c) HA, (d) MI, (e) MP and (f) MR with respect to the d4PDF 10-year return period and depth > 0 m (the color bar represents the population in nos. and the red cross represents the C2 station).	69
5.9	Population exposure to future floods for six SST GCMs (a) CC, (b) GF, (c) HA, (d) MI, (e) MP and (f) MR with respect to the d4PDF 100-year return period and depth > 0 m (the color bar represents the population in nos. and the red cross represents the C2 station).	70
5.10	Agriculture exposure map of 2011 flood (the red cross represents the C2 station).	71
5.11	Cumulative frequency distribution plots for d4PDF past and future climate with respect to the (a) exposed area and (b) average duration.	72
5.12	Comparison between inundation area and rice exposed area for past (HPB) and future (HFB) climates (all six SST GCMs for the future climate experiment).	74
5.13	Rice exposure to past floods for the d4PDF (a) 5-year, (b) 10-year, (c) 50-year and (d) 100-year return period with respect to depth > 0.5 m (the color bar represents the exposed inundation depth in meters and the red cross represents the C2 station).	75
5.14	Rice exposure to future floods for six SST GCMs (a) CC, (b) GF, (c) HA, (d) MI, (e) MP and (f) MR with respect to the d4PDF 10-year return period and depth > 0.5 m (the color bar represents the exposed inundation depth in meters and the red cross represents the C2 station).	76

5.15	Rice exposure to future floods for six SST GCMs (a) CC, (b) GF, (c) HA, (d) MI, (e) MP and (f) MR with respect to the d4PDF 100-year return period and depth > 0.5 m (the color bar represents the exposed inundation depth in meters and the red cross represents the C2 station).	77
6.1	Methodological framework opted for the agriculture damage assessment for (a) 2011 flood as model validation and (b) d4PDF past and future climate in the LCPRB.	84
6.2	Heatmap produced with the fragility curve data for rice growing period in Philippines (values taken from Shrestha <i>et al.</i> , 2019), Myanmar (values taken from Shrestha <i>et al.</i> , 2021) and Japan (values taken MLIT, 2005).	85
6.3	Cropping calendar for wet and dry rice in Thailand (modified based on Shrestha <i>et al.</i> , 2019 and Som-ard <i>et al.</i> , 2022).	86
6.4	Agriculture damage for 2011 flood (the green cross represents the C2 station).	88
6.5	Flood risk curve for agriculture damage based on fragility curve for (a) Philippines, (b) Myanmar and (c) Japan.	89
6.6	Agricultural damage based on three spatial regions (Philippines, Myanmar and Japan) with respect to four return periods (5-year, 10-year, 50-year and 100-year).	90
6.7	Past agriculture damage for the d4PDF (a) 5-year, (b) 10-year, (c) 50-year and (d) 100-year return period with respect to depth > 0 m (the color bar represents the economic damage in million THB and the red cross represents the C2 station).	92
6.8	Future agriculture damage for six SST GCMs (a) CC, (b) GF, (c) HA, (d) MI, (e) MP and (f) MR with respect to the d4PDF 10-year return period and depth > 0.5 m (the color bar represents the economic damage in million THB and the red cross represents the C2 station).	93
6.9	Future agriculture damage for six SST GCMs (a) CC, (b) GF, (c) HA, (d) MI, (e) MP and (f) MR with respect to the d4PDF 100-year return period and depth > 0.5 m (the color bar represents the economic damage in million THB and the red cross represents the C2 station).	94

A.1 Simulated future flood inundation extent and depth for 6SST GCMs (a) CC, (b) GF, (c) HA, (d) MI, (e) MP and (f) MR with respect to the d4PDF 5-year return period and depth > 0 m (the color bar represents the inundation depth in meters and the red cross represents the C2 station). . . .	120
A.2 Simulated future flood inundation extent and depth for 6SST GCMs (a) CC, (b) GF, (c) HA, (d) MI, (e) MP and (f) MR with respect to the d4PDF 50-year return period and depth > 0 m (the color bar represents the inundation depth in meters and the red cross represents the C2 station). . .	121
A.3 Population exposure to future floods for 6SST GCMs (a) CC, (b) GF, (c) HA, (d) MI, (e) MP and (f) MR with respect to the d4PDF 5-year return period and depth > 0 m (the color bar represents the population in nos. and the red cross represents the C2 station).	122
A.4 Population exposure to future floods for 6SST GCMs (a) CC, (b) GF, (c) HA, (d) MI, (e) MP and (f) MR with respect to the d4PDF 50-year return period and depth > 0 m (the color bar represents the population in nos. and the red cross represents the C2 station).	123
A.5 Rice exposure to future floods for 6SST GCMs (a) CC, (b) GF, (c) HA, (d) MI, (e) MP and (f) MR with respect to the d4PDF 5-year return period and depth > 0.5 m (the color bar represents the exposed inundation depth in meters and the red cross represents the C2 station).	124
A.6 Rice exposure to future floods for 6SST GCMs (a) CC, (b) GF, (c) HA, (d) MI, (e) MP and (f) MR with respect to the d4PDF 50-year return period and depth > 0.5 m (the color bar represents the exposed inundation depth in meters and the red cross represents the C2 station).	125
A.7 Future agriculture damage for 6SST GCMs (a) CC, (b) GF, (c) HA, (d) MI, (e) MP and (f) MR with respect to the d4PDF 5-year return period and depth > 0.5 m (the color bar represents the economic damage in million THB and the red cross represents the C2 station).	126
A.8 Future agriculture damage for 6SST GCMs (a) CC, (b) GF, (c) HA, (d) MI, (e) MP and (f) MR with respect to the d4PDF 50-year return period and depth > 0.5 m (the color bar represents the economic damage in million THB and the red cross represents the C2 station).	127

List of Tables

2.1	AGCMs selected and their details used in the study.	12
3.1	Details of the hydrological observation data (daily) used in the CPRB. .	20
3.2	Changes in future C2 station discharge with respect to past climate. The past column show the absolute values (cumecs) and the columns for the six GCMs show the change factor.	30
4.1	Changes in future maximum inundation area and future maximum volume with respect to past climate. The past column show the absolute values (in sq. km. and billion cu. m., respectively) and the columns for the six GCMs show the change factor.	48
5.1	Changes in future exposed population (projected population for SSP5 scenario) with respect to past climate population. The past columns show the absolute values (in number of people) and the columns for the six GCMs show the change factor.	65
5.2	Changes in future exposed population (constant population as past) with respect to past climate population. The past columns show the absolute values (in number of people) and the columns for the six GCMs show the change factor.	66
5.3	Changes in future agriculture exposed rice area and average duration with respect to past climate. The past column show the absolute values (in sq. km. and no. of days, respectively) and the columns for the six GCMs show the change factor.	73

6.1 Past and future changes in agriculture economic damage based on three fragility curves of the Philippines, Myanmar and Japan. The past columns show the absolute values (billion THB) and the columns for the six GCMs show the change factor. 91

Chapter 1

Introduction

1.1 Background

Floods occur when the river overflows its banks and impacts nearby areas, posing a threat to the environment and causing huge financial losses (Merz *et al.*, 2021). More people are impacted by flooding than by any other natural hazards, and it prevents sustainable development (Tellman *et al.*, 2021). Besides their effect on the population, they have the potential to harm the economy and spark societal unrest. Its amplification is gaining worldwide attention due to its large number of assets and property damage. It was predicted that between 2000 and 2019, there would be 651 billion USD in flood losses worldwide (Tellman *et al.*, 2021; UNDRR, 2021). With 46.5 billion USD worth of economic damage and 813 fatalities, the Great 2011 Thailand Flood is recognized as the third-largest financial disaster in history (GFDRR, 2012). Compared to the global average, it is anticipated that Southeast Asian countries such as Thailand, Vietnam, Indonesia, etc. will face significant flood-related economic impacts and damages (Padiyedath Gopalan *et al.*, 2022). In addition, the consequences of flooding impacts are also evident in the agricultural sector, which is vital to the global economy and food production. Research suggests that agricultural crop losses caused by flooding vary from 13-100% in different basins around the globe (Hossain *et al.*, 2020; Shrestha *et al.*, 2019).

This potential for flood risks is expected to be influenced by both alterations in land use and shifts in climate conditions. Changes in the land use of river basins have an impact

on runoff generation, while climate change can additionally increase heavy precipitation and have an impact on snowmelt or catchment wetness (Merz *et al.*, 2021). Studies show that the latter is exacerbating the frequency and intensity of floods, prompting disastrous events and bringing more challenges to future flood prevention (Budhathoki *et al.*, 2022; Devitt *et al.*, 2023). For many locations around the world, there will likely be an increase in flood threats every year. Recent studies suggest that there is a growing concern about the increase in the risk of flooding in Asia (Fabian *et al.*, 2023), Europe (Bertola *et al.*, 2020; Dottori *et al.*, 2018), and America (Chen *et al.*, 2023) due to the effects of climate change. In addition, as a result of the impact of climate change on floods, there is rising concern that in regions with high population densities, large cultivation areas, and large asset counts, the risk of flooding may rise significantly (Tellman *et al.*, 2021). It is crucial to consider that by 2050, the world's population is projected to reach 9.7 billion, intensifying the pressure on agricultural regions to meet the expanding demand for food (Arora, 2019). Due to this impact and significant inter-annual spatial-temporal variability, low-lying topography and permeable surfaces in coastal cities are at a higher risk (Hallegatte *et al.*, 2013). Additionally, a few flooding hot-spots are predicted to emerge across Asia and Africa in the future (Merz *et al.*, 2021). Water managers have new obstacles in preventing floods, which also impede the sustainable development of ecosystems. Therefore, flood risk assessment, a crucial instrument for preventing flood hazards, has excellent practical benefits in flood risk management and can lessen the damage and loss caused by floods. Examining flood risk necessitates frequency analysis, given that the observation time is significantly shorter than the return periods of occurrences. Therefore, these return periods should extend beyond the observation data. (Tanaka *et al.*, 2021).

Advancements in computational power have facilitated the creation of extensive ensembles for investigating extreme occurrences through sampling, eliminating the necessity for statistical models, assumptions about distributions, and extrapolating data (Engeland *et al.*, 2004). This is particularly beneficial when analyzing hydrological extremes, which are highly sensitive to even slight adjustments in statistical model parameters and their extrapolations. This sensitivity often results in considerable uncertainty in predicting severe events. A modeling technique is, of course, dependent upon the caliber of the modeled data; therefore, it is still crucial to validate models using historical data (Van Der Wiel *et al.*, 2019). Despite reduced uncertainty in climate change projections at the global scale owing to compiled evidence (AR6), catchment-scale fu-

ture change projections are still varied, which is possibly due to high uncertainty associated with the large impact of internal climate variability on extreme precipitation that cannot be captured with limited ensembles (Peel *et al.*, 2015). Therefore, previous works on climate change impact assessments on floods in Thailand are limited to overall tendencies such as mean or variance, and it is hard to give a robust estimate of frequency changes in extreme cases with limited sample size, such as the 2011 flood event. To overcome this issue, multi-ensembles covering internal climate variability as much as possible are required for the impact assessments of extreme floods. Large climate ensemble dataset such as the database for policy decision-making for future climate changes (d4PDF) has therefore been developed and employed in a variety of climate change impact studies looking into river discharge, floods, tropical cyclones, storm surges, etc. (Lavender *et al.*, 2018; Mori *et al.*, 2019; Ninomiya *et al.*, 2021; Tanaka *et al.*, 2020). Hence, d4PDF has the potential to detect future changes in extreme flood characteristics.

A large-scale modeling technique can lower uncertainty in future projections of the occurrence of these severe events and enhance estimates of the risk of extreme events in the present climate, especially in large river basins. The Chao Phraya River Basin (CPRB) is one of the principal river basins, occupying 30% of Thailand's geographical extent and 40% of the country's total population. It has been endowing livelihoods, employment opportunities, and developing country's agronomies, contributing to 66% of the gross domestic product (Abhishek *et al.*, 2021; Gunawardana *et al.*, 2021). This basin has been under continuous impacts of floods, droughts, land subsidence, urbanization, an increase in population, etc., especially affecting the lower delta region (Hogendoorn *et al.*, 2018; Loc *et al.*, 2020; Park *et al.*, 2021). Various episodic hydro-meteorological events have hit the CPRB in the past couple of decades, such as floods in 2006, 2011, and 2021; droughts in 2015–2016 and 2019–2020, affecting millions of people and causing large economic damage (Abhishek *et al.*, 2021; Loc *et al.*, 2020). The basin spawns 66% of the nation's Gross Domestic Product (GDP), out of which the Lower Chao Phraya River Basin (LCPRB) generates 78.2% of the CPRB's GDP (GWP, 2017). As a result, for CPRB sustainability, knowing the influence of climate change and its effect on future extreme events is a prerequisite.

Making use of a novel multi-ensemble climate dataset over single model-based climate data, this study aims to explore the impacts of climate change on the assessment of probabilistic flood risk in large-scale basins and evaluate its effect on demography

and agricultural risks in a case study of CPRB. The assessment for extreme streamflow discharge is examined across the entire CPRB, and to conduct a more comprehensive analysis, the study region is redefined as the LCPRB area for the purpose of conducting an assessment on inundation and exposure. Within the LCPRB, a thorough assessment of exposure and risk is performed for the population and agriculture. The case study itself is crucial due to the area's increased economic significance, stemming from its advantageous employment prospects and the potential for farming in the low-lying flood delta.

1.2 Overall objective

The primary aim of this study is to evaluate the impact of climate change on flood inundation, analyze demographic and agricultural exposure to floods, and quantify agricultural economic damages in the Lower Chao Phraya River Basin (LCPRB), Thailand, utilizing the d4PDF dataset.

1.2.1 Specific objectives

- To simulate and analyze the past and future floods using 1K-FRM in the CPRB;
- To simulate and assess the past and future flood inundation using IMCR in the LCPRB;
- To evaluate the past and future flood exposure to the population living in the LCPRB;
- To assess the past and future flood exposure to agriculture in the LCPRB;
- To analyze the future economic damage to agriculture in the LCPRB.

By addressing these objectives, the study aims to provide a comprehensive understanding of the effects of climate change on flood dynamics, demographic vulnerability, and agricultural economic sustainability in the LCPRB through the analysis of the d4PDF dataset.

1.3 Outline of the thesis

The research objectives mentioned above to conduct this thesis are addressed in each separate chapter. The structure of the thesis is elucidated in Fig. 1.1. Before delving into each objective, Chapter 2 covers a detailed description of the study area and the primary data used in this study.

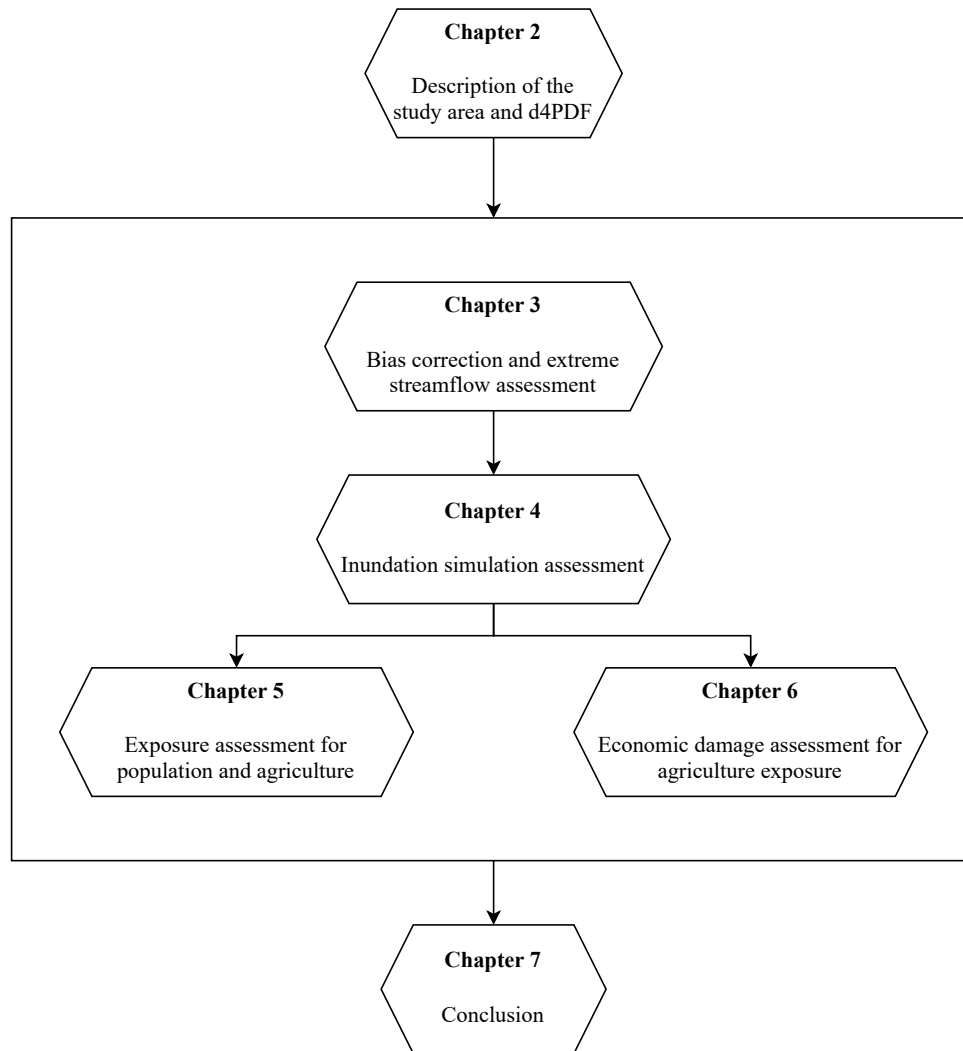


Figure 1.1: Overall outline of the thesis.

Chapter 3 explores a unique method of spatial bias correction for simulated discharge using a river-routing simulation model for the CPRB. Additionally, after the bias correction, this chapter also investigates the effect of climate change on different flood

characteristics using large climate ensembles for probabilistic future flood projection in the CPRB.

Using the simulated lateral tributary discharge and station discharge from Chapter 3, Chapter 4 assesses the impact of climate change on flood inundation using the inundation simulation model concerning flood area and depth for different frequency events of different return periods in the LCPRB.

The inundation output of Chapter 4 is further used in Chapter 5 to explore the flood exposure for two parameters. The first is population exposure, and the second is agricultural exposure to floods in the LCPRB. The analysis is carried out for different high and low-frequency return periods.

Chapter 6 comprises agricultural economic damage and risk assessment. Due to the availability of the data, only rice was selected for the analysis of exposure and damage assessment.

Finally, Chapter 7 comprehends the concluding remarks of this thesis.

Chapter 2

Study area and d4PDF

2.1 Description of study area

This section elaborates on the study area for the river-routing simulation which is the Chao Phraya River Basin and further narrows down to Lower Chao Phraya River Basin for a detailed study of inundation, exposure, and damage assessment. In addition, an overview of the 2011 flooding in Chao Phraya is also explained as it is considered as an important event in terms of flooding in Thailand.

2.1.1 The Chao Phraya River Basin

The Chao Phraya River Basin (CPRB), (99°000 E–101°300 E, 13°150 N–17°000 N) is the largest river basin situated in Thailand which spans about a length of 1,352 km and a drainage area of 170,000 km² from the Shan plateau in the northwest part of Thailand reaching to the south to the Gulf of Thailand. The Ping (36,018 km²), Wang (11,708 km²), Nan (34,557 km²), and Yom (24,720 km²) (Bidorn *et al.*, 2021) are the four major tributaries in the basin. Figure 2.1 shows that from the Northern Mountain territories, the Ping and Wang tributaries amalgamate with the Nan and Yom tributaries at Nakhon Sawan province which is the middle part of CPRB, and form the Chao Phraya River. The river then runs down and passes through Ayutthaya and Bangkok (capital of Thailand) provinces before releasing to the Gulf of Thailand (Loc *et al.*, 2023; Padiyedath Gopalan *et al.*, 2022; Sayama *et al.*, 2015).

The climate in the basin is hot and humid, affected by an Asian tropical monsoon in the north and mild throughout the year in the south which is faced with the marine climate. The basin comprises two seasons - January to April is considered to be the dry season whereas May to December is considered to be the wet season. The monthly average temperature in the basin is 22–28 °C with slight changes. Average rainfall of 1220 mm in the northern mountains, 1360 mm in the central, and 1875–2000 mm in the southern area occurs in the basin, out of which 85% of the rainfall and increasing river discharge happens during the monsoon season (May to December). The water quantity in CPRB changes promptly with seasons with approximately ten times the difference between wet and dry seasons. The basin experiences peak discharge during September and October (Abhishek *et al.*, 2021; Bidorn *et al.*, 2021; Loc *et al.*, 2023).

People in Thailand typically reside in the floodplains since the area is suitable for farming and agriculture. The central provinces receive a huge quantity of water practically every year due to their steep terrain and extensive forests (60% of the area) in the upper CPRB, causing floods in low-lying regions along the Yom and Nan Rivers. Over 3000 dams have been built in the CPRB since 1950 to store monsoon rains and increase agricultural potential during the dry season. The Bhumibol and Sirikit Dams are the two prominent dams in the Ping River and Nan River, respectively, whose purposes are hydropower generation, irrigation, flood control, and salinity intrusion management. During the middle of April 2011, 45% of Bhumibol and 51% of Sirikit dams were filled, which increased to 95% on both dam reservoirs by October 5 and September 14 (Komori *et al.*, 2012; Loc *et al.*, 2020; Mateo *et al.*, 2017; Park *et al.*, 2021).

2.1.2 The Lower Chao Phraya River Basin

The Chao Phraya River, also named the “River of Kings”, is the prime and largest river in Thailand, formed by the convergence of four major rivers in the uplands of northern Thailand, as stated in Section 2.1.1. After the confluence of these four tributaries forming the Chao Phraya River at Nakhon Sawan station (C2), lies the Lower Chao Phraya River Basin (LCPRB) (Bidorn *et al.*, 2021) as shown in Fig. 2.1 (highlighted in red square). This basin consists of salient industrial and agrarian sectors, and Thailand’s capital city, Bangkok, is prime for the nation’s economic development. The LCPRB covers an area of approximately 50,000 km², with crisscross river branches forming a flat river delta. The quantity of water in the river varies drastically with the

2.1. Description of study area

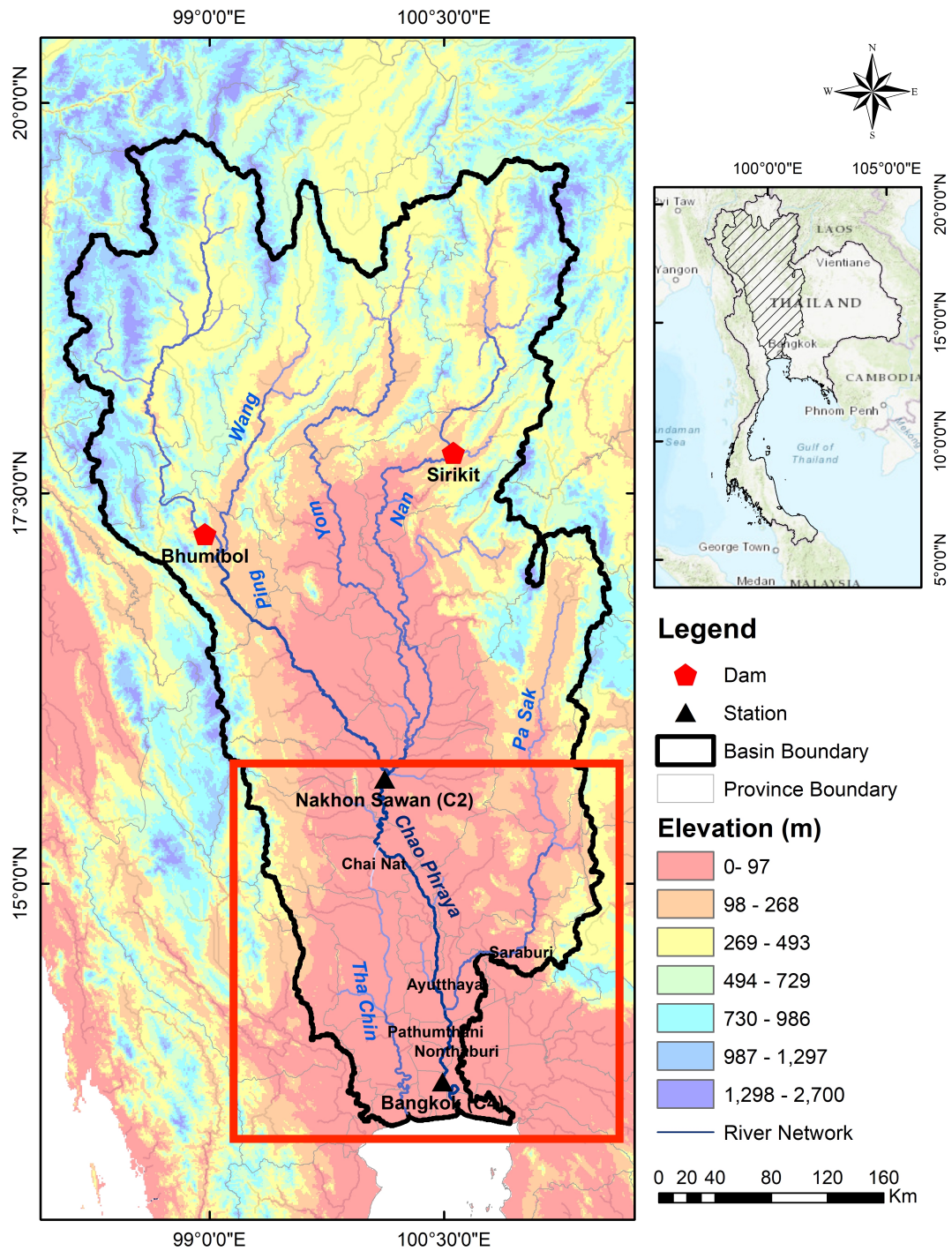


Figure 2.1: Location map of the Chao Phraya River Basin, Thailand (Lower Chao Phraya River Basin, highlighted in the red square).

seasons, with a tenfold variation between the dry and wet seasons. The widening of the river width to 700–800 m is due to the varying discharge during the dry and rainy seasons. As a result, during the rainy season, the stream overflows, carrying a layer of rich material with it, which is useful for the irrigation of paddy fields as it is primarily dependent on natural floods. The basin has been experiencing continuous flooding for several decades due to its low-lying elevation (Abhishek *et al.*, 2021).

River flooding is useful for rice cultivation; however, some downstream cultivation areas are affected when the discharge at the C2 station exceeds 2000 m³/s. In addition to agricultural and industrial areas, communities residing in this area are vastly affected by the increase in river discharge. A large increase in the discharge of more than 3500 m³/s will drastically increase the flood risk, resulting in extensive inundation areas and massive financial damage in the LCPRB. The peak river discharge at the C2 station reached 3500 m³/s in some years, such as 2006 (5960 m³/s), and 2011 (4686 m³/s) which caused extensive damage in the basin (Jamrussri and Toda, 2017). The discharge at the C2 station is crucial for decision-making on the flood control and watershed management of the LCPRB.

Around Chai Nat, the Tha Chin River diverges and merges directly into the Gulf of Thailand. The Chao Phraya River meets the two pivotal tributaries, the Sakae Krang near Uthai Thani and the Tha Pa Sak River near Ayutthaya (Loc *et al.*, 2020). The Chao Phraya River is approximately 3.5 m above the mean sea level at Ayuthaya, and further down south in the Bangkok delta, it reaches barely 1 m above the mean sea level. The delta is a network of waterways that includes the mainstream, major tributaries, and several constructed canals with a slope of 0.00001 to 0.00002. Throughout the delta and across the central plain, the embankments connected with roadways, channels, and railway lines act as a barrier. Low embankments also surround agricultural areas, and hence, floods in the LCPRB near the delta are aggravated by high tides (Liew *et al.*, 2016). In the vicinity of LCPRB, “King’s Dyke” was created after the flood in 1983. The elevated roadways that make up this dike were intended to prevent flooding in the inner city, but they also raised the risk of flooding for urban areas that reside outside of it. Its construction is one instance of how urban design has led to such socio-spatially heterogeneous risks (Tuitjer, 2023). However, to protect the main economically valuable region, the construction of this dyke has a certain value.

2.1.3 Overview of the 2011 Great Thailand Flood

In 2011, a great catastrophic flood hit Thailand, and the people residing in the low-lying areas of the Chao Phraya River were vastly affected. The Great 2011 Thailand Flood is known to be the world's third most expensive catastrophe to date. The rainfall was high throughout the rainy season, and in most of northern and central Thailand, the cumulative rainfall increased by 20–60% and 10–40% between May and October 2011 (Liew *et al.*, 2016). When the two major dams (Bhumibol and Sirikit) reached their full capacity, the surplus water was released towards the south of the Chao Phraya River. This resulted in an escalated spread of floodwater over the Chao Phraya delta plain, rupturing 10 major flood control gates. The C2 station acts as a constricting yet key station, collecting water from upstream channels Ping and Nan and diverging into other tributaries, losing water to the delta (Loc *et al.*, 2020). The Ayuthaya region withstood the floodwaters for several weeks until October 11, 2011, eventually flooding the region with flood depths of more than 2 m, which lasted until several months later (Meesuk *et al.*, 2017). Around 2 million people were affected, with a fatality rate of 400. Tentatively, 1400 mm of rainfall occurred alone in the wet season of 2011, resulting from flood-hit typhoons and depressions that hit the northern part of the CPRB. In October 2011, Nakhon Sawan received a peak discharge of 4686 m³/s. Approximately USD 46.5 billion worth of economic damage and loss ravaged Thailand during the 2011 flooding (Sayama *et al.*, 2015).

Several factors contributed to this level of disastrous and costly flood events. Higher river flow due to continuous heavy rainfall for a prolonged duration was one of the prime reasons. The other factor was topology, which comprises a gentle slope downstream and a high volume of water passing through the bottlenecked river system. It led to a large volume of water upstream, which broke the control structures, making the downstream unable to handle it (Komori *et al.*, 2012). Additionally, land use in the basin was also another component, as the planners fell short in developing the capital city and nearby industrial parks to withstand the indefatigable flood. Bangkok and its surrounding provinces are situated in the former flood delta, which replaced the natural waterways and marshlands with urban and sub-urban metropolises (Engkagul, 1993). Land subsidence in the region due to large groundwater extraction also promoted flood damage, making several areas in the region vulnerable. A lack of proper water management as the country progresses from agronomy to an industrial country

was also one of the elements contributing to the 2011 flood impact (Haraguchi and Lall, 2015).

2.2 Multi-ensemble climate change scenario dataset, d4PDF

Table 2.1: AGCMs selected and their details used in the study.

SST Model	Driving GCM	Institute	Country
CC	CCSM4	National Centre for Atmospheric Research	USA
GF	GFDL CM3	Geophysical Fluid Dynamics Laboratory	USA
HA	HadGEM2-AO	National Institute of Meteorological Research	Korea
MI	MIROC5	Univ. Tokyo and Japan Agency for Marine-Earth Science and Technology (JAMTEC)	Japan
MP	MPI-ESM-MR	Max Planck Institute for Meteorology	Germany
MR	MRI-CGCM3	Meteorological Research Institute	Japan

The database for Policy Decision-making for Future climate changes (d4PDF) was created by a joint project of the Meteorological Research Institute (MRI) of the Japan Meteorological Agency (JMA), the Atmosphere and Ocean Research Institute of the University of Tokyo, Disaster Prevention Research Institute of Kyoto University, National Institute of Environmental Study, Japan Agency for Marine-Earth Science and Technology (JAMSTEC), and University of Tsukuba (http://search.diasjp.net/en/dataset/d4PDF_RCM_3D_Plev) in order to project the future climates at various global warming levels by running numerous climate simulations using a high-resolution global atmospheric model AGCM-3.2 at a 60-km resolution and then dynamically downscaling with a regional atmospheric model at a 20-km and 5-km resolution around Japan (Mizuta *et al.*, 2017). Hence, the global climate experiment was used in this research. For both experiments, four climate scenarios: the non-global warming, the past, +1.5 K, +2 K, and +4 K warmer climates were employed.

The boundary conditions were based on Mizuta *et al.* (2017) where the past climate simulation was driven by the observed sea surface temperatures (SST) and sea ice for 60 years from 1951–2010 with 100 variations of small perturbation comparable to observation errors yielding 6000-year data in total (hereinafter, past climate); the future

climate simulation was driven by six representatives of the projected SST patterns (see Table 2.1) from CMIP5 (Mizuta *et al.*, 2017) with the same perturbation setting and performed for 60 years yielding 5400-year data (hereinafter, future climate) (Ishii and Mori, 2020; Mizuta *et al.*, 2017).

These SST general circulation models (GCMs) have been used in several studies around the globe for climate change projections for various applications. Chen *et al.* (2022) studied the future variation of extreme precipitation from southern China to northeast Asia using the d4PDF data. Yang *et al.* (2018) assesses the past and future storm surges on the Korean peninsula. Similarly, using d4PDF data, the future flood risks in significant river basins of Japan along with its economic damage were analyzed (Tanaka *et al.*, 2021, 2020). Apart from wide global implementation, these six SST models have been used in the nearby region, the Mekong River basin, which is a transboundary basin in East and Southeast Asia, for the assessment of uncertainty in water resources and the projection of flood inundation (Meema *et al.*, 2021; Try *et al.*, 2020). Based on these, this study uses the most widely used combination of the past climate experiment and the 4-degree rise scenario in global mean temperature (hereinafter, the 4-degree rise / +4K warming experiment) (Mizuta *et al.*, 2017; Mori *et al.*, 2019) to explore the impact of the most severe temperature increase on flooding in the CPRB.

Chapter 3

Climate change impact assessment on extreme river discharge using 1K-FRM in the CPRB

This chapter aims to ascertain the difference between spatial bias heterogeneity of streamflow in the CPRB. The upstream major dams and the outlet of the basin are examined with two-step bias correction and compared with a more practical bias correction only at the outlet of the basin. The former clarified that, due to the large effect of downstream bias, the upstream bias effect is considered negligible thus the two approaches resulted in similar future projections. Through this comparison, streamflow bias in the past and future climate experiments are corrected considering its spatial characteristics for robust assessments of quantitative impacts of climate change. The + 4 K warmer climate will increase the frequency of the 2011 flood and enhance 100-year flood peak discharge by 1.1–1.6 times than the past climate. The future flood in the basin, which starts predominantly in September in the present climate, is likely to begin in September and August with a prolonged duration of floods of around 10–50 days. The CPRB is expected to experience elevated flood volume, earlier flood occurrence, and longer flood duration indicating rigorous forthcoming floods.

This chapter is largely based on the publication: Budhathoki, A., Tanaka, T., Tachikawa, Y., (2022). Correcting streamflow bias considering its spatial structure for impact assessment of climate change on floods using d4PDF in the Chao Phraya River Basin, Thailand. *Journal of Hydrology: Regional Studies* 42, 101150. <https://doi.org/10.1016/j.ejrh.2022.101150>

3.1 Introduction

The presence of increased greenhouse gases in the atmosphere leads to notable impacts related to climate change and global warming. These changes affect several hydrological elements, including evapotranspiration, infiltration, and surface runoff. Innumerable studies have been carried out on climate change impact assessments on river discharge and water availability (Budhathoki *et al.*, 2021; Casale *et al.*, 2021; Hughes and Farinosi, 2020; Jahandideh Tehrani *et al.*, 2021; Li *et al.*, 2016). Environmental, ecological, and socio-economic sectors, such as agriculture, industry, hydropower, and biodiversity protection, rely on the ability to estimate water availability under varying climatic circumstances and hydrological changes, both in the near and far future (Didovets *et al.*, 2020; Li *et al.*, 2016; Liu *et al.*, 2021; Wannasin *et al.*, 2021). Climate change-induced floods are expected to disproportionately impact developing nations rather than developed ones, particularly Southeast Asian nations (Padiyedath Gopalan *et al.*, 2022). According to regional impact assessments in Thailand, the country will experience a change in high-intensity rainfall falling between -5% in the dry season to raising to 36.5% in the wet season annually (Champathong *et al.*, 2013; Chaowiwat *et al.*, 2019). Studies with several GCMs show that average annual discharge, as well as maximum annual flows, will surge up between 6.8% and 38.4% with rising rainfall in the CPRB towards the end of the 21st century (Hunukumbura and Tachikawa, 2012; Kure and Tebakari, 2012; Ligaray *et al.*, 2015).

Experts have endeavored to find the most appropriate climate change model for forecasting severe events, aiming to aid decision-makers and end users. The d4PDF dataset appears as a promising model because it can handle uncertainties of both internal variability and external forcing conditions (Maneechot *et al.*, 2023). The benefits of utilizing distinct databases for various research objectives are founded on the presence of thousands of years of past and future climate datasets (Mizuta *et al.*, 2017). The evaluation of future climate changes in the form of T-year rainfall events is made possible without statistical extrapolation by these large ensembles. Through the d4PDF model, advancements in uncertainty handling and predictions of extreme events are achieved by leveraging the advantages offered by multiple SST GCMs (Try *et al.*, 2020).

The d4PDF, however, still contains the model bias even after achieving such huge ensemble simulations (Tanaka *et al.*, 2019b; Watanabe *et al.*, 2020). Hence, a prominent approach for addressing biases in GCM outputs is the quantile-quantile mapping (QQM)

bias correction technique, which is used to enhance the accuracy of climate forecasts and hydrological simulations (Piani *et al.*, 2010; Tong *et al.*, 2018). In this method, the GCM data of a grid cell is adjusted using the QQM, which links observational climate data from the same or surrounding grid cells and has been found to be very efficient at eliminating biases from climate model outputs while keeping shifts in climate frequency and variance (Elshamy *et al.*, 2009; Ines and Hansen, 2006). Many streamflow impact assessments lag the correlation structure in their bias, which needs to be considered (Maraun, 2016). This issue would be critical in the CPRB, where approximately 80% of precipitation is consumed by evapotranspiration, i.e., runoff is considered a residual in terms of the water cycle (Wichakul *et al.*, 2013; Zhao *et al.*, 2022). Therefore, as an alternative, bias correction to GCM runoff data has been lately called to attention to reduce the uncertainty, and results show improved river discharge calculations (Ibarra *et al.*, 2021), in particular in Thailand or the Indochina peninsula (Duong *et al.*, 2014; Ram-Indra *et al.*, 2020a). However, it is still challenging due to the necessity of preparing reference runoff data that requires precise land surface simulations. A more direct approach, streamflow bias correction, is considered in a few studies (Farmer *et al.*, 2018), possibly due to the combination of small observation and simulation sample sizes, runoff bias heterogeneity, and human intervention such as dam control and/or irrigation. Due to the long record of streamflow observations and large ensemble climate simulations such as d4PDF, the sample size issue can be addressed. Nevertheless, the latter factors need regional-scale analysis of the bias structure in the selected river basin. After the spatial bias structure is clarified through rigorous discussions, streamflow bias correction could be adopted as a strategy. Although such a basin-specific approach is hard to apply uniformly to the entire globe, it is crucial to compile regional studies for a comprehensive understanding as a whole.

This chapter aims to discuss robust streamflow bias correction in the CPRB, considering the spatial contrast in bias between upstream and downstream, and to present impact assessments on floods using d4PDF. There is a unique topography of the CPRB where the inflows to the Bhumibol and Sirikit Dams represent upstream mountainous catchments. Hence, the upstream GCM bias and the corrected inflows at the two major dams following the middle stream bias, which is corrected at Nakhon Sawan, a major stream gauge in the downstream area, are explored. Additionally, we compare the two-step bias correction with the bias correction of simulated discharge only at Nakhon Sawan (single-step bias correction). Based on the general efficacy of the two-step bias

correction and its performance in the CPRB, the bias-corrected d4PDF is applied in the basin to analyze its future floods in a +4 K warming condition. This quantitative impact assessment based on huge ensemble climate simulations with robust bias correction can be advantageous for future flood risk assessment, damage estimations, and policymaking in the CPRB.

The remainder of this chapter is assembled as follows: The framework implemented for this chapter is explained in Section 3.2. Moreover, after the explanation of the data used for this chapter in Section 3.3, the river flow routing model and its application are elaborated in Section 3.4. A unique method of spatial bias correction for simulated discharge using a large climate ensemble is described in Section 3.5. In addition, the d4PDF past and future impacts on floods, its comparison with the 2011 flood and the characteristics of d4PDF floods in CPRB are shown in Section 3.6.

3.2 Framework for bias correction and river-routing simulation

The overall methodology opted in this chapter is shown in Fig. 3.1. This study simulates streamflow through river routing simulations from runoff outputs of d4PDF. The most controversial point of this approach is neglecting spatial bias structure in climatic variables as well as runoff. Hence, this chapter proposes to incorporate bias correction for upstream dam inflows at Bhumibol and Sirikit before the direct correction at the downstream station (hereinafter, Two-Step Correction (TSC)) as shown in the red-colored dotted box. As a far more straightforward alternative, the blue-colored dotted box which shows the bias correction at C2 without bias correction at two upstream dams of the basin (hereinafter, Single-Step Correction (SSC)) is tested. Indeed, SSC is a commonly used bias correction method by quantile mapping. A comparison of the results of the two approaches and an examination of how effective SSC is compared to TSC as a more complicated method is done. This validation is opted as CPRB contains contrasting basin climates between upstream and midstream areas. Bias-corrected streamflow data at C2 is then analyzed to evaluate the impact of climate change on flood peak / volume, its duration, and the starting season. The details of the methodological steps are shown in the following sections.

Table 3.1: Details of the hydrological observation data (daily) used in the CPRB.

Station ID	Station Name	Type	Location	Duration	Source
BB	Bhumibol	Dam Inflow	Ping	1965-2011	EGAT, Thailand
SK	Sirikit	Dam Inflow	Nan	1974-2011	EGAT, Thailand
C2	Nakhon Sawan	Discharge	Chao Phraya	1979-2017	RID, Thailand

3.4 River routing model 1K-FRM and its application

1K-FRM, a distributed river flow routing model with a spatial resolution of 10-km is used (<https://hywr.kuciv.kyoto-u.ac.jp/products/1K-DHM/1K-DHM.html>). To convert the runoff generated by the land surface model (SiBUC) embedded in the GCM into river discharge, this kinematic wave model is used where all the rectangular units channel the water downstream based on flow direction. The continuity equation for each rectangular unit is shown in

$$\frac{\partial Q}{\partial t} + \frac{\partial A}{\partial x} = q_L(x, t) \quad (3.1)$$

where, t is time; x is distance from the rectangular unit's top (m); A is cross-sectional area (m^2); Q is discharge (m^3/s); $q_L(x, t)$ is the lateral inflow per unit length of channel unit given as d4PDF runoff generated by MRI AGCM 3.2 (m^3/s). MRI-AGCM 3.2 outputs 3-hour averaged surface and baseflow runoff, both of which are added as $q_L(x, t)$ in the continuity Eq. (3.1). The one-dimensional momentum Manning's equation is used to route the water which regulates the open channel flow characteristics.

$$Q = \alpha A^m \quad (3.2)$$

$$\alpha = \frac{\sqrt{i_0}}{n} \left(\frac{1}{B} \right)^{m-1} \quad (3.3)$$

where, i_0 is slope; n is Manning's roughness coefficient; m is the river cross-sectional parameter ($=5/3$); the model parameters of the flow model B which is the width of flow is determined by $B = aS^c$, Here, S is the catchment area at the calculated points, and $a = 1.06$ and $c = 0.69$ are constant parameters. The value of n is determined to be

3.4. River routing model 1K-FRM and its application

0.03 m^{-1/3} s for the channel when the catchment area at the calculated point is larger than 250 km² and 11.0 m^{-1/3} s for the slope when the catchment area is smaller than 500 km² (Duong *et al.*, 2013; Tachikawa *et al.*, 2011). The topological dataset is hydrological data and maps based on 30-second digital elevation and flow direction data, Shuttle Elevation Derivatives at Multiple Scales (HyDroSHEDS) (Lehner, 2005) upscaled at 10-km spatial resolution for the flow routing model 1K-FRM (Duong *et al.*, 2013). The downstream area of the Yom River (see Fig. 3.1) is frequently flooded in the middle stream area, which is expressed by applying the following linear reservoir model to downstream cells as shown in Eq. (3.4) and Eq. (3.5)

$$\frac{dS}{dt} = I - Q \quad (3.4)$$

$$S = kQ \quad (3.5)$$

where, S is the flooded storage, I is the upstream inflow discharges to a target cell, Q is the river discharge considering the delay due to inundation around the cell, and k is the model parameters indicating the delay of flood peaks between inflow I and river discharge Q . Duong *et al.* (2013) used 1K-FRM to compare the changes in flow for the past and future climates under changing climates for the Indochina Peninsula. In order to represent the spatially distributed topography of the Chao Phraya River Basin, this flow routing model has been successfully used by Wichakul *et al.* (2013) and Hunukumbura and Tachikawa (2012).

The monthly operations of the Bhumibol (1.3 billion m³) and Sirikit (0.9 billion m³) dams are modeled to store water during the wet season and release it during the dry season, based on Wichakul *et al.* (2013). It is estimated that the normal downstream water resource demands are 200 m³/s for the Bhumibol dam and 250 m³/s for the Sirikit dam. Further, during the wet season, the amount of water discharged is governed by a minimum/maximum reservoir storage capacity and spillway capacity. When reservoir storage is less than the maximum, both dams release roughly 15% and 30% of the natural inflow to sustain downstream flow. Due to the limited storage capacity of the dam, they must entirely release the water when a dam's storage capacity approaches its limit (6000 m³/s and 3200 m³/s for the Bhumibol and Sirikit dams, respectively).

3.5 Spatial bias correction at upstream and downstream

Numerous studies have used QQM for GCM bias correction for a variety of climatic variables (Bennett *et al.*, 2011; Kumar Mishra and Herath, 2015; Mishra and Herath, 2011). These studies targeted a single model ensemble and corrected its bias from observation data with comparable record lengths. Such procedures become complicated when multiple ensembles such as in the d4PDF dataset which has a larger sample size than observation data. There are several possible ways of bias correction, particularly for the selection of model quantiles to compare with observation ones: each ensemble, aggregation of all members, a median member as a baseline, and an arbitrary ensemble as a baseline. Chen *et al.* (2019) investigated the difference in performance among them and verified that the median ensemble-based correction showed robust performance. A similar approach is applied by Tanaka *et al.* (2020) which estimates the median of d4PDF ensembles at each percentile as a baseline to compare with observation ones. Hence, in this analysis, the same method is employed: the median of 100 ensembles is calculated in order to identify the bias correction factors. The QQM procedures are formulated in Eq. (3.6) and Eq. (3.7).

$$R_i = \frac{F_{obs}^{-1}(F_{\tilde{x}_{raw,i}}(\tilde{x}_{raw,i}))}{\tilde{x}_{raw,i}} \quad (3.6)$$

where, R_i is the bias correction factor for i -th order statistics of the target variable ($i = 1, 2, \dots, 60$); $\tilde{x}_{raw,i}$ is the median of a target streamflow variable among 100 ensembles; $F_{\tilde{x}_{raw,i}}(x)$ is its empirical cumulative probability; $F_{obs}^{-1}(P)$ is the inverse function of the empirical cumulative probability P of the observation data for the target variable. Unambiguously, the bias correction factors are determined such that among 100 ensembles of 60-year data, the cumulative probability of their median match that of observation as for the target variable. The target variables are wet (May to December) and dry (January to April) season total inflows and the hydrograph flood volume (total volume over $2000 \text{ m}^3/\text{s}$) at C2, all of which are annual data. Then, the raw simulation daily discharge at the day d in the i^{th} rank year for j^{th} member for the target variable, $Q_{raw,j,i}(d)$ is corrected to $Q_{bc,j,i}(d)$ by:

$$Q_{bc,j,i}(d) = R_i Q_{raw,j,i}(d) \quad (3.7)$$

3.6 Results and discussion

This section unravels the application of the river flow routing model and spatial bias correction in the upstream and middle stream of the CPRB for an impact assessment of climate change. Additionally, an insightful aspect of flood characteristics such as changes in re-occurrences, commencing month, and time span of future floods due to the effects of climate change is elaborated in this section.

3.6.1 d4PDF past and future extreme river flow impact assessment

The raw d4PDF past runoff data for 100 ensembles is first used in the river flow routing simulation with 1K-FRM. The simulated 100 ensemble dam inflows to Bhumibol and Sirikit are sorted and for each dam, their median is calculated at each percentile as a baseline to calculate the bias ratio by Eq. (3.6). Fig. 3.2 (a) and (b) show the cumulative probability plot of d4PDF dam inflows before/after bias correction at Bhumibol and Sirikit respectively. The raw d4PDF data (grey) are underestimated in comparison to the observed data (black) for both dams. After the bias correction, the median of corrected data (blue) should match the observation and as a result, each corrected ensemble spreads around the observation plot. The corrected daily inflow data is again used as input to 1K-FRM to simulate downstream river discharge with dam operations and middle stream inundation as described above.

The cumulative plot at C2 is shown in Fig. 3.2 (c). As per the Royal Irrigation Department (RID), the downstream part of the CPRB has a discharge capacity of $2000 \text{ m}^3/\text{s}$ over which flooding occurs at some downstream reaches. Thereby, the bias correction at the C2 station is done for the total amount of discharge over $2000 \text{ m}^3/\text{s}$ (hereinafter, hydrograph flood volume). After streamflow simulations with bias-corrected dam inflows, it is found that in contrast to the dam inflows, downstream river discharge overestimated the observed data, which implies that middle stream runoff is overestimated. As demonstrated here, the final output of river discharge is often affected by spatial heterogeneity of runoff (or its original climate) bias, even resulting in the opposite direction; therefore, it is suspected that the presence of bias correction at upstream dams (SSC or TSC) affects the future projections of downstream streamflow. Therefore, this chapter further investigates its impact as a case study in the CPRB.

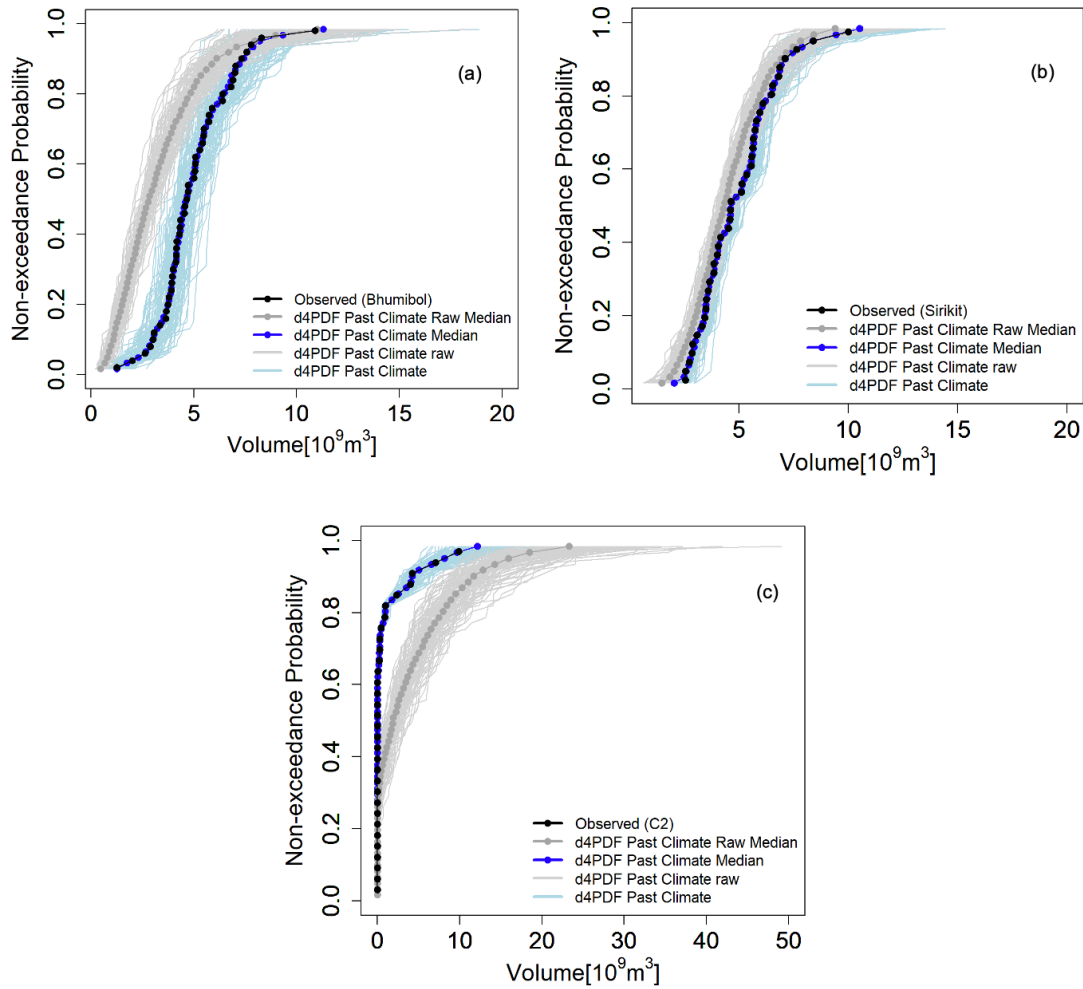


Figure 3.2: Cumulative probability plot of observed (black dots), raw (light-gray lines), and corrected (light-blue lines) ensemble for wet season volume at (a) Bhumibol, (b) Sirikit, and (c) for hydrograph flood volume at C2. The gray dots show the median of raw ensembles as a baseline of bias correction. The median of corrected ensembles (blue dots) perfectly matches observation data.

3.6. Results and discussion

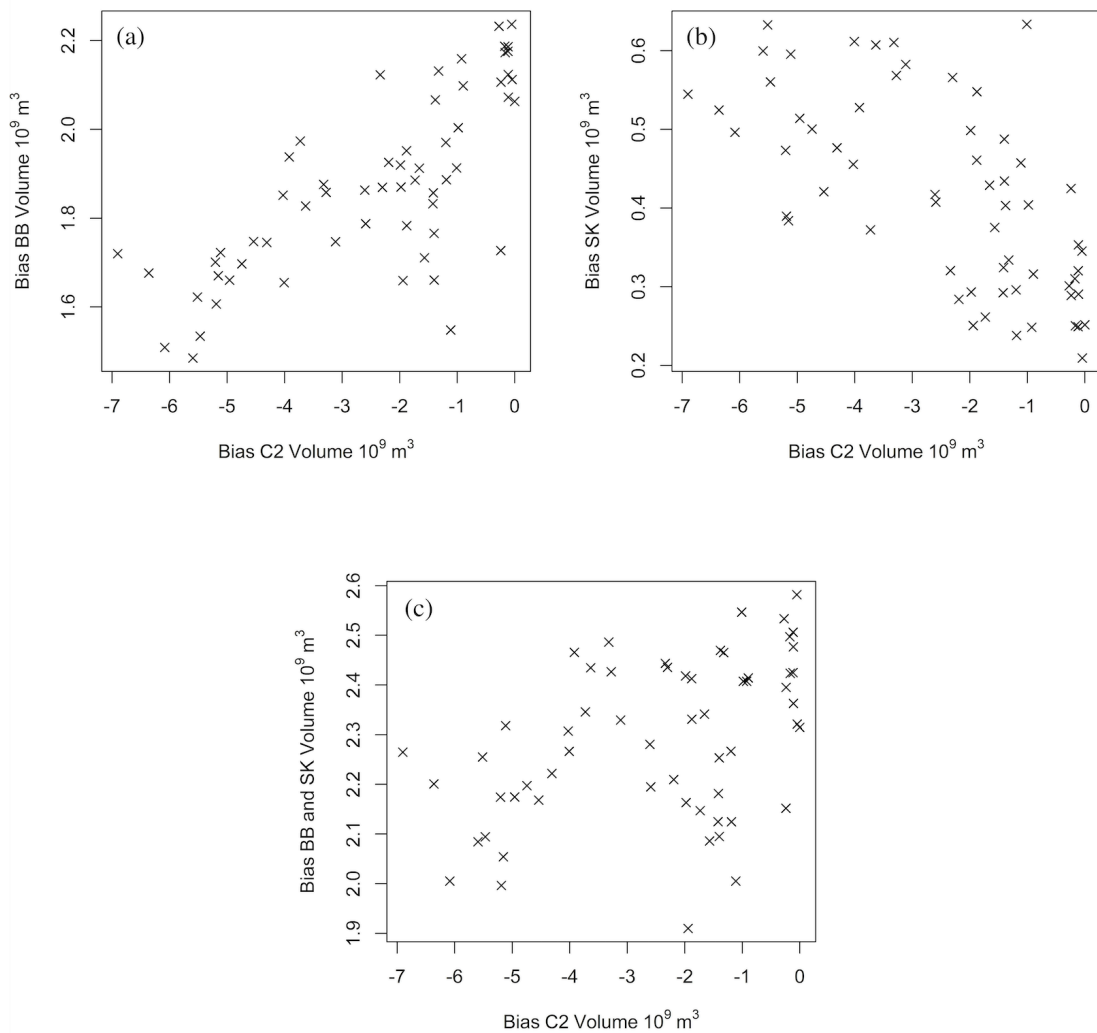


Figure 3.3: Scatter plot between bias of wet-season volume in the (a) Bhumibol and (b) Sirikit dams and (c) their total with respect to that at C2.

The magnitude of bias in wet-season streamflow volume for the inflows at the upstream dams and middle stream river discharge at C2 is compared in Fig. 3.3. It shows that the bias in the Bhumibol dam is higher than in the Sirikit dam. The bias in the wet-season volume at C2 is much larger than the bias in the Bhumibol and Sirikit dams as well as their total, indicating that the upstream bias correction at the dams does not contribute significantly to the future projection of downstream discharge in this particular river basin. This is verified by applying both SSC and TSC to future projections in Section 3.6.1.2.

3.6.1.1 Bhumibol and Sirikit dam inflows

Fig. 3.4 shows the same plot as Fig. 3.2 (the Bhumibol and Sirikit dam inflows), adding the bias-corrected future projections for the six SST ensembles (red) in wet season volume. Dry season volume analysis is also done in this chapter to compare the bias of dam operation. The future discharge volume is going to be magnified in both dams during the wet season period. The intensification of the future volume is higher in the Bhumibol dam than in the Sirikit dam. There is a slight increase or almost similar future trend at the Sirikit dam, whereas, at the Bhumibol dam, the future volume is going to increase. The mean increase ratio for 100-year volume for the six SST ensembles is likely going to be between 1.3-1.5 times the past climate for the Bhumibol dam and 1.2-1.4 times the past climate for the Sirikit dam. Fig. 3.4 shows that for both Bhumibol and Sirikit dams, the future volume (red) is higher than in the past (blue). In both cases, the cumulative probability higher than 0.9 for all SST ensembles shows greater volume than in the past. This indicates that future dam operation rules (such as rule curves) need updates to avoid adverse effects on downstream flooding.

3.6. Results and discussion

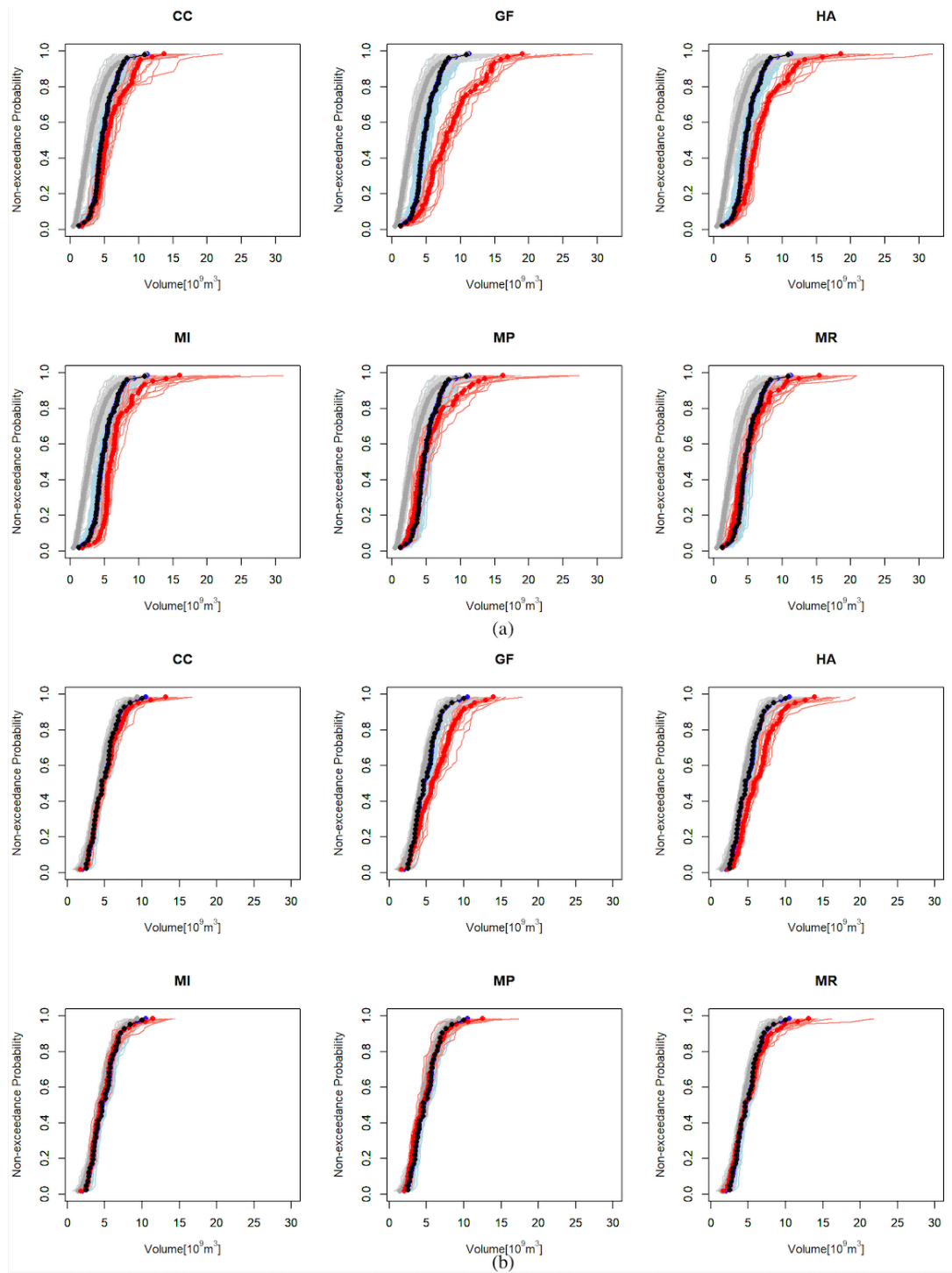


Figure 3.4: Cumulative probability plot of observed (black dots), raw (light-gray lines), corrected (light-blue lines), and projected future (light-red lines) ensemble for wet season volume at (a) Bhumibol, (b) Sirikit. The gray dots show the median of raw ensembles as a baseline of bias correction. The median of corrected ensembles (blue dots) perfectly matches observation data. The median of the future ensembles (red dots) shows an increasing trend.

3.6.1.2 C2 station

Fig. 3.5 shows the future changes in hydrograph flood volume at C2 with (a) SSC and (b) TSC, respectively. In both cases, all SST ensembles show a clear increasing trend (red). As for the bias correction approach, both SSC and TSC show a similar trend. The mean increase ratio for 100-year volume for the six SST ensembles is likely going to be between 1.1–1.5 times the past climate by SSC and 1.1–1.6 times the past climate by TSC. The downstream area of the C2 station is dominated by many industrial and agricultural areas. This increase in future hydrograph flood volume might alter downstream activities drastically. Due to the large C2 bias in the future climate, similar to the past climate, the upstream dam bias correction is insignificant in this particular case study. In general, however, the TSC is more prominent and robust as it tries to reduce bias correction uncertainty with multi-step corrections; therefore, the TSC bias correction is opted for further analysis of flood characteristics in the study.

The bias correction of discharge is one of the main considerations of this study. Studies show that the land surface model generates runoff data that incorporates the direct effects of land cover in GCM simulation techniques. As a result, the bias correction of runoff and river discharge in GCMs may adapt to different types of land cover settings, which is to a greater degree effective than the bias correction of precipitation (Mizushima *et al.*, 2019; Ram-Indra *et al.*, 2020a, 2020b). The bias correction of the discharge method with an adequate statistical performance taking into account non-stationary conditions is an effective method for the estimation of future discharge (Manee *et al.*, 2016).

3.6. Results and discussion

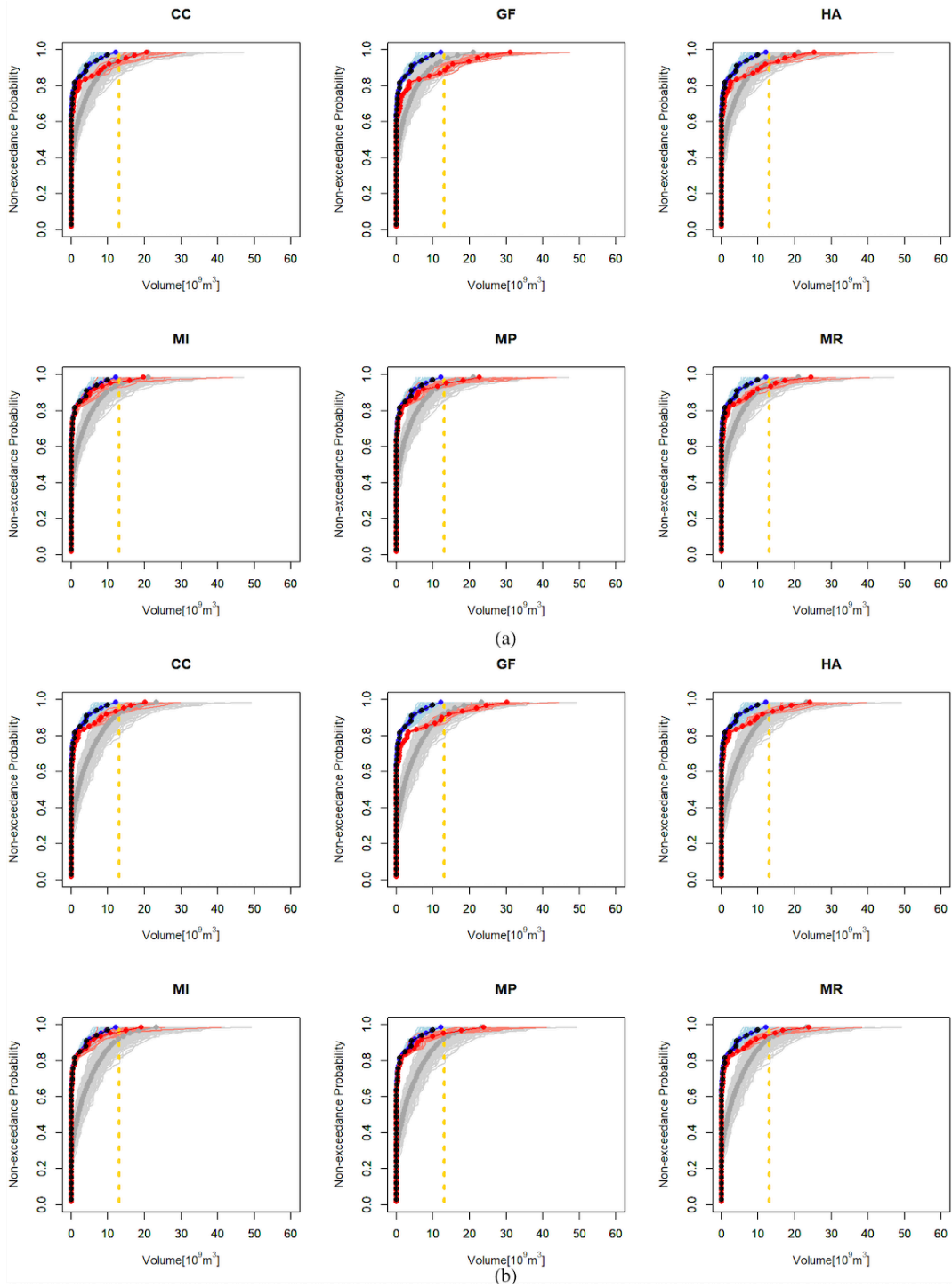


Figure 3.5: Cumulative probability plots of observed (black dots), raw (light-gray lines), corrected (light-blue lines), projected future (light-red lines) ensemble and 2011 flood volume (yellow dotted lines) for hydrograph flood volume at C2 (a) SSC, (b) TSC. The gray dots show the median of raw ensembles as a baseline of bias correction. The median of corrected ensembles (blue dots) perfectly matches observation data. The median of the future ensembles (red dots) shows an increasing trend.

Table 3.2: Changes in future C2 station discharge with respect to past climate. The past column show the absolute values (cumecs) and the columns for the six GCMs show the change factor.

Return Period [years]	Past [cumecs]	Change in discharge					
		CC	GF	HA	MI	MP	MR
5	4336.8	1.3	1.5	1.4	1.1	1.2	1.4
10	4668.4	1.3	1.6	1.3	1.1	1.3	1.4
50	4955.1	1.3	1.6	1.4	1.1	1.5	1.5
100	5267.6	1.5	1.7	1.5	1.2	1.7	1.5

3.6.2 Future extreme river flow characteristics

3.6.2.1 Return period

The annual maximum peak discharge and hydrograph flood volume for each return period at C2 are shown in Fig. 3.6 (a) and (b). The maximum discharge is going to be higher than in the past climate experiment. More severe floods are likely to occur more frequently, i.e., with a shorter return period. Fig. 3.6 (a) and (b) show that the return period of the 2011 flood discharge is approximately 70 years, whereas the return period of 2011 total volume is tentatively 120 years. The peak discharge may increase slightly, whereas, for the same or shorter return period, the volume of the flood is going to be huge. It also shows that a reduced return period of similar or higher discharge and volume than the 2011 flood for all SST members is expected in the future. The 100-year return period flood is likely to be more than 1.1–1.7 times in the future, as shown in Table 3.2. This implies that the frequency of floods is also likely to increase, and a higher volume of floods in the future will result in more severe economic damage than in the past. Similar studies in the basin show that the increase in future discharges is expected to be between 28% and 40% (Kure and Tebakari, 2012; Ponpang-Nga and Techamahasaranont, 2016) in overall agreement with this study showing a 10–70% increase. In addition, the mean monthly discharge in the basin is likely to increase in all the months, and the flood risk in the future projection periods is likely to increase, according to a flood frequency analysis utilizing the annual maximum daily flow record in the CPRB (Wichakul *et al.*, 2015). Kotsuki *et al.* (2014) also suggests that at the C2

station, in the future, an increased annual runoff is likely to occur due to the increase in precipitation.

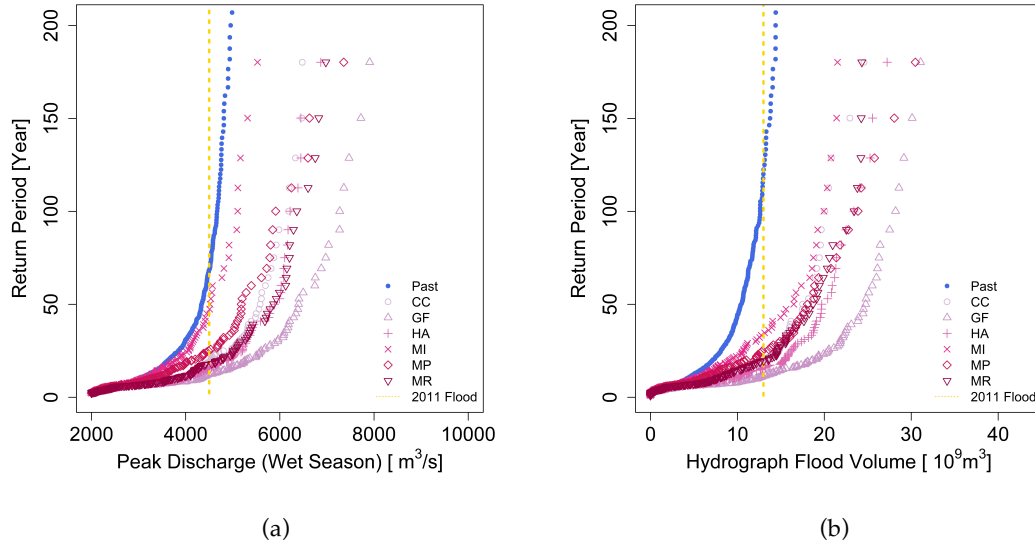


Figure 3.6: (a) Peak discharge and (b) hydrograph flood volume at each return period for wet season in past climate and six SST ensembles of 4-degree rise experiments at C2.

3.6.2.2 Shift in flood onset

The change in flooding is also assessed in terms of a shift in flooding (over $2000 \text{m}^3/\text{s}$) onset in Fig. 3.7, indicating that the typical flood starting month, i.e., the most frequent starting month, is going to shift from predominantly September in the past climate (blue) to both August and September equally (and even June and July at certain frequencies) in the future climate. Among the six SST GCM ensembles, MI shows a relatively similar pattern to the past climate, corresponding to the closer future change ratio of peak discharge in Fig. 3.6 (a). Table 3.2 shows that there is an increase in discharge for the six SST GCM ensembles with respect to the return period in the CPRB. This implies that the projected shift in flood occurrence month in Fig. 3.7 is caused by the overall increase in annual maximum discharge. This undeniably shows that longer and earlier occurrences of floods are likely to happen for all SST GCM members. Previously, there used to be rare occurrences of floods during June and July, whereas, in

the future, frequent flood events are likely to turn up during these months too. Similar results can be observed when the occurrence of floods in the future starts in the month of June in the basin (Kitpaisalsakul *et al.*, 2016). Therefore, planning for adaptation to different crop cultivations, especially rice, which is a major source of income for people residing in Chao Phraya, would be an urgent need.

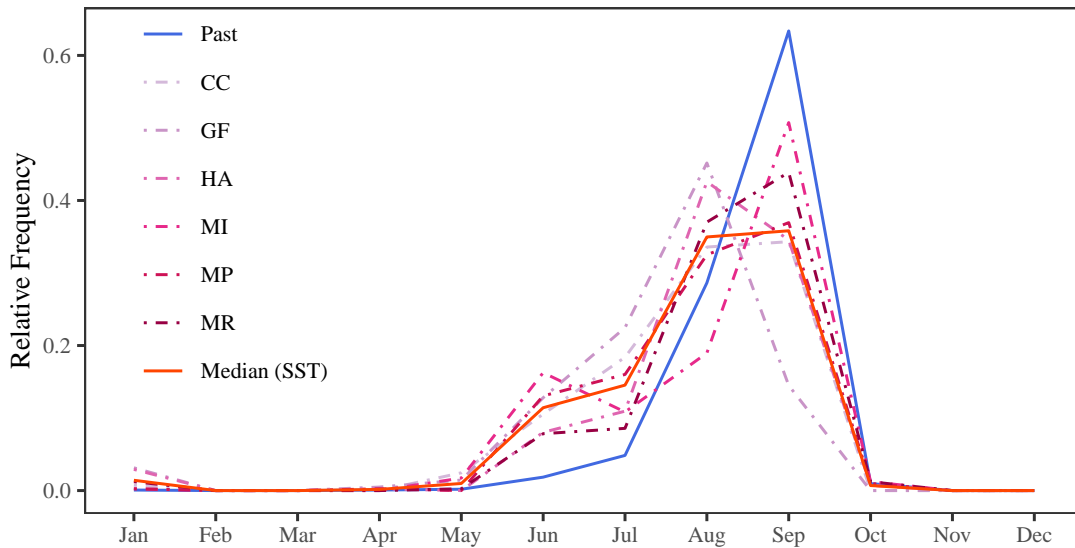


Figure 3.7: Starting period of the flood in the past and six SST future members in the CPRB (the blue dashed line shows the past climate experiment; light dashed lines show each SST ensemble; the red solid line shows the median for the 4-degree rise experiment) at C2.

3.6.2.3 Duration of flood

As a result, flood duration, defined as the total number of days when daily discharge is over $2000 \text{ m}^3/\text{s}$ at C2, is likely to be longer in the 4-degree rise climate (red) compared to the past climate (blue), as shown in Fig. 3.8. On average, floods used to occur approximately 70 days annually during the past, which will shoot up to 80–120 days annually in the future, based on SST members. This means that in the future, the flood duration is going to be extended by approximately 10–50 days. Higher flood volume, early occurrence of flooding, and prolonged duration of flooding show the future is going to be more intense and persistent. During the 2011 flood, the floods lasted from 3 weeks to 3 months, depending on the various provinces, which affected a large pop-

ulation, posing a threat to the capital city (Jular, 2011). Frequent floods and prolonged duration are likely to affect the economic, social, and environmental aspects of the basin and influence a large population depending on the CPRB for their sustainability (Abhishek *et al.*, 2021). Therefore, understanding the past flood characteristics to be prepared for future flood damage is essential (Komori *et al.*, 2012).

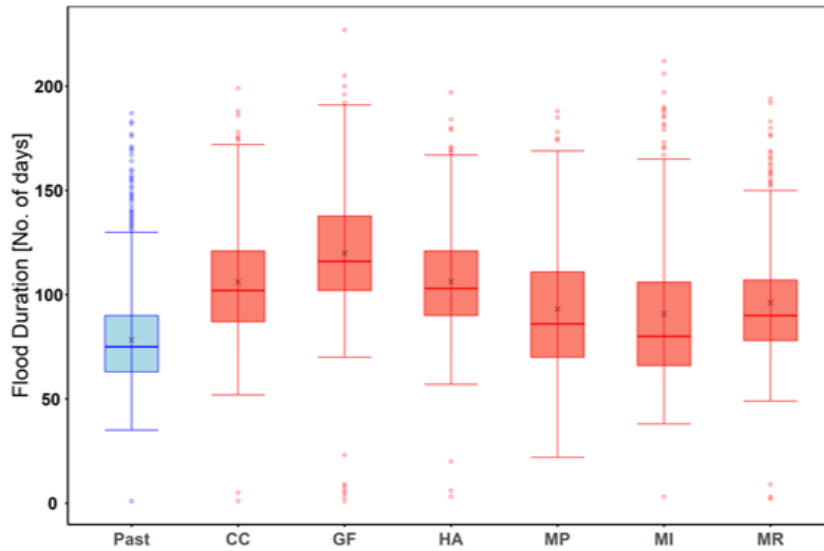


Figure 3.8: Duration of floods in past and six future SST members in the CPRB (blue: past climate experiment; red: 4-degree rise experiments) at C2.

3.7 Conclusions

The CPRB in Thailand is strategically located in the heart of Southeast Asia’s mainland, making it one of the most vulnerable to the effects of climate change due to increased floods. Despite the obvious necessity for revealing its impact, a single solid answer to this question is hard to obtain due to the large catchment area in a contrasting climate and geography with human interventions such as streamflow control. This presents challenges to climate simulations, bias correction, and hydrological modeling. Climate simulation challenges have been addressed recently with large ensemble experiments such as the d4PDF; however, the bias correction of such large ensembles for multiple climate variables or unobserved runoff is a far more challenging task. In this background, this chapter explored the applicability of streamflow bias correction considering its spatial bias heterogeneity for the d4PDF dataset and assessed the impacts of

future floods due to a 4-degree rise in global mean temperature corresponding to the end of the 21st century in the Representative Concentration Pathway (RCP) 8.5 scenario.

To achieve this, large ensemble runoff data from d4PDF was translated into streamflow using the 1-km Flow Routing Model (1K-FRM) customized in the CPRB with the dam operation module for the two major upstream dams, the Bhumibol and Sirikit dams, as well as a simple representation of middle stream overflow using a validated linear reservoir model. The bias of the obtained dam inflows was identified and corrected using the QQM method, and then the bias-corrected dam inflows were used in 1K-FRM again to obtain the discharge at C2, with upstream bias eliminated and middle stream bias remaining. These results were compared with the observed river discharge at C2 and then corrected. This TSC approach was considered to realize robust bias removal even if the bias is in the opposite direction between upstream and midstream catchments, as demonstrated in this study. Due to the large biases present in the middle stream catchment (revealed as bias in C2 in the TSC approach), the upstream bias correction is nominal, which implies similitude results between the multi-step bias correction and a simpler bias correction at C2 in the case of d4PDF, which was also verified by comparing the future projections with both bias corrections. However, this might not be the case in other large basins, and it might be interesting to see the effect that helps to reduce the uncertainty that lies in the model. In addition, the characteristic change of raw simulation data due to statistical bias correction is noticed. This is due to the limited observation data and hence, other approaches such as observation parametric function can be explored for future studies. Results show that the future hydrograph flood volume with respect to both spatial bias correction techniques is expected to increase with respect to the past. Furthermore, the impact assessment of future floods showed that in the future, floods are likely to be more prominent, and their profound effects are going to be much higher than the 2011 flood in Thailand in both SSC and TSC bias correction techniques. Elevated hydrograph flood volumes, earlier flood occurrences, and longer flood durations indicate that forthcoming floods are likely to be more rigorous. The increase in 100-year floods by 1.1–1.7 times with a larger duration exceeded by 10–50 days with respect to the past climate was observed. There is an urgent need for climate change adaptation to avoid future economic, social, and environmental destruction like or higher than the 2011 flood. Hydrological extremes such as floods are caused by several factors in addition to climate change, such as lo-

3.7. Conclusions

cal vulnerability and/or spatial heterogeneity of people and property, which were not considered in this chapter. Consequently, the hydrograph flood volume change cannot perfectly explain the resulting inundation and economic damage. In particular, the literature still lacks knowledge about such social factors which is a barrier to quantitative flood risk assessment in Southeast Asian countries (Leitold *et al.*, 2021) compared to Europe or the United States, where flood damage estimation procedures are manualized.

Chapter 4

Climate change impact assessment on flood inundation using IMCR in the LCPRB

This chapter aims to make a robust assessment based on a large ensemble d4PDF dataset and a flood inundation model for the LCPRB. In order to establish comprehensive inundation and physically grounded scenarios, simulations are conducted for numerous low- and high-frequency flooding events. Events with a hydrograph flood volume surpassing $2000 \text{ m}^3/\text{s}$ are specifically chosen for both past (1951–2010) and future (2051–2100) climates. The simulation outcomes reveal that, in comparison to the historical climate, the inundation area (with a depth greater than 0 m) is anticipated to increase by an average of 1.0–1.4 times for both 10-year and 100-year events. Similarly, the critical area (depth exceeding 0.45 m and 3 m) is projected to grow by an average of 1.0–1.3 times for 10-year events and 1.1–1.3 times for 100-year events. The maximum volume is predicted to escalate by 1.0–1.4 times for 10-year events and 1.1–1.4 times for 100-year events compared to the past climate with a depth greater than 0 m. The findings of this chapter are useful for flood exposure and risk assessment.

This chapter is largely based on the publication: Budhathoki, A., Tanaka, T., Tachikawa, Y., (2023). Assessing extreme flood inundation and demographic exposure in climate change using large ensemble climate simulation data in the Lower Chao Phraya River Basin of Thailand. *Journal of Hydrology: Regional Studies*, 50, 101583. <https://doi.org/10.1016/j.ejrh.2023.101583>

4.1 Introduction

The profound effect of impacts on hydro-meteorological parameters due to anthropogenically induced climate change plays a crucial role in increasing flood risk in Asian regions (Hu *et al.*, 2019; Try *et al.*, 2020). Furthermore, urbanization also significantly contributes to increased flood risk since cities with dense populations are typically located in low-lying terrains and thus are particularly susceptible to flooding (Abhishek *et al.*, 2021; Amnuaylojaroen and Chanvichit, 2019). Emerging evidence shows that climate change is likely raising the likelihood of high rainfall events and catastrophic flood occurrences around the globe, particularly in Southeast Asia (Ajjur and Al-Ghamdi, 2022; Huang and Swain, 2022; Padiyedath Gopalan *et al.*, 2022). The catastrophic flood events coupled with climate change are projected to pose severe damage in Southeast Asia compared to the global average (Padiyedath Gopalan *et al.*, 2022). Therefore, it is highly essential to provide a sturdy future projection of the resulting inundation simulations as a result of climate change to assist regional flood risk management.

Regional climate change studies for extreme floods are now supported by a large ensemble approach (Mitchell *et al.*, 2017; Tanaka *et al.*, 2020; Yang *et al.*, 2018). A high-resolution multi-ensemble dataset, d4PDF (Mizuta *et al.*, 2017) is one of the major products available at a global scale. The application of large ensemble climate simulation results from d4PDF datasets to generate past and future ensemble flood risk has been widely used in various regions (Tanaka *et al.*, 2018; Try *et al.*, 2020). By integrating the d4PDF dataset into the impact assessment models, it is feasible to estimate water-related hazards with return periods of thousands of years in any geographical location (Ishii and Mori, 2020). Hence, to reinforce the impact of climate change on flood magnitude in Thailand, Budhathoki *et al.* (2022) applied d4PDF to the entire CPRB with a robust bias correction by multi-site correction and found that all extreme discharge characteristics (peak, volume, starting month, duration) are expected to be more severe in the 4-degree rise climate scenario at the C2 station, a pivotal reference station in the basin.

Extreme floods pose substantial threats to both property and human lives. Elevated inundation levels increase the vulnerability of individuals and property, with inundation depth commonly used as a gauge for the intensity of floods (Zhang *et al.*, 2019). In addition, the role of assessing risk is notably impacted by the extent of the inundation

area, which is a factor obtainable through the use of hydrological models. Hydrologic models can help with risk assessment by providing an understanding of the depth and extent of the inundation region. Hydrologic and hydro-dynamic models (HEC-HMS, SWAT, RRI, etc.) are useful resources for assessing flood hazards (Bai *et al.*, 2019; Liu *et al.*, 2022; Yamamoto *et al.*, 2021). These models simulate the physical processes of floods by simulating flood parameters such as peak discharge, inundation area, and inundation depth. Researchers have employed these models to replicate past events, analyze changes in runoff, and estimate flood hazards resulting from extreme rainfall events with specific return periods in the context of climate change scenarios (Mishra *et al.*, 2018; Yang *et al.*, 2023; Zhang *et al.*, 2019). As a shallow water inundation model, this chapter uses the simulation of flood inundation performed by IMCR, which integrates a 1-D river flow and a 2-D overflow model (Tanaka *et al.*, 2015). A system for automatic connection acquires upstream river discharge and lateral inflow from the 1K-FRM model (Chapter 3) (Tanaka *et al.*, 2015). As a result, the simulation is limited to particular floodplain regions.

On these backgrounds, to assess a probabilistic flood inundation with respect to the impact of climate change, this chapter simulates the flood inundation at present and in the future, utilizing the large ensemble of d4PDF data. The estimates are done based on the inundation area and depth for various return periods. Particularly, high-frequency (5-year and 10-year) and low-frequency (50-year and 100-year) flooding events are evaluated for the impact assessment on inundation. This is to identify if climate change will have a significant impact on the likelihood of “less frequent but high-consequence” flood disasters.

The remaining part of this chapter is organized as follows: The chosen framework is illustrated in Section 4.2. Following the discussion of the data employed in this chapter in Section 4.3, Section 4.4 details the inundation model and its application. Subsequently, Section 4.5 elucidates the results of the model validation of the 2011 flood and its application to assess the impact of climate change on flood inundation for both high- and low-frequency return period events.

4.2 Framework for flood-inundation simulation

In this chapter, a flood inundation model is developed to analyze flood simulations for the LCPRB in the year 2011, past climates, and future climates. The experimental design is depicted in Fig. 4.1. Initially, the model is employed to simulate the 2011 flood for validation purposes, as illustrated in Fig. 4.1 (a), comparing the model results with the actual case. Following the validation, an assessment of the impact of climate change is conducted for both past and future climates from the d4PDF dataset, as depicted in Fig. 4.1 (b).

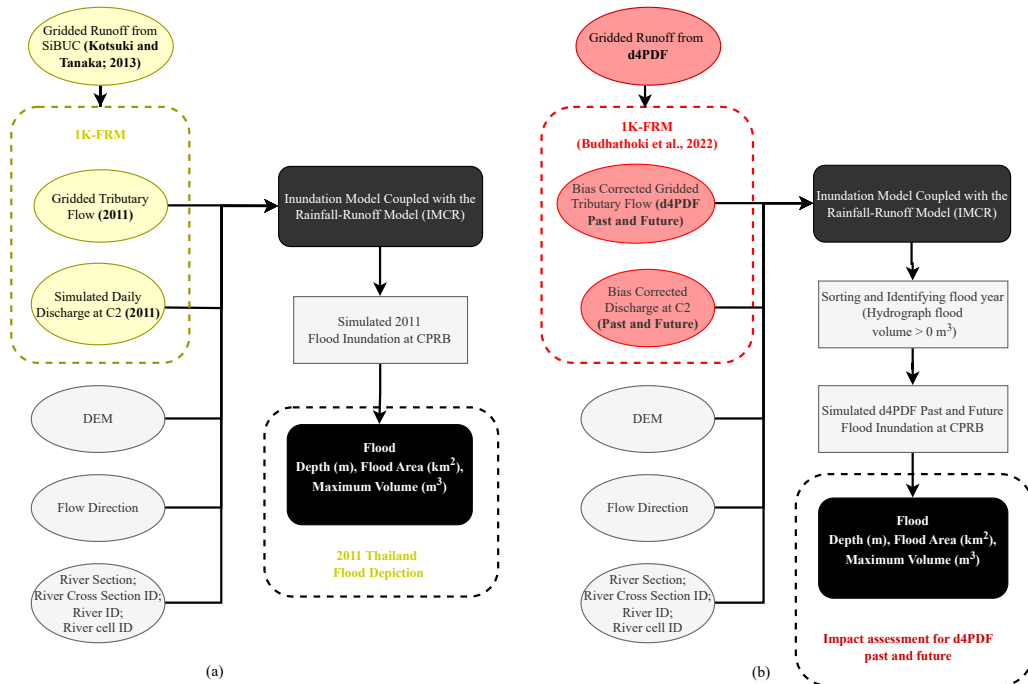


Figure 4.1: The overall methodological framework opted for the inundation simulation (a) 2011 flood for model validation and (b) d4PDF past and future climate.

4.3 Streamflow and topography data

Some of the data used in this chapter is the output of Chapter 3, river-routing simulation. The lateral tributary flow and daily river discharge at the C2 station serve as inputs for the inundation simulation. Both gridded tributary and station discharge

data are utilized for the 2011 flooding as well as for simulations representing the d4PDF past and future climate.

Furthermore, topography data is essential for the inundation model and is obtained from various sources. For the one-dimensional river flow simulation, local surveying data from Sayama *et al.* (2015) is utilized. Two-dimensional elevation data covering the LCPRB region is sourced from the Multi-Error-Removed Improved-Terrain Digital Elevation Model (MERIT DEM) by Yamazaki *et al.* (2017), which is upscaled from the original 30 arc-seconds (~90 m) to 60 arc-seconds (~2 km). The Manning's roughness coefficient for rivers and floodplains is set at $0.05 \text{ m}^{-1/3}\text{s}$. These diverse datasets are not only crucial for 2011 model validation but are also employed in the context of the d4PDF past and future climate simulations.

4.4 Inundation Model Coupling Rainfall-runoff model (IMCR) and its application

As outlined in Section 4.1, the inundation simulations in this study make use of the IMCR model, depicted in Fig. 4.2, which is a two-dimensional flood model designed for the analysis of inundation depth and area. This model is constructed based on the river flow and flood flow models for the LCPRB. The one-dimensional channel flow is used to compute the grid of the river section, and the two-dimensional floodplain flow is used to compute the grid of the flood section. Both river and floodplain flows are governed by the local inertial equations, whose momentum and continuity equations for the two-dimensional case are shown below:

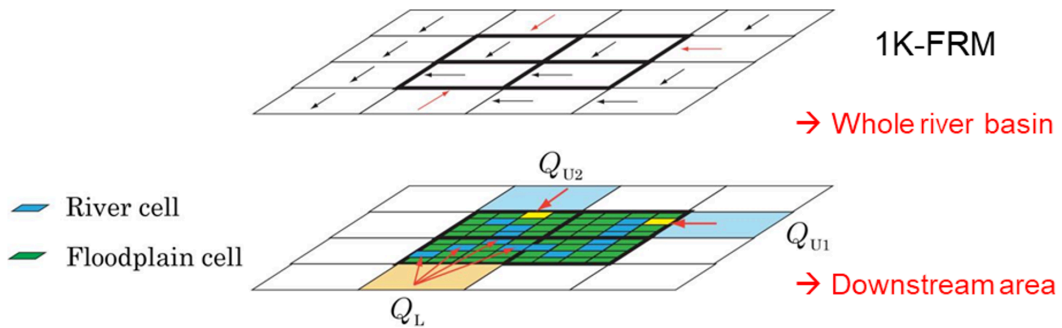


Figure 4.2: Inundation Model Coupling Rainfall-runoff model (IMCR).

X-direction momentum equation

$$\frac{\partial q_x}{\partial t} + gh \frac{\partial(h+z)}{\partial x} + \frac{gn^2|q_x|q_x}{h^{7/3}} = 0 \quad (4.1)$$

Y-direction momentum equation

$$\frac{\partial q_y}{\partial t} + gh \frac{\partial(h+z)}{\partial y} + \frac{gn^2|q_y|q_y}{h^{7/3}} = 0 \quad (4.2)$$

Continuity equation

$$\frac{\partial h}{\partial t} + \frac{\partial q_x}{\partial x} + \frac{\partial q_y}{\partial y} = q_0 \quad (4.3)$$

Where, q_x , q_y are the unit discharges in the x – *direction* and y – *direction* respectively, h is the water depth, Z is the riverbed elevation, g is the gravity acceleration, x is the flow path distance and t is the time.

This chapter selects the 2011 flood for model validation because it represents the most severe flood damage to date in the CPRB, and following it, the basin still lacks significant hydrological and hydrodynamical infrastructures that are in practice. For the validation of the 2011 flood, first, the gridded runoff data is simulated using a land surface model (SiBUC) forced by the observed precipitation in the CPRB, which is obtained from Kotsuki and Tanaka (2013). This is then used as an input to the 1K-FRM, a 1-km resolution flow routing model as stated in Chapter 3 to obtain gridded tributary discharge and daily river discharge at the C2 station, which is then used as the input to the IMCR model. The 1K-FRM model setup is the same as Budhathoki *et al.* (2022).

As can be seen from Fig. 4.2, the gridded resolution in the IMCR model is smaller than in the 1K-FRM model, 2-km and 10-km, respectively, in this case. Therefore, the inundation model processes the 10-km 1K-FRM data results into 2-km data as an input. Such a coupling of the river routing model to the inundation model is facilitated based on Tanaka *et al.* (2019a). After the simulation of the IMCR model, different indices such as flood depth, flood area, and maximum volume are calculated for the 2011 flood. The flood/inundation area is the maximum area submerged (flood depth > 0 m) during a flood event, whereas the maximum volume is the total volume of the maximum depth multiplied by the area of each grid cell. The simulated flood area is validated with the data from the Thailand Flood Monitoring System (TFMS) (<https://flood.gistda>.

or.th/) provided by Geo-Informatics and Space Technology Development (GISTDA), Thailand.

For past and future climate simulations, the d4PDF runoff data is used as the input to the 1K-FRM model, which is simulated using the SiB land surface model (Hirai *et al.*, 2007). Like the model validation simulations, the 1K-FRM outputs simulated daily discharge at the C2 station and gridded tributary river discharge, which are then used as inputs to IMCR.

The simulated daily river discharge is bias-corrected before being used as a boundary condition for the IMCR model. The bias correction method is the quantile-quantile mapping technique and also considers the spatial structure of river discharge bias (Budhathoki *et al.*, 2022). Another boundary condition to the IMCR model is the lateral tributary flows along the target river lines. Since the simulated tributary discharge from 1K-FRM is based on d4PDF gridded runoff data, it is assumed to overestimate actual lateral inflow similar to the C2 station. Hence, the same bias correction to the simulated lateral tributary flow is applied (i.e., the same bias correction factor to daily river discharge as that at the C2 station). The lower boundary condition is given as a steady flow condition.

To reduce the computational burden of 2-dimensional inundation simulations by IMCR, this chapter identifies flood years when the annual maximum river discharge at the C2 station is over 2,000 m³/s, above which some downstream is flooded (Komori *et al.*, 2012) using these river discharge products (Budhathoki *et al.*, 2022). As a result, 2,700 flood years out of 6000 years of past climate and 405 flood years out of 900 years for each SST ensemble GCM for the future +4K rise experiment are simulated in this chapter. Similar to the 2011 flood, the parameters such as the flood depth, flood area are analyzed for past and future d4PDF.

4.5 Results and discussion

This section describes the application of the inundation simulation model for an impact assessment of climate change on flood inundation. The results of the 2011 flood and the validation and implementation of inundation simulation are elaborated in this section. The results of two high-frequency events (5-year and 10-year) and two low-frequency

events (10-year and 100-year) for the d4PDF past and future climate are also discussed in this section.

4.5.1 2011 inundation simulation

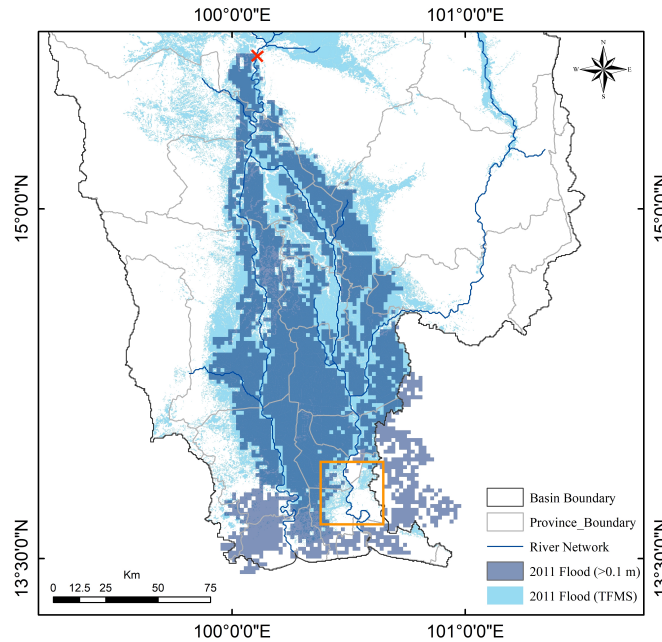


Figure 4.3: Simulated maximum inundation area for the 2011 flood in comparison to satellite remote sensing data from TFMS flood map for 2011. The red cross in the figure represents the C2 station and orange box represents the King's Dyke in the LCPRB.

The spatial distribution of the maximum inundation area simulated using IMCR and the 2011 flood area based on satellite remote sensing data from TFMS are shown in Fig. 4.3 as a validation of the inundation simulation. The maximum inundation area for the 2011 simulation is 11256 km². The inundation area is well represented, including King's Dyke (shown in the orange box in Fig. 4.3) in the basin, which is an economic hub and where large populations are settled. The Bangkok metropolitan region is protected by King's Dyke to protect from river flooding, and no flooding in the region (a whole area in the lower floodplain) can also be observed. This indicates that the IMCR implemented with the MERIT-DEM is a good representation of this reality. It also shows that the inundation extent is fairly simulated in comparison to the remote sensing data and the results shown in the hydrological sensitivity analysis of CPRB based on the RRI model evaluated by Sayama *et al.* (2017). The simulation ac-

curately depicts the overall scope of the flooding, particularly towards the southern part of Nakhon Sawan. The flooding in the Saraburi and Ayutthaya regions (southern and central parts, respectively) is a significantly valuable region, especially in terms of agriculture and industries, which is also well depicted in this simulation.

The 2011 flood event in Thailand is considered a once in a 70- to 100-year flood event, according to several studies (Budhathoki *et al.*, 2022; The World Bank, 2012). Therefore, this chapter compares the d4PDF past and future climate simulations for 50-year and 100-year events as low-frequency flooding events. Similar results are also shown in other studies (Komori *et al.*, 2012; Loc *et al.*, 2023) for the 2011 case. Additionally, to make use of the large probabilistic dataset, 5-year and 10-year high-frequency return periods are also evaluated.

4.5.2 d4PDF past and future inundation simulation

From simulated discharge at the C2 station, the flood years (2700 for the past and 405 for each future GCM) are selected as sufficient coverage for representation, as explained in Section 4.4. Fig. 4.4 (a) and (b) illustrate the past and future d4PDF comparison for inundation area and maximum volume, respectively, based on different return periods.

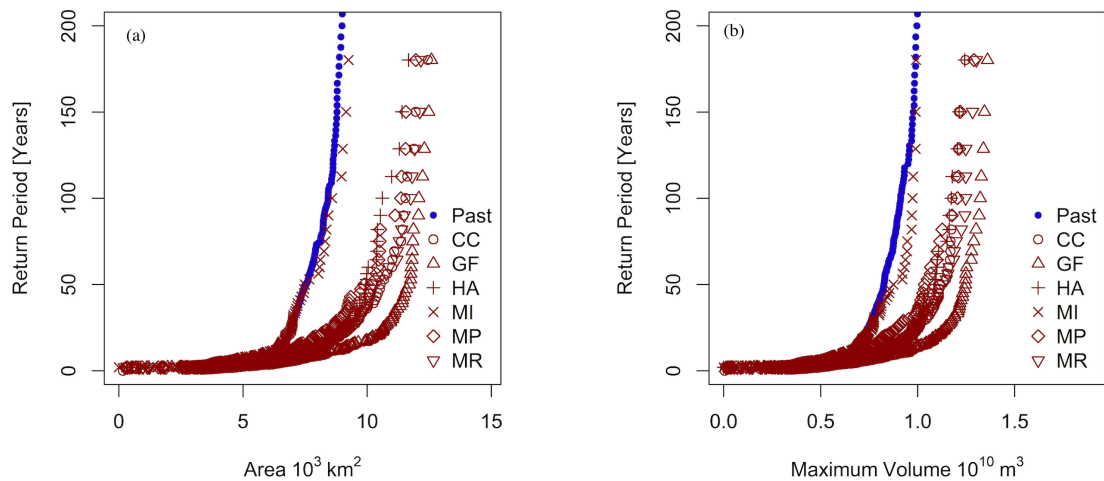


Figure 4.4: Comparison between past and future (six SST GCMs) d4PDF (a) inundation area and (b) inundation maximum volume.

All the future SST ensembles show that for both high and low-frequency return peri-

ods, there is an increase in inundation area and maximum volume compared to the past climate experiment (Fig. 4.4 (a) and (b)) with a certain spread by different scenarios of the future SST. Although the member MI shows the smallest increase and a similar trend to the past climate, most ensembles show a significant increase in the probability distribution. The results of the inundation simulation (IMCR) also correspond with the river-routing simulation (1K-FRM) discharge, as in the study undertaken by Budhathoki *et al.* (2022).

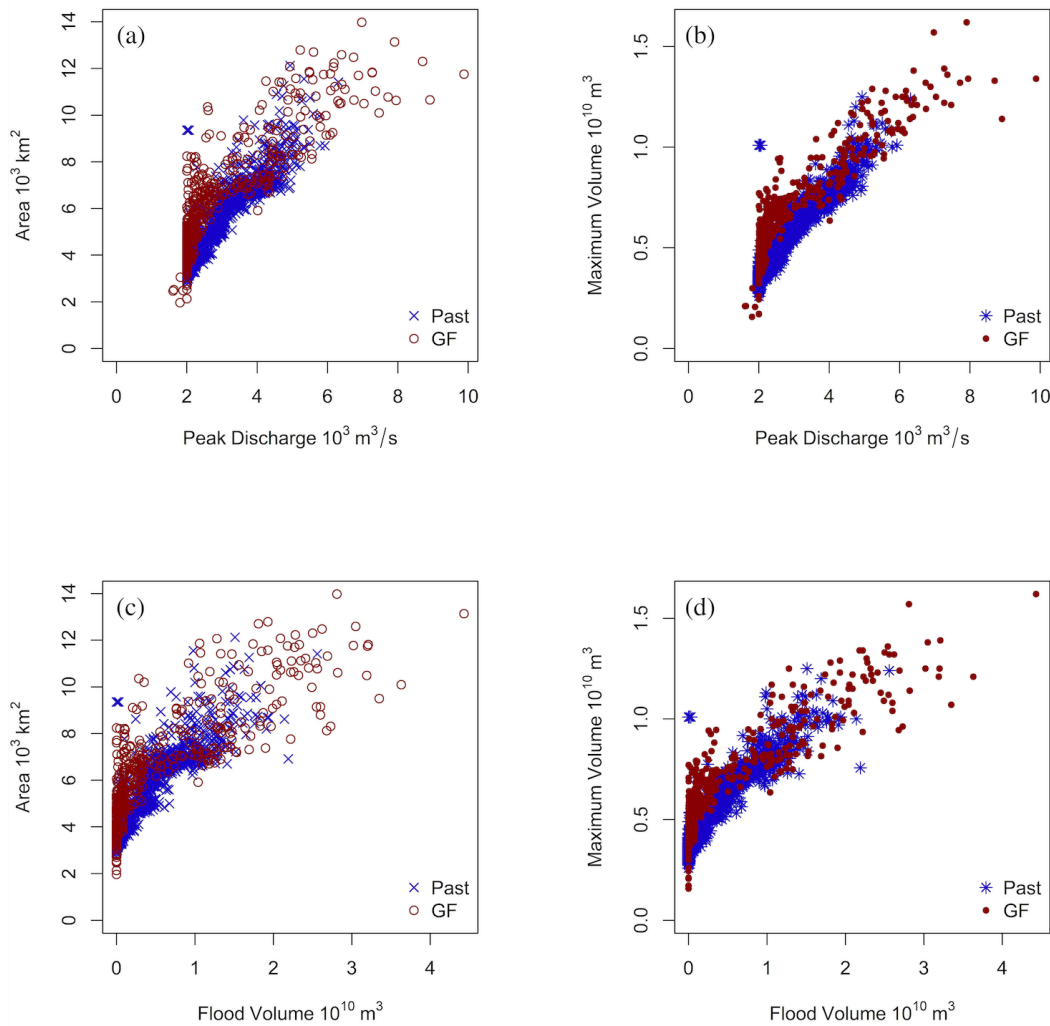


Figure 4.5: Comparison plots of peak discharge with inundation (a) area (b) maximum volume; and hydrograph flood volume with inundation (c) area and (d) maximum volume for the past and future (GF) climate.

To analyze the attribution of hydrograph characteristics at C2 station (upstream bound-

ary) to the simulated inundation and its future change, inundation area and volume from IMCR (inundation simulation) are compared with the peak discharge and hydrograph flood volume (total discharge volume over $2,000 \text{ m}^3/\text{s}$) at C2 station from 1K-FRM (Chapter 3) in Fig. 4.5. The future climate scenario (red) shows a higher magnitude in both peak discharge and flood area or volume compared with the past climate scenario (blue), indicating that future extremes are going to be higher. The gradient for both (a) and (b) of Fig. 4.5 becomes milder for high peak discharge, resulting in a large extent of inundation area and volume for both the past and future. Note that there is not much difference in the relationship between peak discharge and the flood indices between the past and future in each figure, indicating that the physical relationship between the climates is similar. Similarly, for Fig. 4.5 (c) and (d), the comparisons between inundation area and maximum volume with the hydrograph flood volume (volume greater than $2000 \text{ m}^3/\text{s}$ discharge capacity) are shown for GF. Both the comparisons correspond to past and future trends, keeping the physical properties the same. For all four cases, both flood area and maximum volume of the future climate scenario tend to be at the higher range of the past climate scenario. It may be due to the same peak discharge (Fig. 4.5 (a) and (b)), but the inundation is likely to be more severe due to other factors such as hydrograph flood volume (and vice versa in Fig. 4.5 (c) and (d)). This indicates that both hydrograph flood volume and peak discharge at the C2 station as a reference station equally contribute to the future increase of downstream flood area and volume. The results are also in line with the other five SST ensemble GCMs (CC, HA, MI, MP, and MR), and only one representative GCM (GF) is shown in this chapter.

The most affected area across the basin depicted an inundation depth of 2.1–4 m for a return period of 50-year flood, while the most affected area across the basin for the return period of 100-year and 200-year depicted an inundation depth between 4.1 and 6 m. According to Shakti P. C. *et al.* (2022), most of the LCPRB area, including the industrial park (central part of the LCPRB), shows maximum depths of greater than 3 m to be highly critical for disaster preparedness and management. The inundation depth of 0.45 m is assessed in this chapter based on the discussion among the authors, as greater than this elevation is commonly considered property loss due to flooding in Japan (Kobayashi *et al.*, 2016). Therefore, this chapter also analyzes the inundation area over 3 m (hereinafter, the critical flood area) for different return periods. Table 4.1 shows the change ratio in inundation parameters for both high- and low-frequency

Table 4.1: Changes in future maximum inundation area and future maximum volume with respect to past climate. The past column show the absolute values (in sq. km. and billion cu. m., respectively) and the columns for the six GCMs show the change factor.

Depth [m]	Return Period [years]	Past	CC	GF	HA	MI	MP	MR
Change in maximum inundation area								
> 0	5	4932.0	1.4	1.7	1.5	1.0	1.2	1.5
	10	7204.0	1.3	1.4	1.2	1.0	1.1	1.3
	50	9191.6	1.4	1.6	1.3	1.0	1.3	1.4
	100	10307.8	1.4	1.4	1.2	1.0	1.3	1.4
> 0.45	5	3340.0	1.3	1.6	1.4	1.0	1.2	1.4
	10	4872.0	1.3	1.4	1.3	1.0	1.1	1.3
	50	6560.0	1.4	1.6	1.3	1.0	1.3	1.4
	100	7328.0	1.3	1.4	1.3	1.0	1.3	1.4
> 3	5	360.0	1.2	1.3	1.2	0.9	1.1	1.2
	10	440.0	1.2	1.3	1.2	1.0	1.1	1.2
	50	548.0	1.2	1.3	1.2	1.0	1.2	1.2
	100	576.0	1.2	1.3	1.2	1.1	1.1	1.3
Change in maximum volume								
> 0	5	5.1	1.3	1.6	1.4	1.0	1.2	1.4
	10	7.4	1.3	1.4	1.3	1.0	1.1	1.2
	50	9.9	1.3	1.5	1.3	1.0	1.3	1.4
	100	10.9	1.3	1.4	1.3	1.1	1.3	1.4
> 0.45	5	4.7	1.4	1.6	1.4	1.0	1.2	1.4
	10	6.9	1.3	1.4	1.3	1.0	1.1	1.2
	50	9.3	1.4	1.5	1.3	1.0	1.3	1.4
	100	10.3	1.3	1.5	1.3	1.1	1.3	1.4
> 3	5	1.3	1.2	1.3	1.2	0.9	1.1	1.2
	10	1.7	1.2	1.3	1.2	1.0	1.1	1.2
	50	2.2	1.2	1.3	1.2	1.0	1.2	1.2
	100	2.3	1.2	1.4	1.2	1.1	1.2	1.3

events. The results show that the inundation area increases by 1.0–1.7 times and 1.0–1.6 times the past climate for high- and low-frequency events, respectively, for depths greater than 0 m in all six SST GCMs. Similar results can be observed in depths > 0.45 m. Whereas for the critical depth, MI shows a slight decrease in inundation area,

4.5. Results and discussion

but the other five SST GCMs show an increase in the spread of 1.1–1.3 times the past climate for both high- and low-frequency events. The critical flood area shows a similar increasing ratio for most of the SST GCMs as the whole flood area, indicating that with the increase in flood magnitude, not only the flood area will expand but also the flood depth will become deeper, particularly in critical zones.

In addition to the inundation area, the maximum volume is also calculated in the study. For high- and low-frequency events, the maximum volume is likely to increase 1.0–1.6 times and 1.0–1.5 times in the past, respectively, across all 6 SST GCMs. Just like the inundation area, the maximum volume is also expected to increase at a similar ratio for depths greater than 0.45 m and 3 m.

4.5.2.1 Inundation maps of high and low frequency flooding events

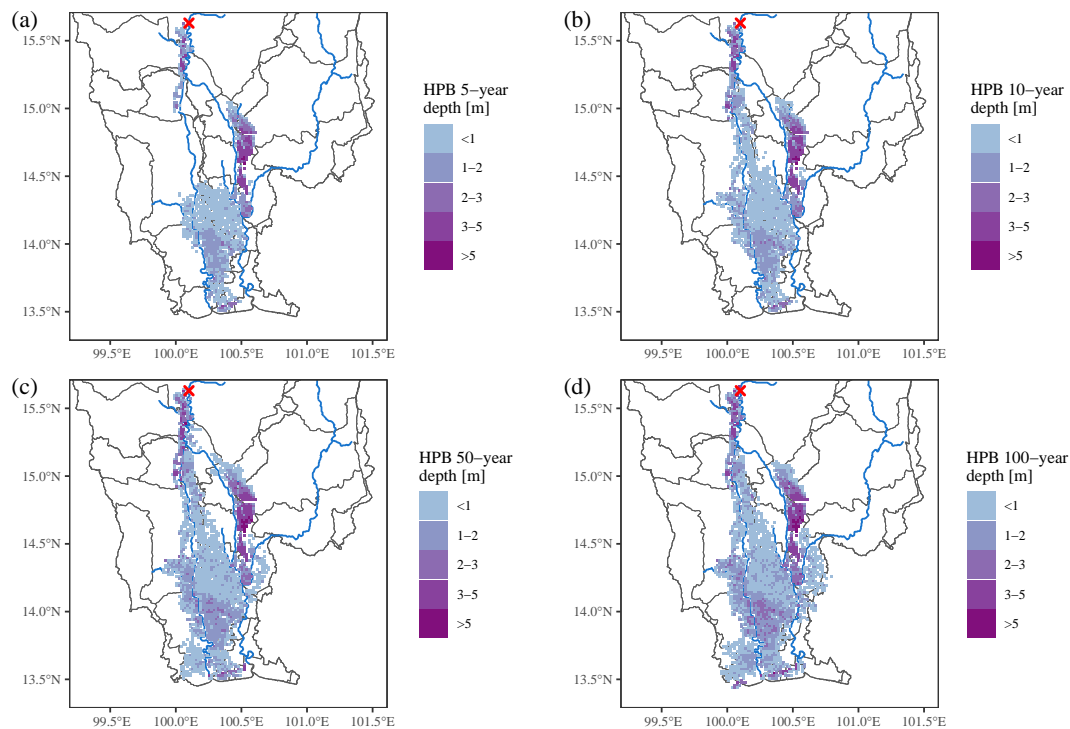


Figure 4.6: Simulated past flood inundation extent and depth for the d4PDF (a) 5-year, (b) 10-year, (c) 50-year and (d) 100-year return period with respect to depth > 0 m (the color bar represents the inundation depth in meters and the red cross represents the C2 station).

Fig. 4.6 (a-d) show the past climate flood inundation extent and depth for the d4PDF

5-year, 10-year, 50-year, and 100-year return periods, respectively, for the depth > 0 m. Fig. 4.7 (a-f) and Fig. 4.8 (a-f) illustrate the future flood inundation extent and depth for six SST GCMs for 10-year and 100-year return periods, respectively for depth > 0 m. As expected, the inundation spread is greater for low-frequency events than for high-frequency events.

Since the 2011 flood was similar to the 70- to 100-year flood in the LCPRB, there is an urgent need for adaptation and mitigation measures to be adopted in the basin to prepare for severe situations in the future.

Additionally, the King's Dyke area, as shown in Fig. 4.3 is also protected for the past and future +4K warming scenarios in all six SST GCMs, which can be clearly observed in Fig. 4.6 as well as Fig. 4.7 and Fig. 4.8. For both high- and low-frequency events, the least inundation extent is shown by MI across all the analyzed depths (0 m, 0.45 m, and 3 m). In contrast, GF shows the maximum increase in inundation extent across all analyzed depths (0 m, 0.45 m, and 3 m) for both high- and low-frequency events. Other SST GCMs such as CC, HA, MP, and MR show results close to GF towards a higher inundation extent. On average, it is evident from the figures that almost all the cases for future SST GCMs (except MI) show higher area and maximum volume than the past climate for a 10-year and 100-year flood. Similar maps are produced for a 5-year and 50-year return period, which are shown in Fig. A.1 (a-f) and Fig. A.2 (a-f) respectively.

4.5. Results and discussion

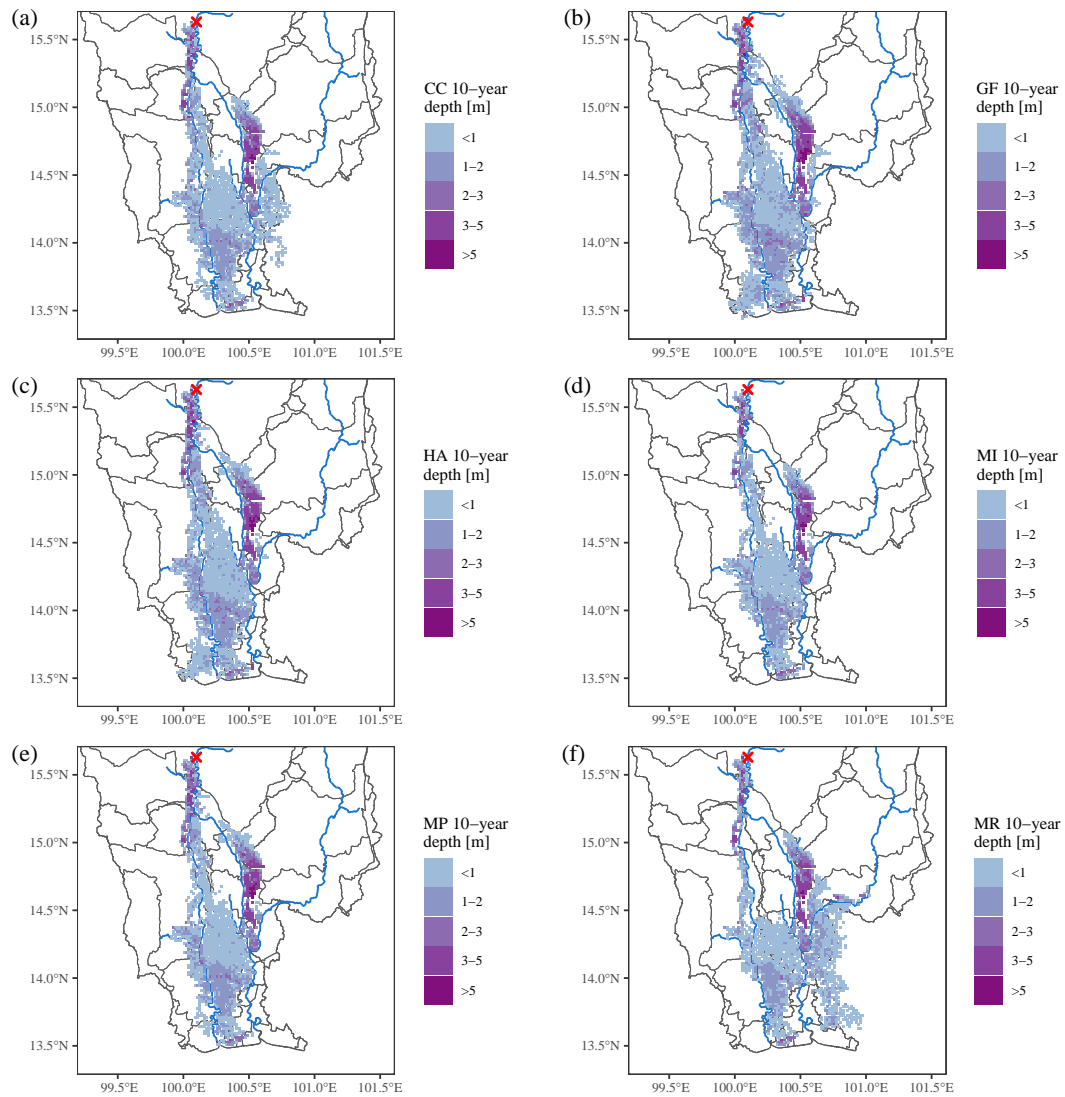


Figure 4.7: Simulated future flood inundation extent and depth for six SST GCMs (a) CC, (b) GF, (c) HA, (d) MI, (e) MP and (f) MR with respect to the d4PDF 10-year return period and depth > 0 m (the color bar represents the inundation depth in meters and the red cross represents the C2 station).

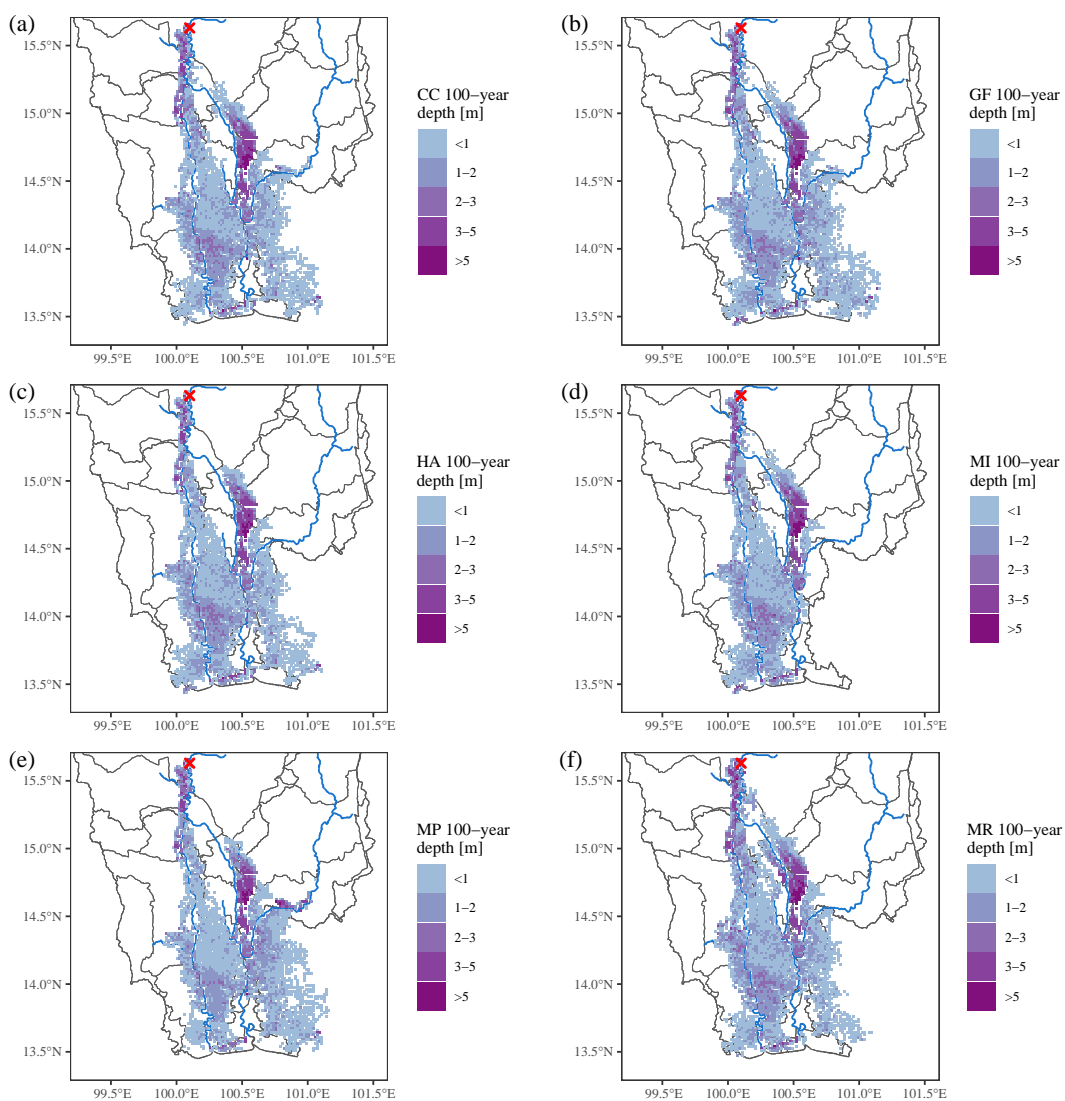


Figure 4.8: Simulated future flood inundation extent and depth for six SST GCMs (a) CC, (b) GF, (c) HA, (d) MI, (e) MP and (f) MR with respect to the d4PDF 100-year return period and depth > 0 m (the color bar represents the inundation depth in meters and the red cross represents the C2 station).

The findings of this simulation are consistent with other regional as well as global research. The analysis of Yang *et al.* (2023) shows that under the SSP126 scenario (the most sustainable route), the 100-year historical flood with respect to the return period in the Chao Phraya region will rise by 1.63 times, while it will rise by 4.55 times under the SSP370 scenario (the most pessimistic rocky-road pathway). This also validates that extreme d4PDF flooding is likely to be more intensive. It shows that the intensified inundation extent and depth are likely to be affected more if further adaptation

and mitigation approaches are not undertaken. Studies in the future climate change impact assessment on the Chao Phraya flooding under various climate change scenarios for 100-year flooding show the spatial characteristics over the basin making this region prone to flood risk (Kotsuki *et al.*, 2014; Liew *et al.*, 2016; Yang *et al.*, 2023). Additionally, using three GCMs, MRI-CGCM3, MIROC5, and HadGEM2-ES, the flood inundation in the Ciliwung River Basin of Indonesia, the inundation area is likely to increase by 1.2 times for depths < 1.5 m, and for depths > 1.5 m, it is likely to increase by 1.5 times for 100-year floods in the future (Mishra *et al.*, 2018). Another study in the Hadahe River Basin of China emphasizes that the increase in inundation area is likely to increase with the inundation depth. The results show that the future inundation area for depths between 1.0–2.0 m, 2.0–3.0 m, and > 3 m is projected to increase by 5.4%, 12.3%, and 22% for RCP 8.5 in the basin (Zhang *et al.*, 2019). These studies suggest that measures for the reduction of emissions are suggested as the effects on the inundation area are higher for the RCP 8.5 scenario, which is also similar to the +4K warming scenario.

4.6 Conclusions

The LCPRB is the predominant region in the Southeast Asian region. Also being home to the capital city of Thailand, Bangkok, this basin is also crucial, as several industries and agricultural production contribute to the economy of Thailand. The basin is prone to frequent river floods from the Chao Phraya River, affecting residential as well as economic zones. Hence, this chapter analyzes flooding in the basin in terms of flood area and depth with the help of a large ensemble climate simulation dataset (d4PDF) and flood-inundation simulations. The analysis is carried out for low- and high-frequency events to utilize the 2700-years (out of 6000-years) of the past and 2430-years (out of 5400-years) of future climate for a +4K increase in temperature. In addition to the inundation depth > 0 m, depths > 0.45m and 3 m were also carried out.

The future 5-year and 10-year flooding for +4K rise is likely to increase in terms of both maximum volume and inundation area compared to the past climate. However, the future 50-year and 100-year flooding for +4K rise is likely to be more severe in terms of both inundation area and maximum volume compared to the past climate for all the cases of analyzed depths. Approximately, the inundation area is likely to increase by

1.3, 1.2, 1.3, and 1.3 times across all depths for 5-year, 10-year, 50-year, and 100-year return periods, respectively. On average, across six SST GCMs and three analyzed depths, similar results were observed for maximum volume. Moreover, there is not much difference in the relationship between peak discharge and the flood indices between the past and future, which indicates that the physical relationship kept between the d4PDF climates is similar. In addition, the inundation area for all the cases well represents the King's Dyke region, which also suggests that the DEM used in the basin well represents the actual study area. The output of this chapter can be utilized for risk and economic damage assessment for various sectors to depict the overall scenario for the past and future.

There is uncertainty in hazard models, brought on mainly by an incomplete representation of complicated local drainage networks, which limits evaluations of flood exposure in this study. This could be further explored for potential research in the region.

Chapter 5

Demographic and agriculture exposure assessment in the LCPRB

This chapter aims to analyze the impacts of climate change on population demographics and agriculture exposure to high- and low-frequency floods. Population exposure for different flood depths (greater than 0 m, 0.45 m, and 3 m) is analyzed to check the effects on population at varied flood levels. The d4PDF multi-ensemble analysis shows that the exposed population based on the SSP5 scenario is likely to decrease despite the increase in inundation extent in the LCPRB. The exposed population in the future, with respect to the SSP5 scenario “Taking the Highway,” is expected to decrease on average by 0.7–0.9 times in comparison to the past climate for depth > 0 m. However, keeping the population constant as in the past, the exposed population is likely to increase on average by 1.3–1.4 times in comparison to the past climate for depth > 0 m. In addition, rice exposure for depths higher than 0.5 m is also assessed in this chapter, and results show that the exposed area is likely to increase on average by 1.2–1.4 times the past climate, and the exposed duration is likely to increase by 1.1–1.2 times the past climate. Several sectors have been hit by the impact of climate change, and action is required for adaptation and mitigation in the affected sectors.

This chapter is partially based on the publication: Budhathoki, A., Tanaka, T., Tachikawa, Y., (2023). Assessing extreme flood inundation and demographic exposure in climate change using large ensemble climate simulation data in the Lower Chao Phraya River Basin of Thailand. *Journal of Hydrology: Regional Studies*, 50, 101583. <https://doi.org/10.1016/j.ejrh.2023.101583>

5.1 Introduction

The impacts of climate change on floods ultimately affect water resources, population, agriculture, ecosystems, etc. The detrimental effects of floods have been worse during the last century and are expected to get worse in the future due to population growth and economic expansion (Merz *et al.*, 2021). In addition, a number of studies have studied the CPRB from a hydrological and hydrodynamic perspective (Padiyadath Gopalan *et al.*, 2022; Sriariyawat *et al.*, 2022; Yang *et al.*, 2023). Numerous flood models have, therefore, been developed to identify exposed, vulnerable flood areas and possible water depths (Eccles *et al.*, 2021; Luo *et al.*, 2018; Nandi and Reddy, 2022; Padulano *et al.*, 2021; Pinos and Timbe, 2019). However, its translation into future projections under the combined impact of climate and socio-economic changes is less studied (Miller and Hutchins, 2017; Sebastian *et al.*, 2019). Instead, there is a need for flood risk assessment to expand the target to population or gross domestic product (GDP) at a global scale (Arnell and Gosling, 2016; Dottori *et al.*, 2018), as well as at a regional scale (Tanoue *et al.*, 2020). As a next step, future projections of extreme floods and their translation into flood extent and demographic exposure are essential to support regional decision-making.

In addition, the consistent flooding during the rainy season endangers already planted crops and seriously harms water and road infrastructure. Agriculture is one of the sectors that is most susceptible to climatic fluctuations, and hence yields are typically anticipated to drop most dramatically in nations at lower latitudes on a global scale (Parker *et al.*, 2019; Stevanović *et al.*, 2016). In the near past, 24% of agriculture around the globe was situated in regions that frequently experienced flooding (IPCC, 2014), and by 2050, it is anticipated that main grains in Asia, such as wheat and maize, will see average yield losses of 8% (Parker *et al.*, 2019). Hence, understanding flood exposure in the context of the effects of climate change is crucial for sustainable development.

Recently, the regional effects of climate change have been evaluated using ensemble climate databases to capture the spatio-temporal climatic variability of flooding. Based on hundreds of heavy rainfall occurrences in a large climate database, it is feasible to assess the likelihood of the occurrence of exceptionally heavy rainfall and potential flood disasters for past and future climates (Economou and Garry, 2022; Tebaldi and Knutti, 2007). Therefore, using a large ensemble high-resolution database to identify the potential disaster for future climate is highly needed for the development of

flood management strategies. This dataset, coupled with hydrodynamic simulations, is widely adapted for capturing the flooding events of different return periods in several basins (Budhathoki *et al.*, 2022; Tanaka *et al.*, 2020; Try *et al.*, 2023).

Predicting flood threats and the harm they cause depends heavily on the use of distributed hydrodynamic models in the low floodplain area. There is a large uncertainty in exposure and vulnerability assessments due to the dependency on hazard models that rely on incorporating swift anthropogenic changes, topographic data, and insufficient calibration data (Ward *et al.*, 2015). However, a tool that takes into account the intricate relationships between river parameters, land surface information, and climate variables is highly beneficial (Try *et al.*, 2023). In order to forecast flood behavior at the scale of a river basin, IMCR is a two-dimensional diffusive wave model widely used in various river basins, such as Tanaka *et al.* (2017); Tanaka *et al.* (2020). This model has shown reasonably good performance in large river basins such as the Chao Phraya River Basin of Thailand to compute the flood simulations, as well as reduced its computational time compared to other two-dimensional models as shown in Chapter 4.

Therefore, the overall objective of this chapter is to evaluate the demographic and agricultural exposure by making use of the simulated floods. The assessment is done with respect to the impacts of climate change results from Chapter 4 for different return periods and flood levels. Specifically, population exposure under flood depths higher than 0.45 m and 3 m is also undertaken in this study as typical and critical levels, respectively, accounting for future population change. Whereas considering the damage assessment in Chapter 6 for rice cultivation, flood depth greater than 0.5 m is also analyzed in this study. Understanding the combined effects of societal and climatic changes on those affected by flooding would be helpful in estimating future flood risk in rapidly urbanizing communities.

The remainder of this chapter is assembled as follows: The overall framework opted for in this chapter is described in Section 5.2. The data used explicitly for this chapter is mentioned in Section 5.3. Followed by it, Section 5.4 describes the method of coupling the inundation results from Chapter 4 with the population and rice cultivation data mentioned in Section 5.3. Section 5.5 elaborates on the impact assessment on the affected population and agriculture with respect to the d4PDF climate data for both high- and low-frequency return periods and different flood depths.

5.2 Framework for exposure assessment

This section aims to determine the probabilistic flood exposure to population and agriculture. In particular, low- and two high-frequency return periods assessment is carried out at different flood levels for the demography and agricultural crop. The overall methodological framework opted in the study is shown in Fig. 5.1.

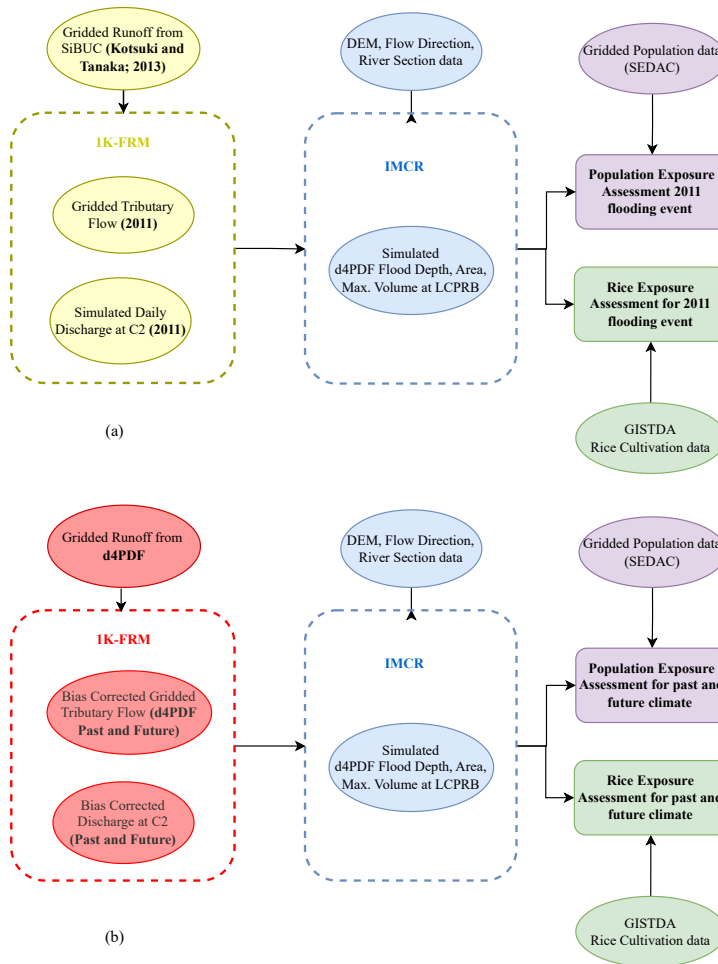


Figure 5.1: Methodological framework opted in this chapter for the demographic and agriculture exposure assessment for (a) 2011 flood and (b) d4PDF past and future climate in the LCPRB.

5.3 Exposure data

The simulated floods for different return periods are taken from the outputs of Chapter 4. In addition, the two other data used as input in this study for the exposure assessment are the population density and the rice production area in the LCPRB. In a large-scale area, satellite remote sensing data appears to be creating spatially accurate visualizations of the localized consequences of damage caused by floods with adequate spatial resolution (Wang *et al.*, 2022). Hence, this study uses satellite data for the evaluation of demographic and agricultural exposure for accurate visual representations, considering its spatial dimension in the LCPRB.

5.3.1 Population data

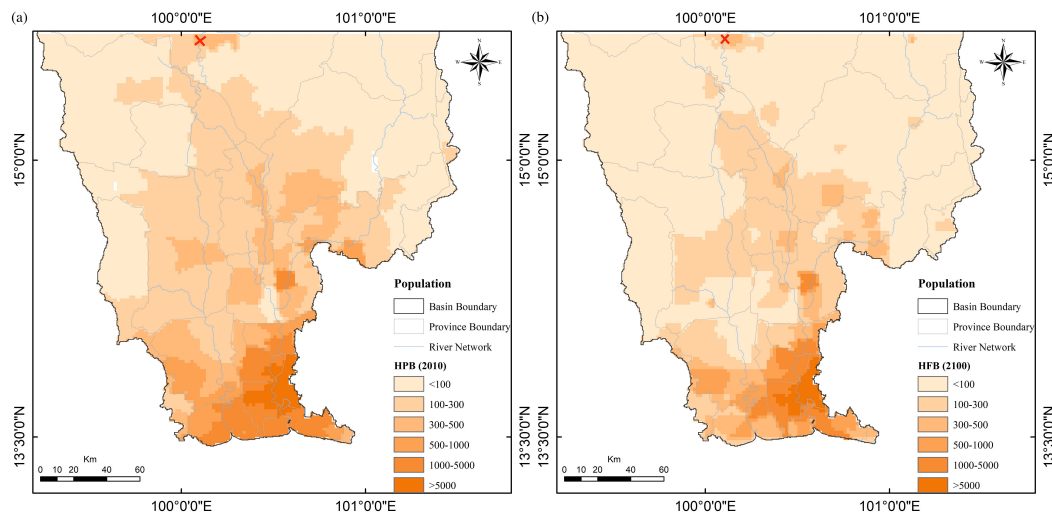


Figure 5.2: Spatial population distribution in the LCPRB based on the GWP SEDAC dataset for (a) 2010 and (b) 2100 (SSP5) (the red cross in both (a) and (b) represents the C2 station).

Population density data to analyze past and future population exposure in the LCPRB is required for the demographic exposure assessment. However, the governmental population data is not publicly available (Tierolf *et al.*, 2021), including the future projections of these data in many Southeast Asian countries. Therefore, as a widely available dataset, the Gridded Population of the World (GPW) from the Socioeconomic Data and Applications Center (SEDAC) at 30 arc-seconds (~ 1 -km) resolution (<https://sedac.ciesin.columbia.edu/data/collection/gpw-v4>) is employed. For 2011 and past

climate cases, the data for 2010 were utilized as population estimates available for 5 target years: 2000, 2005, 2010, 2015, and 2020 in GPW version 4. The gridded population for depths greater than 0 m is shown in Fig. 5.2 for (a) 2010 and (b) 2100. The number of people and projected number of people are 19,510,069 for 2010 and 13,523,685 for 2100, respectively. The figures clearly show that the projected 2100 population is going to decrease, especially in the central and northern parts of the LCPRB.

The dataset further includes future gridded projections of the population based on the Shared Socioeconomic Pathways (SSP) scenarios. These projections are calculated based on a parameterized gravity-based downscaling model to generate spatial population change projections that are quantitatively consistent with SSP national population and urbanization projections, and qualitatively consistent with SSP narrative assumptions about spatial development patterns (Gao and O'Neill, 2021; Gao and O'Neill, 2020; Jones and O'Neill, 2016). For future predictions, data for the SSP5 (fossil-fueled development) scenario for the year 2100 are used because the +4K increase scenario corresponds to RCP 8.5 towards the end of the century.

5.3.2 Agricultural data

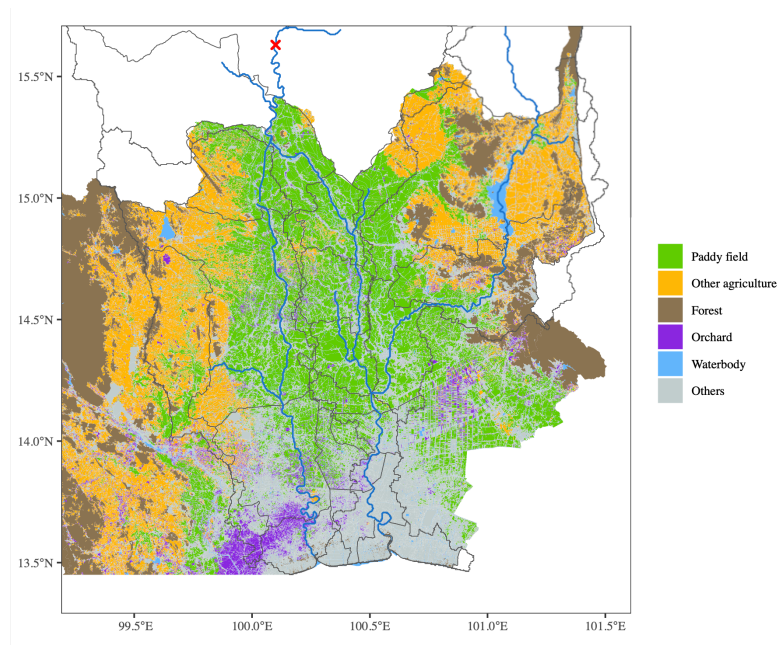


Figure 5.3: Landuse map modified based on LDD data for 2015 in the LCPRB (the red cross represents the C2 station).

5.3. Exposure data

The rice cultivation data for the whole of Thailand is taken from the Geo-Informatics and Space Technology Development Agency (GISTDA) (<https://rice.gistda.or.th>), which is further masked to LCPRB for the utilization in this study. The data available and used in this study is for the year 2023. Rice is the major crop in the region; therefore, wet-season rice is used as the crop for agriculture exposure assessment in the LCPRB. For further reference, the landuse map produced in the data from the Land Development Department (LDD) is shown in Fig. 5.3. In the north and central part of the CPRB, the rice area does not increase due to the higher cost of inputs, including fertilizer, pesticides, and energy. In addition, Yuan *et al.* (2022), states that there is stagnant rice cultivation in south-eastern countries such as Thailand, Vietnam, Myanmar and the Philippines. Therefore, in this study, we assume that the rice cultivation area is constant (i.e., 2023 cultivation area) for the 2011 flood event, d4PDF past and future climate rice exposure. Fig. 5.4 shows the percentage rice cultivation coverage in the LCPRB in 2023, and the total rice cultivation area is about 11,172 km².

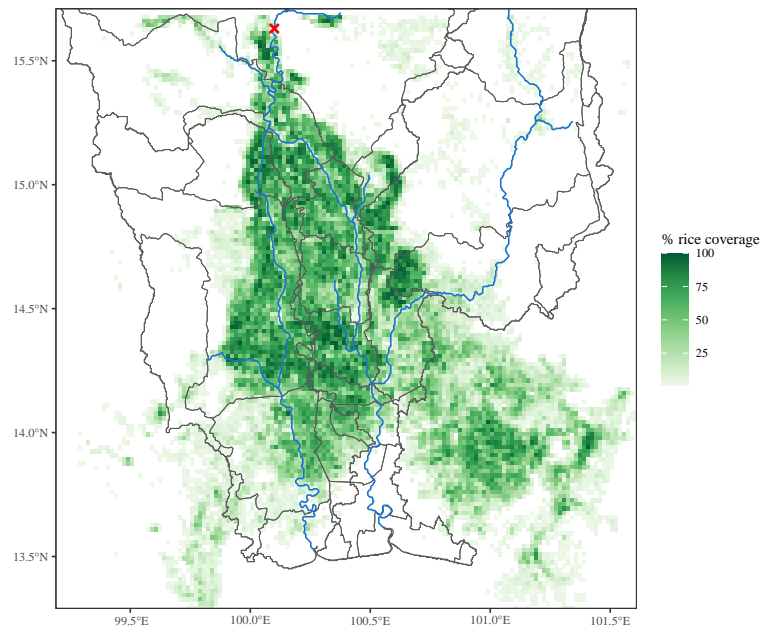


Figure 5.4: Percentage rice cultivation area based on GISTDA data for 2023 in the LCPRB (the red cross represents the C2 station).

5.4 Methodology for exposure assessment

5.4.1 Population exposure

To understand the effects on the population, this study investigates the exposed population to the 2011 flood. The translation of inundation depths to population exposure is based on gridded SEDAC population data as mentioned in Section 5.3. Similarly, both the past and future climate simulations are translated into population exposure for different inundation depths (based on the results of Chapter 4) for flood exposure assessment. The 2010 population density data is used for the estimation of 2011 and past climate floods, whereas the 2100 projected data is for the SSP5 “Taking the Highway” scenario. Different flood levels are analyzed in the study to have a clear depiction of exposure. For the population exposure assessment, three cases of depth greater than 0 m, 0.45 m, and 3 m are analyzed as in Chapter 4.

5.4.2 Agricultural exposure

From inundation simulations in Budhathoki *et al.* (2023), the inundation depth, area, and duration are calculated for 2011, and d4PDF past and future climate experiments for the depth greater than 0.5 m for high-frequency events (5-year and 10-year) and low-frequency events (50-year and 100-year) using the inundation simulation model IMCR as mentioned in Chapter 4. Overall performance of extreme river discharge and inundation extent in 2011 are validated (Budhathoki *et al.*, 2022 ; Budhathoki *et al.*, 2023). These inundation simulation results are then overlaid with rice cultivation data to derive into flood rice exposure in each experiment. As for the assessment on damage estimation on rice cultivation (which is done in Chapter 6), fragility curves estimated in the Philippines and Myanmar show no damage below 0.5; therefore, rice cultivation area with flood water depth larger than 0.5 m is counted as exposure. Hence, in this chapter, a threshold of 0.5 m is set for the evaluation.

5.5 Results and discussion

This section explores the exposure assessment for different return periods and depths for two major aspects. The demographic and agricultural aspects are explored for the

2011 flood, d4pDF past and future climate.

5.5.1 Population exposure assessment

5.5.1.1 2011 population exposure

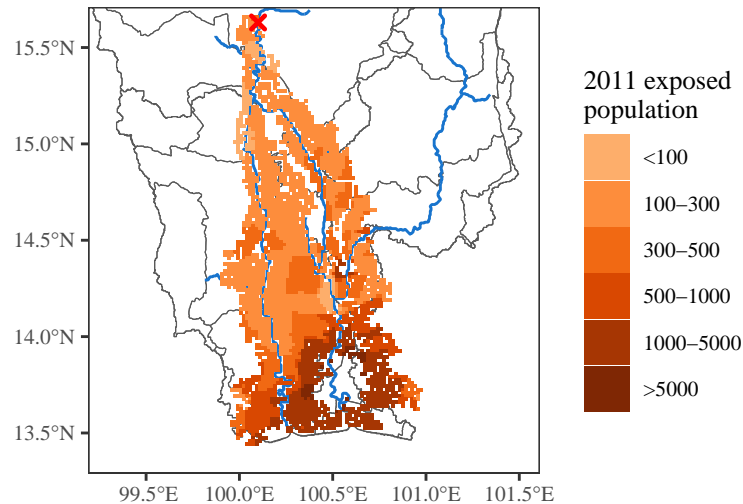


Figure 5.5: Population exposure map of 2011 flood (the red cross represents the C2 station).

Thailand’s 2011 flood presents comprehensive examples of how water resources may materialize in a complicated matter of geography, culture, and political management through flood catastrophes. With continuous flooding occurring in Thailand, it saw its worst floods in more than half a century. The inundation information, thus overlaying population information in the basin, is crucial for the evaluation of flood risks. Such assessments are highly needed to avoid any impulsive decisions, considering the demographic situation (Smith *et al.*, 2019). Therefore, to understand the effects on the population, this study looks into the exposed population in the 2011 flood. Fig. 5.5 shows the population exposure map throughout the LCPRB, which is calculated by overlaying the flood inundation area with the population data for the 2011 flood. This figure indicates that most of the population that surrounds Bangkok (the central lower part of the basin) is more highly affected than the northern part of the LCPRB. The total number of populations exposed below C2 was found to be 8,832,743 for depths greater

than 0 m.

5.5.1.2 d4PDF past and future population exposure

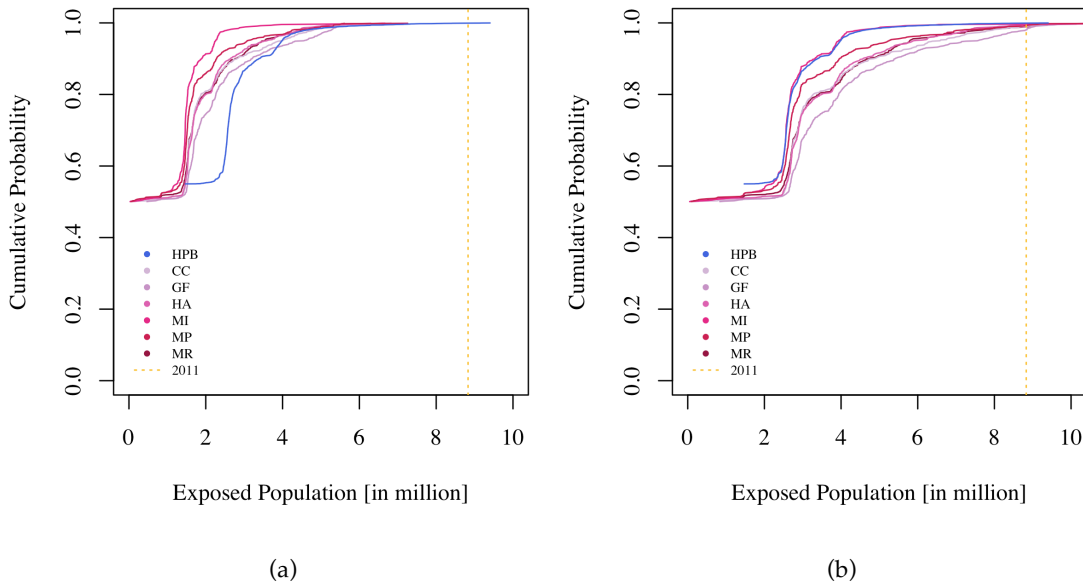


Figure 5.6: Cumulative frequency distribution plots for d4PDF past and future climate with respect to the exposed population for (a) SSP5 projected population and (b) constant population as d4PDF past climate.

Following the 2011 population exposure, this study examines the population exposure for the d4PDF past and future scenarios for different flood depths and return periods. Towards the end of the century, based on the projected population for SSP5, the population exposed is likely to decrease. Fig. 5.6 (a) clearly shows the decrease in future population compared to past climate for all SST GCMs. It is expected to be around 0.6–0.9 times and 0.6–1.1 times compared to the past climate for different SST ensembles in high-frequency and low-frequency return period and depth greater than 0 m, respectively, as shown in Table 5.1. Similar results are expected for depths greater than 0.45 m and 3 m. This states that even with the increase in depth, the exposed population ratio is expected to be similar.

Table 5.1 shows the overall change in population exposure in the future climate with respect to the past climate. The total population exposed to flood inundation is approximately 5,585,602 nos. (depth > 0 m), 3,692,536 nos. (depth > 0.45 m), and 210,326

nos. (depth > 3 m) for the 100-year return period in the past climate. The d4PDF past climate shows that Bangkok and its nearby provinces are more highly populated than the upstream region. However, due to the presence of King’s Dyke surrounding the Bangkok region, people in this region are less likely to be affected by river flooding. However, moving toward the Ayutthaya and Saraburi (central and eastern) regions, where a large industrial, agricultural, and residential area lies, the exposed population due to flooding is higher.

Table 5.1: Changes in future exposed population (projected population for SSP5 scenario) with respect to past climate population. The past columns show the absolute values (in number of people) and the columns for the six GCMs show the change factor.

Depth [m]	Return Period [years]	Past [Nos.]	Change in exposed population (projected population for SSP5)					
			CC	GF	HA	MI	MP	MR
> 0	5	2705415	0.7	0.8	0.7	0.6	0.6	0.7
	10	3384710	0.8	0.9	0.8	0.6	0.7	0.8
	50	4619138	1.0	1.1	1.0	0.6	0.9	1.0
	100	5585602	0.9	1.0	0.9	0.6	0.9	1.0
> 0.45	5	1830604	0.7	0.8	0.7	0.6	0.6	0.7
	10	2294965	0.8	0.9	0.8	0.6	0.7	0.8
	50	3129120	1.0	1.1	0.9	0.6	0.9	0.9
	100	3692536	1.0	1.0	0.9	0.6	0.9	0.9
> 3	5	115637	0.7	0.7	0.7	0.5	0.6	0.7
	10	130256	0.7	0.9	0.8	0.6	0.6	0.7
	50	172704	0.9	1.0	0.9	0.6	0.8	0.9
	100	210326	0.7	0.8	0.8	0.7	0.7	0.8

Additionally, this study also looked into the impact on the exposed population in the future, keeping the change in population constant for different depths, as shown in Table 5.2. Fig. 5.6 (b) shows that if the population is kept constant as present climate then the population exposure is likely to increase for all SST GCMs and the results are likely to be completely different than Fig. 5.6 (a). In addition, for a high-frequency return period, the change in exposed population in the future is likely to rise by 1.3 times and for a low-frequency return period, it is likely to rise by 1.5 times the past

climate-exposed population for depths greater than 0 m and 0.45 m. Similarly, for depths greater than 3 m, the exposed population is likely to increase by 1.1 times and 1.3 times for high-frequency and low-frequency events, respectively.

Table 5.2: Changes in future exposed population (constant population as past) with respect to past climate population. The past columns show the absolute values (in number of people) and the columns for the six GCMs show the change factor.

Depth [m]	Return Period [years]	Past [Nos.]	Change in exposed population (constant population as past)					
			CC	GF	HA	MI	MP	MR
> 0	5	2705415	1.2	1.5	1.3	1.0	1.1	1.3
	10	3384710	1.4	1.6	1.4	1.0	1.2	1.4
	50	4619138	1.7	1.9	1.6	1.0	1.5	1.7
	100	5585602	1.6	1.6	1.5	1.0	1.5	1.6
> 0.45	5	1830604	1.2	1.4	1.3	1.0	1.1	1.2
	10	2294965	1.4	1.6	1.4	1.0	1.1	1.3
	50	3129120	1.6	1.9	1.5	1.0	1.5	1.6
	100	3692536	1.6	1.6	1.4	1.0	1.5	1.6
> 3	5	115637	1.1	1.2	1.1	0.9	1.0	1.1
	10	130256	1.2	1.4	1.3	1.0	1.1	1.2
	50	172704	1.4	1.6	1.4	1.0	1.3	1.4
	100	210326	1.2	1.4	1.3	1.1	1.3	1.3

In this case, the increasing ratio is constant between area and exposure, and hence, the added inundation area, especially towards the southern part of LCPRB, should be similarly populated. This also states that for the projected population case, the climate change impact may cancel the impact of population exposure due to the decline in population towards 2100. The population growth of the SSP5 scenario for Thailand based on fertility, mortality, migration, and education scenarios (Jones and O'Neill, 2016; Kc and Lutz, 2017) is used as an input in the study. Since Thailand is grouped under "low fertility countries," where the population growth rate is expected to be low towards the end of the century, this study also shows a similar rate for the exposed population.

Fig. 5.7 shows the past climate population exposure maps for (a) 5-year, (b) 10-year,

5.5. Results and discussion

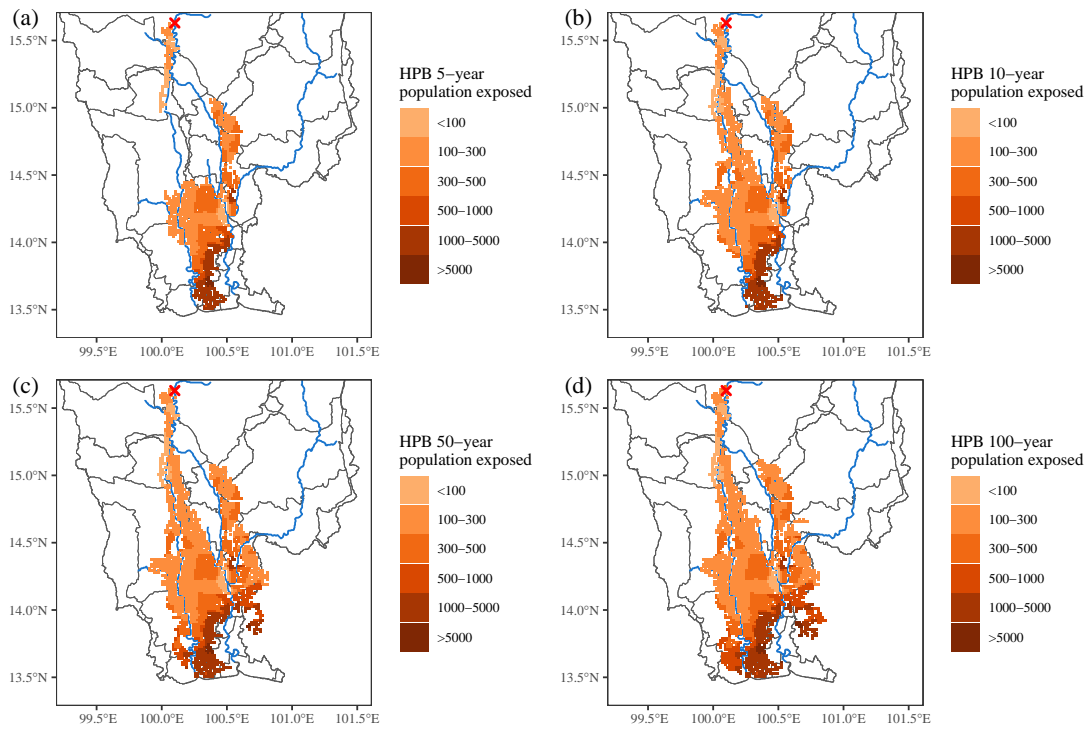


Figure 5.7: Population exposure to past floods for the d4PDF (a) 5-year, (b) 10-year, (c) 50-year and (d) 100-year return period with respect to depth > 0 m (the color bar represents the population in nos. and the red cross represents the C2 station).

(c) 50-year, and (d) 100-year return periods. For the past climate exposure for different return periods, it is clear that the urban region (central southern part), which also contains the capital city, is highly exposed to depths greater than 0 m. However, towards the end of the 21st century, the intensification is less for both high- and low-frequency events than in the past climate. This may be due to the decrease in population towards the end of the century. However, it can be clearly observed that low-frequency events like 2011 will have a larger population exposure than the more commonly occurring high-frequency events. Fig. 5.8 (a-f) and Fig. 5.9 (a-f) show the future gridded exposed population maps to depths greater than 0 m flooding for 10-year and 100-year respectively. Other maps of the 5-year and 50-year return periods are shown in Fig. A.3 (a-f) and Fig. A.4 (a-f) respectively. Hence, managing riverine flooding in addition to urban flooding is likely to be a challenge, especially with the increase in urban population. Therefore, to reduce the increased incidence of the exposed population to flooding, reliable flood mitigation and adaptation strategies are required.

Research carried out for 100-year flood-exposed populations under climate change in 14 main catchments around the globe using SEDAC gridded population data similar to this study shows that there is a decrease in population exposed to flooding in the catchments that contain dams. Boulange *et al.* (2021) and Tierolf *et al.* (2021) state that in Thailand, after 2040, similar to decrease in flooding, the exposed population is expected to decrease by 11%. Whereas, in contrast, Gu *et al.* (2020) states that there is an increase in extreme flood exposure to the population and a decrease in population exposure to moderate floods. There was an increase of 11.6% and 9.7% in the exposed population with respect to flood magnitude in the SSP5 scenario. Future analyses of risks associated with global floods would also profit from the development of plausible future population projections that consider population behavior in terms of migration, adaptation, movement during warning measures, etc.

5.5. Results and discussion

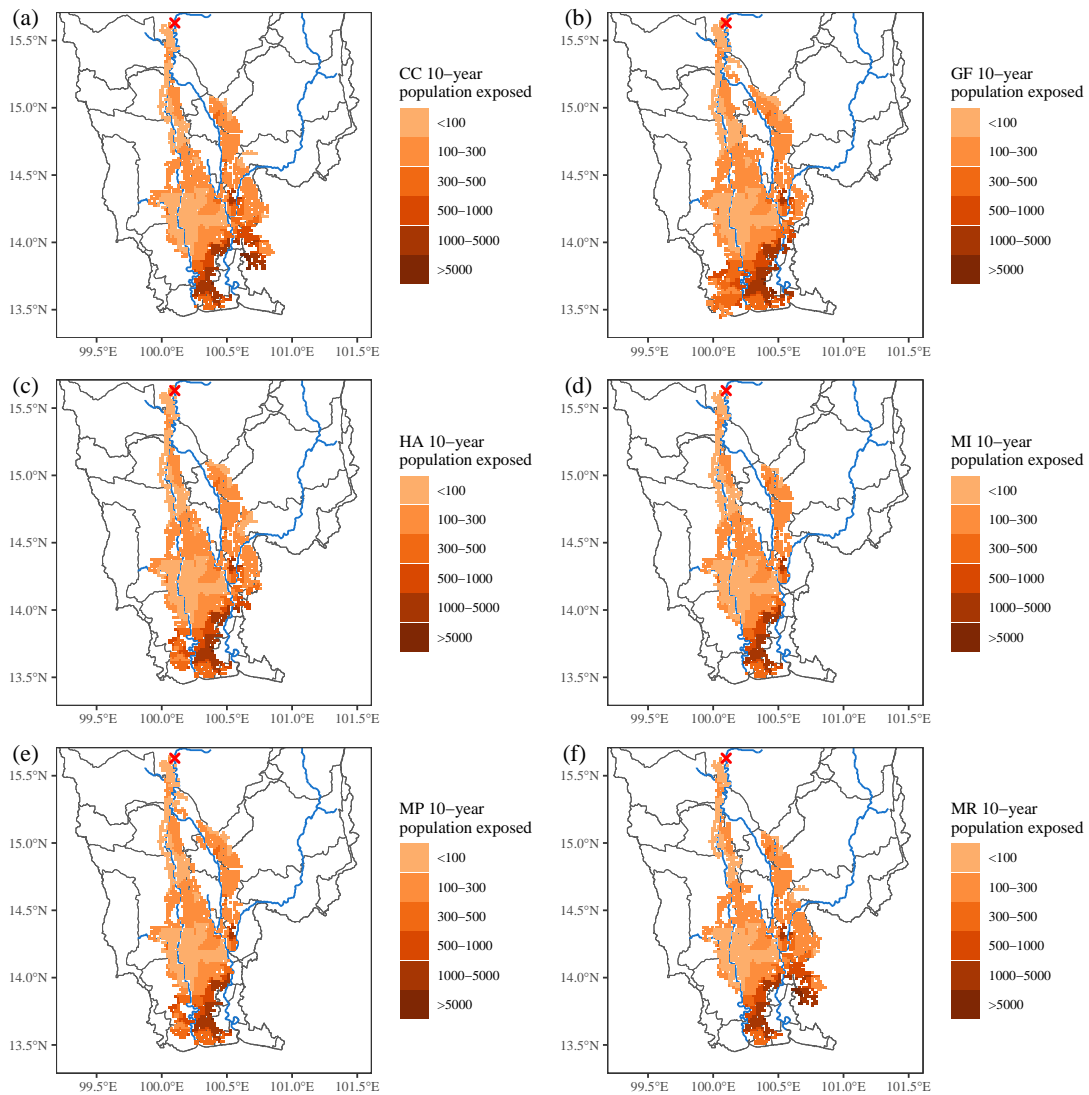


Figure 5.8: Population exposure to future floods for six SST GCMs (a) CC, (b) GF, (c) HA, (d) MI, (e) MP and (f) MR with respect to the d4PDF 10-year return period and depth > 0 m (the color bar represents the population in nos. and the red cross represents the C2 station).

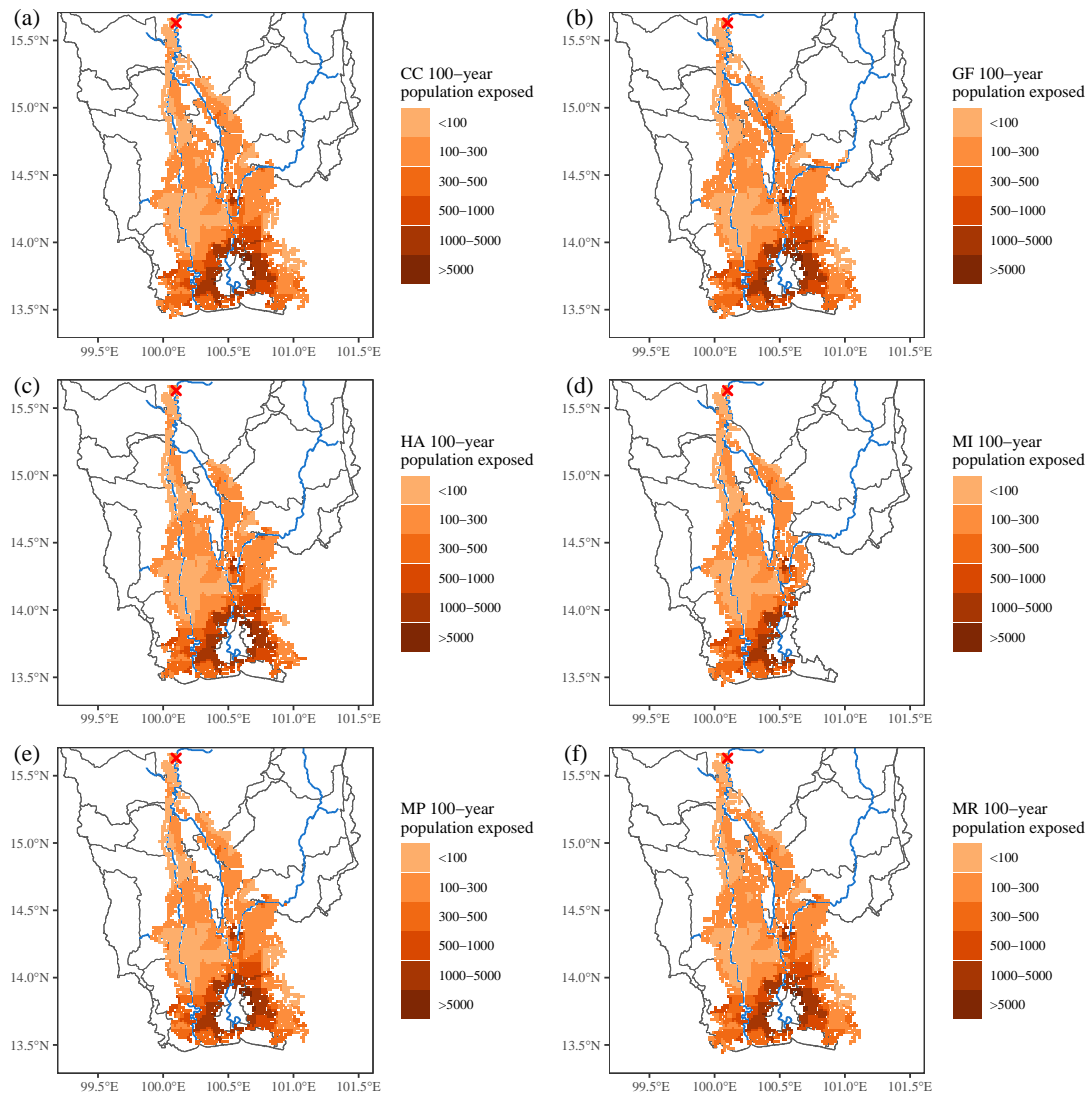


Figure 5.9: Population exposure to future floods for six SST GCMs (a) CC, (b) GF, (c) HA, (d) MI, (e) MP and (f) MR with respect to the d4PDF 100-year return period and depth > 0 m (the color bar represents the population in nos. and the red cross represents the C2 station).

5.5.2 Agricultural exposure assessment

5.5.2.1 2011 agriculture exposure

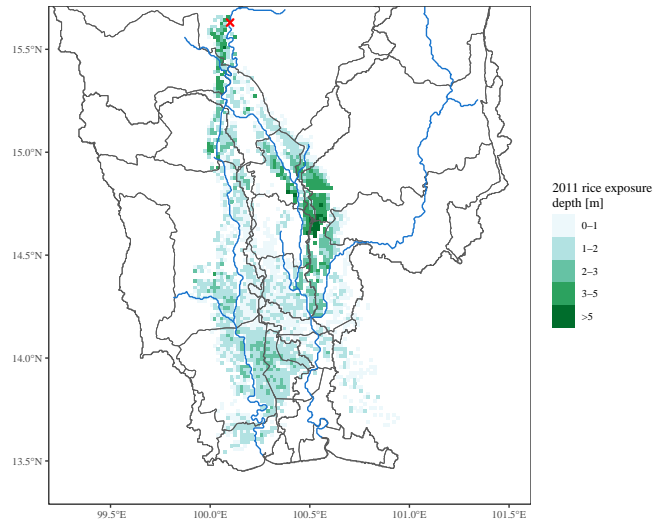


Figure 5.10: Agriculture exposure map of 2011 flood (the red cross represents the C2 station).

Rice has been a major crop in Thailand, providing for the local people as well as exporting internationally. In 2011, rice cultivation faced a huge loss due to the prolonged duration of floods. The exposed duration of the flood in rice cultivation during the 2011 flood was approximately 68 days. As stated above, the rice cultivation area in the region is saturated; hence, for the past and future, we will use the same rice cultivation area as in 2023 for 2011, the past, and 4 degree rise future. Fig. 5.10 shows the exposed rice cultivation area for the year 2011. The exposed area is 4879 km² for a depth greater than 0.5 m.

5.5.2.2 d4PDF past and future agriculture exposure

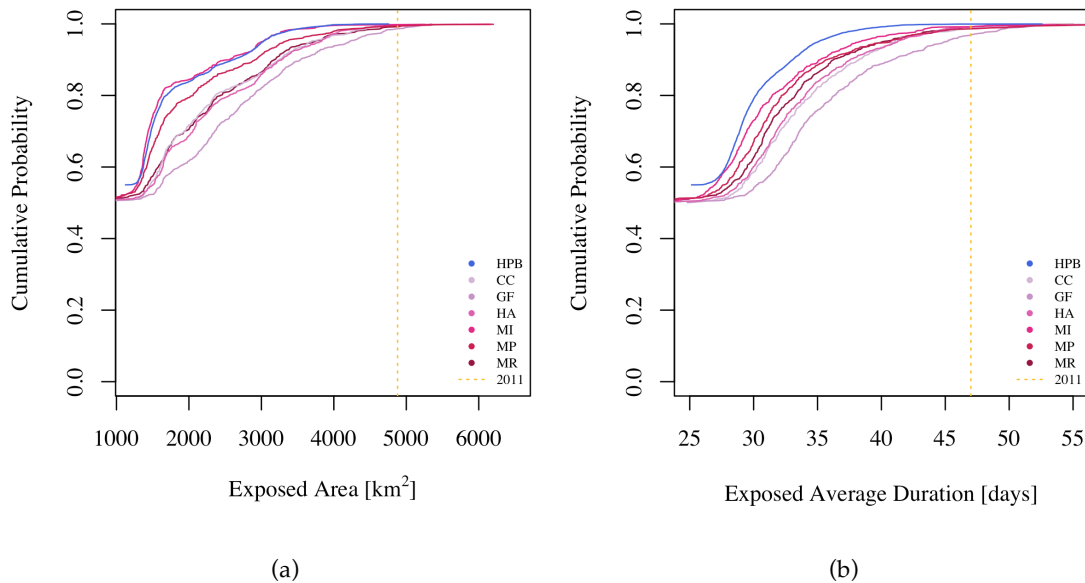


Figure 5.11: Cumulative frequency distribution plots for d4PDF past and future climate with respect to the (a) exposed area and (b) average duration.

After the 2011 exposure assessment to rice cultivation, d4PDF past and future assessments are carried out in this study for depth greater than 0.5 m with the inundation simulation results and rice cultivation area in the region. The inundation simulation results are taken from Budhathoki *et al.* (2023) and the rice cultivation data is taken from GISTDA as mentioned in Section 5.3. As shown in Table 5.3 and Fig. 5.11, GF has the highest increase in rice exposure, while the MI shows similarity to past climate. Fig. 5.11 (a) clearly illustrates that for the same cumulative probability, future rice exposure is likely to be greater. This could severely affect the rice-dependent regions, as Thailand is one of the major rice-exporting countries. It is interesting to note that the 2011 simulated rice exposure is higher than the past d4PDF case, which states that 2011 was one of the worst hits in terms of rice exposed area in the past few decades. Fig. 5.11 (b) also clearly shows that even by a few days, for the same cumulative probability, the future exposed average duration is likely to be more than the past climate. The increase in exposed duration increases with the increase in the return period. It is interesting to note that even though MI is similar to the past climate in terms of flood area (also peak discharge or flood volume in Chapter 3), duration in MI is longer than

that in the past climate. This is also common with Section 3.6 flood duration analysis.

Table 5.3: Changes in future agriculture exposed rice area and average duration with respect to past climate. The past column show the absolute values (in sq. km. and no. of days, respectively) and the columns for the six GCMs show the change factor.

Return Period [years]	Past	CC	GF	HA	MI	MP	MR
Change in exposed rice area							
5	1684.0	1.4	1.7	1.5	1.0	1.2	1.4
10	2613.4	1.2	1.4	1.3	1.0	1.1	1.2
50	3363.7	1.3	1.4	1.2	1.0	1.2	1.3
100	3638.2	1.2	1.4	1.2	1.0	1.2	1.3
Change in exposed average duration							
5	30.2	1.1	1.2	1.1	1.0	1.1	1.1
10	33.1	1.2	1.2	1.1	1.1	1.1	1.1
50	37.7	1.2	1.3	1.2	1.1	1.2	1.2
100	39.6	1.2	1.3	1.2	1.1	1.3	1.2

The d4PDF past climate rice exposure area is 1684 km², 2613 km², 3363 km², and 3638 km² for the 5-year, 10-year, 50-year, and 100-year return periods, respectively. Table 5.3 shows the change in rice exposure for high and low-frequency flooding events with respect to the past climate for depths greater than 0.5 m. Almost all the cases of SST GCMs show an increase in rice exposure. Results show that rice exposure is likely to increase 1-1.7 times and 1-1.4 times in the future climate compared with the past climate for high- and low-frequency, respectively. On average, even though there are fewer exposed areas, higher increases are likely to be expected for the high-frequency events than the low-frequency events.

Moreover, in addition to evaluating the rice-exposed area, this chapter also assesses the average duration of the rice exposure. As shown in Table 5.3, with respect to the past climate, the average exposed duration is likely to increase in the future. The exposed average duration for rice is expected to increase about 1-1.2 times and 1.1-1.3 times the past climate for the high and low-frequency events, respectively. The future expansion of rice cultivation in the area will surpass the average duration of exposure. This might be attributed to the proximity of the rice fields to the river channel, which accelerates the drainage of water through the river, leading to this outcome.

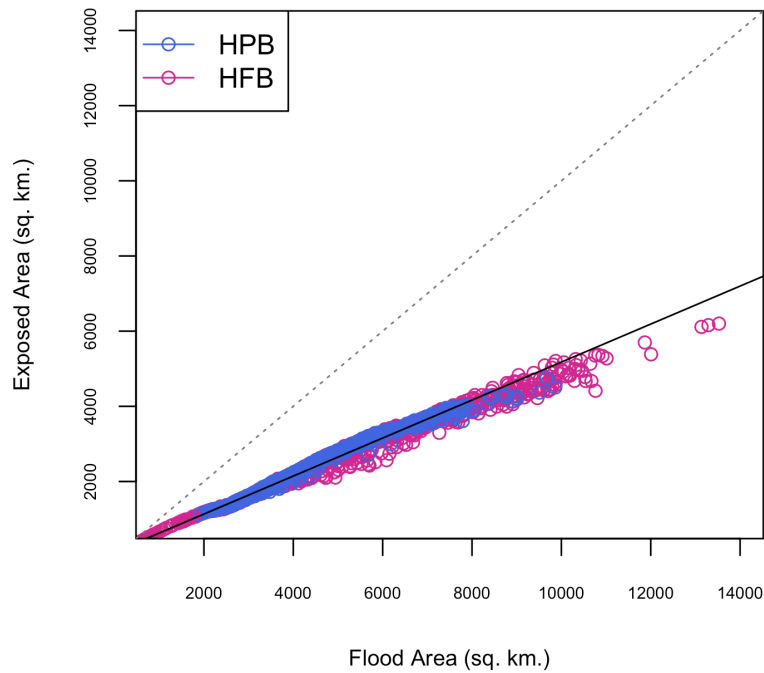


Figure 5.12: Comparison between inundation area and rice exposed area for past (HPB) and future (HFB) climates (all six SST GCMs for the future climate experiment).

The relationship of d4PDF past/future exposed area and inundation area is plotted in Fig. 5.12 to explore how flood area is translated into rice exposure area. The blue color (HPB) indicates the past climate whereas the red color (HFB) indicates the future climate of all six SST GCMs. Obviously, the rice-exposed area is less than the inundation area. Furthermore, both past and future climate experiments have a similar linear relationship. Consistent relations between past and future climates imply that exposed areas simply increase as flood areas expand in the LCPRB.

5.5. Results and discussion

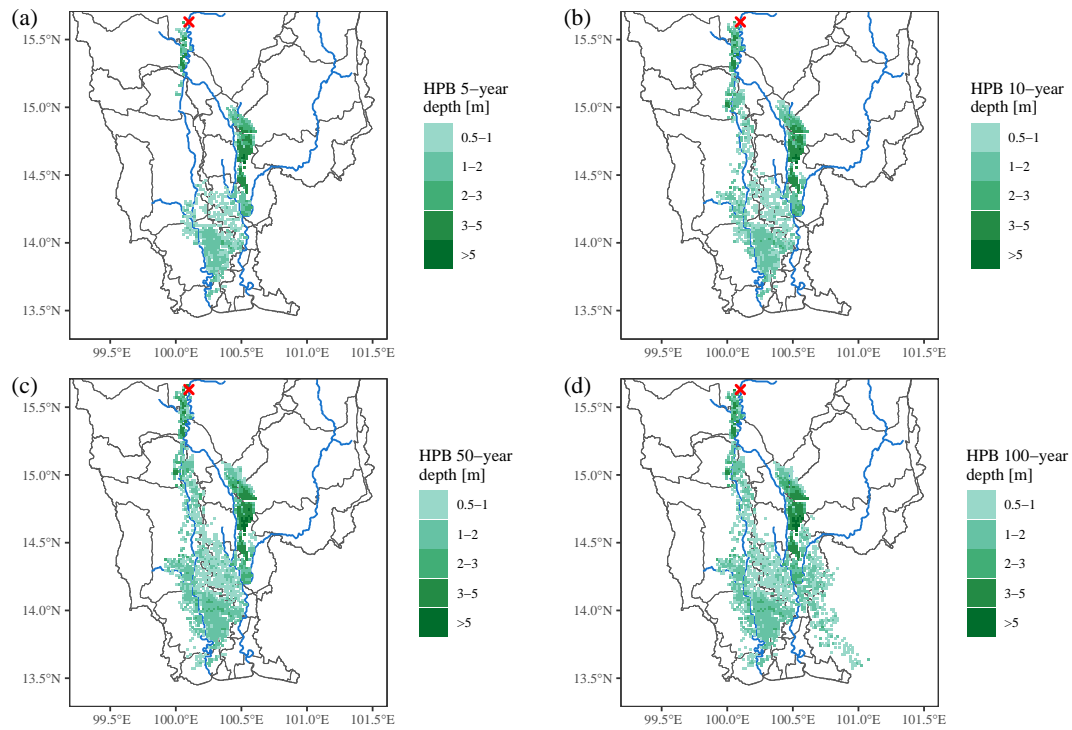


Figure 5.13: Rice exposure to past floods for the d4PDF (a) 5-year, (b) 10-year, (c) 50-year and (d) 100-year return period with respect to depth > 0.5 m (the color bar represents the exposed inundation depth in meters and the red cross represents the C2 station).

Fig. 5.13 illustrates the d4PDF past inundation for high-frequency return periods ((a) 5-year and (b) 10-year) and low-frequency return periods ((c) 50-year and (d) 100-year). The d4PDF future rice exposure for six different SST GCMs is shown in Fig. 5.14 (a-f) for the 10-year return period and Fig. 5.15 (a-f) for the 100-year return period. As expected, the exposed area increases with the return period. The 5-year and 50-year exposure maps are shown in Fig. A.5 (a-f) and Fig. A.6 (a-f), respectively. It clearly shows that the future exposure to rice cultivation areas is going to be greater. In addition, with the increase in the return period, the exposed area is also increasing, affecting a large rice cultivation area.

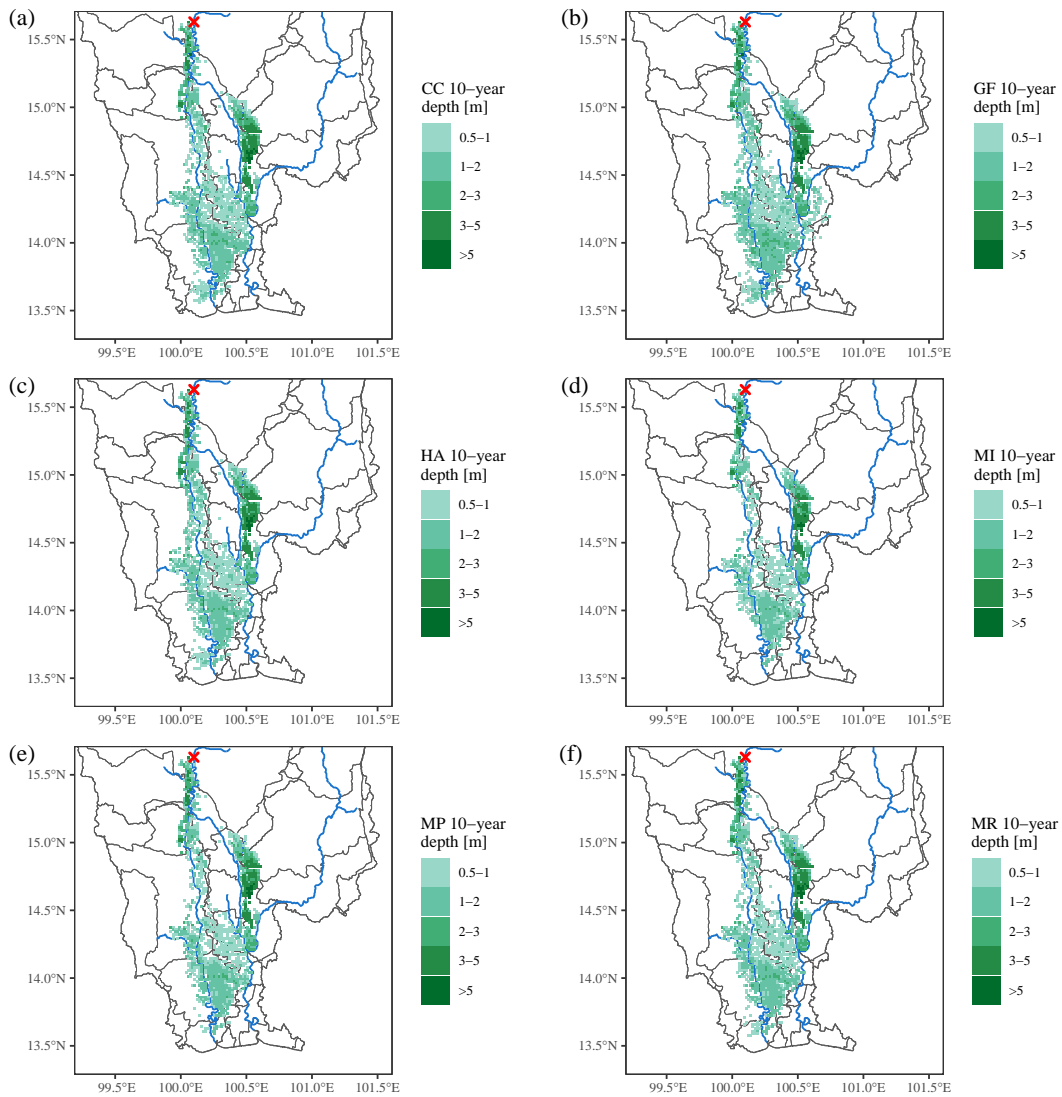


Figure 5.14: Rice exposure to future floods for six SST GCMs (a) CC, (b) GF, (c) HA, (d) MI, (e) MP and (f) MR with respect to the d4PDF 10-year return period and depth > 0.5 m (the color bar represents the exposed inundation depth in meters and the red cross represents the C2 station).

5.5. Results and discussion

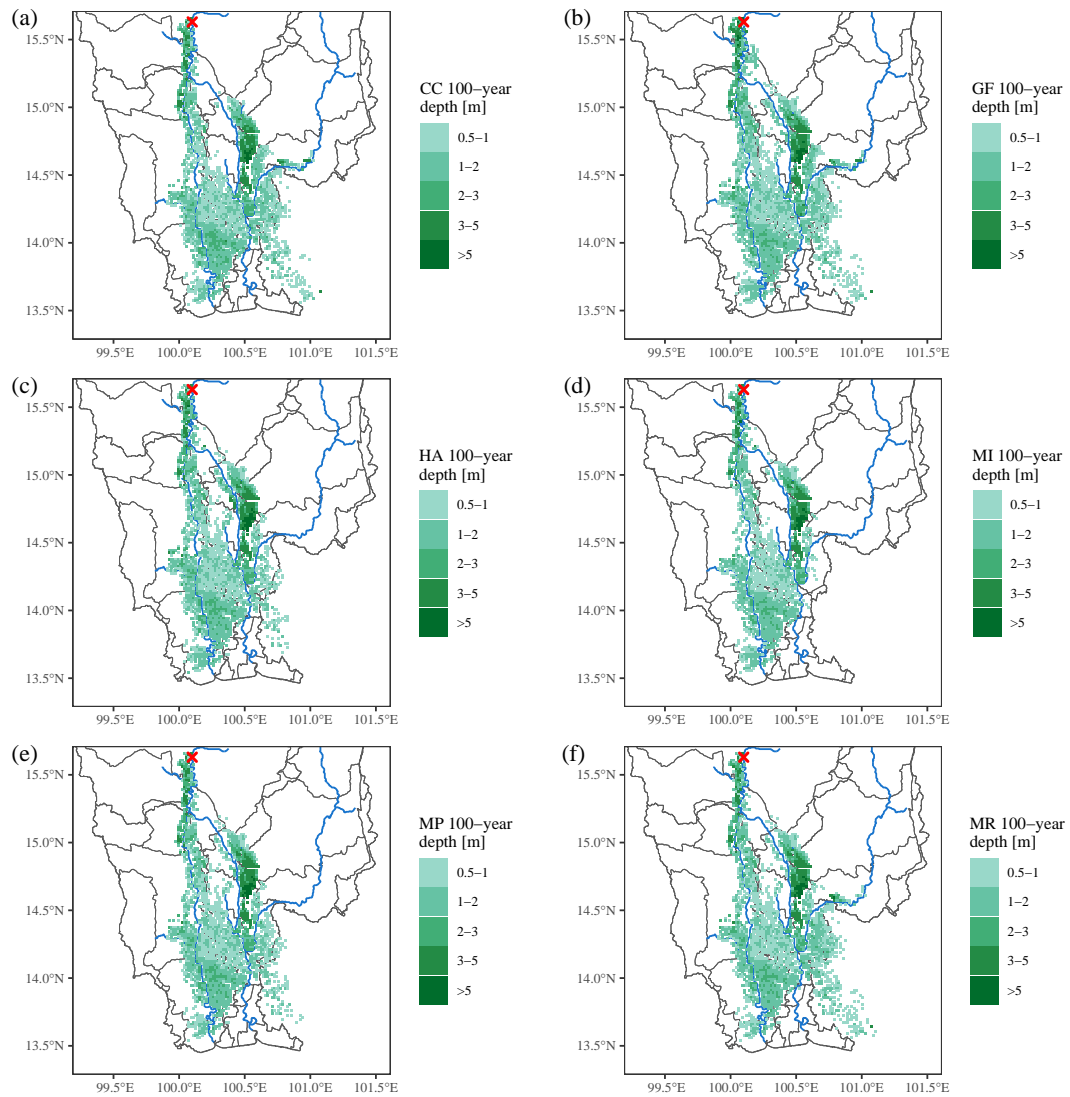


Figure 5.15: Rice exposure to future floods for six SST GCMs (a) CC, (b) GF, (c) HA, (d) MI, (e) MP and (f) MR with respect to the d4PDF 100-year return period and depth > 0.5 m (the color bar represents the exposed inundation depth in meters and the red cross represents the C2 station).

A study in the Philippines also highlights that the decrease in crop exposure leading to decreased crop production is mainly due to the enlarged inundation area along with the submergence period. This could also be a reason for future decreases in the land that is available for irrigated lowland crop varieties (Wang *et al.*, 2022). Another study with a similar climate in the Mekong River Basin also states that almost 39% of the rice farming land is in threat, especially 24% of the rice area, which is exposed to sustained floods lasting more than 3 months (Wassmann *et al.*, 2019). Shrestha *et al.* (2019) also

states that floods occur almost every year in LCPRB, affecting large crop areas, and hence flood risk assessment in agriculture areas is critical in this basin for planning and implementing mitigation measures and preparedness efforts to avoid future flood damage to crops.

5.6 Conclusions

The LCPRB inhabits a large population and is part of the rice bowl of Thailand. Due to several opportunities, a lot of people reside in the capital city and its surrounding provinces. This chapter analyzes the impact on the population by combining climate projections with population projections. This chapter incorporates the impact on agriculture, particularly rice coupling, with its cultivation area and climate projections.

Future low-frequency events such as 50-year and 100-year flooding for +4K rise are likely to be more severe in terms of exposed area and duration compared to the past climate. The exposed population in the future is likely to decrease 0.7–0.9 times as much as the past climate across all return periods and SST GCMs for depths greater than 0 m. Similar results are expected for depths greater than 0 m and for depths greater than 0.45 m and 3 m. However, the analysis conducted by keeping the population change constant in the future suggests that the flood exposure is likely to increase by 1.2 times for high-frequency and 1.5 times for low-frequency floods on average for depths greater than 0 m. This states that the climate change impact is significant in the basin as is the demographic change. Due to the decrease in projected population towards the year 2100, the climate change impact nullifies with population exposure. The overall analysis of this study indicates that higher return period events are expected to affect more people than lower return period events, even if combined effects of climate change and population loss will not increase overall population exposure.

The low- and high-frequency event analysis for the rice exposure is carried out in this study, and the results clearly show the increase in rice exposure area in the future with respect to past climate. On average, rice exposure is expected to increase 1.3 times for high-frequent events and 1.2 times for low-frequent events in terms of exposed areas for six SST GCMs. On the other hand, the exposed average duration for rice is expected to increase 1.1 times and 1.2 times in the future with respect to high- and low-frequency events, respectively. The increase in exposed rice area in the future is higher than the

exposed average duration. This could be because the rice area is near the river channel, causing the water to drain through the river channel faster.

This states that the future exposure for population is likely to decrease with the trend in decreasing population. However, keeping the constant population as past climate and constant rice cultivation area, the exposure is likely to increase in the future, causing suffering and higher losses to the local people. Therefore, actions are required in terms of structural and non-structural measures for better adaptation and mitigation approaches to support the inhabitants by the respective agencies and ministries. In addition, there is uncertainty in hazard models, which is brought on mainly by an incomplete representation of complicated local drainage networks, which limits evaluations of flood exposure. Population data may also be uncertain due to the use of a global data set. In addition, the effect on rice cultivation is also likely to worsen affecting the local as well as global rice-dependent nations.

Chapter 6

Agricultural damage assessment in the LCPRB

This chapter aims to assess the economic damage to agriculture production in the LCPRB and to develop a flood risk curve for an agricultural crop. Rice is used as the major agricultural crop in the LCPRB, therefore, its economic damage based on flood depth and duration is evaluated in the region. The whole CPRB is considered a rice bowl of Thailand, and the LCPRB also consists of a significant amount of rice cultivation land. In the LCPRB, flooding due to climate change has a large impact on rice cultivation, leading to decreased yield and production for the local people as well as exports. This reduction has severe monetary damage, which ultimately impacts the GDP of the nation. For the 2011 flooding, the simulated results show economic damage of 11.25 billion THB for rice cultivation in the LCPRB. Future damage will likely increase by 1.2–1.4 times the past climate. Future results for extremely low-frequency events show higher damage than the 2011 flooding, where the 2011 flooding is likely to be one of the most extreme cases in terms of damage with respect to the past climate.

6.1 Introduction

Globally, the effects of climate change have gradually increased in recent years, increasing the intensity and frequency of severe events (Abeysekara *et al.*, 2023). Droughts, floods, heat waves, and other catastrophic natural catastrophes might occur if components causing climate change are not quickly eliminated. Flood events, in particular, have continued to wreak devastation in many regions and countries (Adelodun *et al.*, 2023). Furthermore, the agricultural sector has been severely impacted by flooding brought on by climate change, and this situation is only predicted to get worse in the future. The prevalence and severity of flood catastrophes have increased in recent decades, particularly in South and Southeast Asia, and are expected to increase further in the next few decades (Ahmad *et al.*, 2023). Natural resource-based developing nations are more likely to be hit hard by climate change-induced flooding in agriculture than more prosperous nations. To begin with, agriculture is the primary source of income for a larger proportion of people residing in developing countries. Secondly, the agricultural sector is the backbone of many developing countries' economies, and thirdly, these countries have less adaptive capacity to cope with the effects of climate change than the developed nations (Abeysekara *et al.*, 2023; Ahmad *et al.*, 2023). Crop yield and production have pounding repercussions due to the increase in depth and duration of floods, which is the resulting effect of climate change.

Southeast Asia has been locally consuming a decent amount of rice and contributing to 40% of global rice exports for the past 50 years (Yuan *et al.*, 2022). Additionally, studies report that climate change susceptibility is causing a 10% decline in grain yields, particularly in Southeast Asia (Eka Suranny *et al.*, 2022), whereas globally, rice demand is increasing by 30% (Yuan *et al.*, 2022). Hence, there is a major question about Southeast Asia continuing to be a major rice exporter amidst the changing climate, stagnant yields, and saturated cultivation land. To reduce future flood damage to agriculture, a quantitative estimate of economic damage and risk under climate change is highly needed.

Thailand's economy remains greatly dependent on agriculture, particularly for jobs in the area, despite the country having achieved great progress in recent years (Tingting and Chuang, 2010). The LCPRB is an important region - a considerable number of people reside here as it is home to a number of significant industries and large agricultural areas, including the capital city Bangkok. It also includes the Chao Phraya Delta,

which is regarded as one of the world's principal rice-exporting areas (Kotera *et al.*, 2016).

Therefore, this chapter aims to achieve a probabilistic assessment of economic damage to agriculture production due to floods in the LCPRB. Rice has been an important plantation in the LCPRB, and with the limited availability of data, this study is carried out using only rice cultivation data. An in-depth study of probabilistic return periods along with a few low (50-year and 100-year) and high (5-year and 10-year) frequency events particularly to calculate the change and visualize spatial maps have been analyzed for further assessment. In addition to the evaluation of flood inundation, there is a necessity for a thorough flood risk evaluation with the available hazard and vulnerability data. Hence, to address this, this study also identifies the risk curve for rice cultivation due to floods that are affected by climate change. The result of the translation of the inundation assessment (Chapter 4) to the rice exposure assessment (Chapter 5) has been used in this study to identify the rice damage assessment due to climate change impacted floods, including the flood risk curve.

The remainder of this chapter is assembled as follows: The overall framework opted in this chapter is explained in Section 6.1.1. In addition, after the explanation of agricultural data used, particularly for this chapter in Section 6.2, Section 6.3 describes the evaluation criteria used in this study for economic damage assessment. Section 6.4 explains the results of damage assessment validation by comparing them with the 2011 flood damage and its application to assess the probabilistic agricultural economic damage and risk in the LCPRB.

6.1.1 Framework for agricultural economic damage assessment

This section aims to explain the framework for economic damage assessment for agricultural products (i.e., rice). The assessment is carried out for flood levels greater than 0.5 m. The overall methodological framework is shown in Fig. 6.1.



Figure 6.1: Methodological framework opted for the agriculture damage assessment for (a) 2011 flood as model validation and (b) d4PDF past and future climate in the LCPRB.

6.2 Fragility curve, cropping calendar and rice data

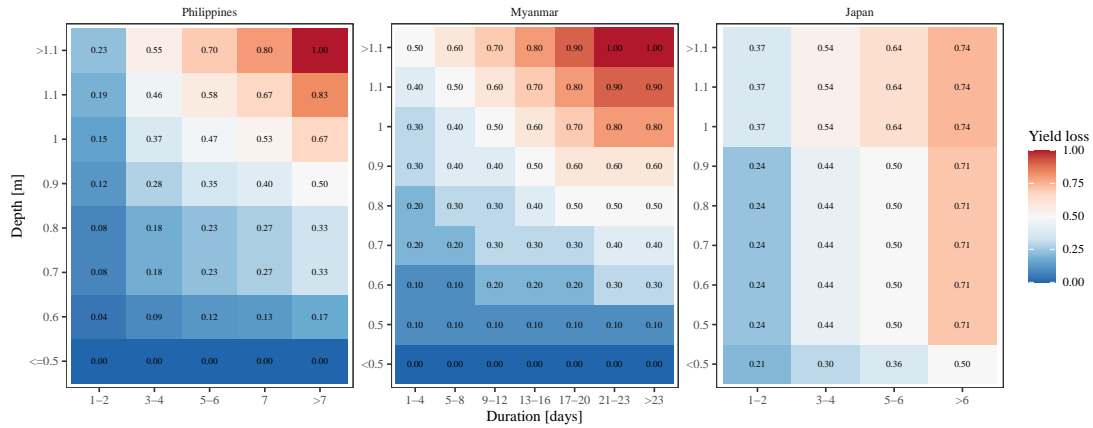


Figure 6.2: Heatmap produced with the fragility curve data for rice growing period in Philippines (values taken from Shrestha *et al.*, 2019), Myanmar (values taken from Shrestha *et al.*, 2021) and Japan (values taken MLIT, 2005).

Firstly, the economic assessment of rice cultivation is carried out based on the rice damage curve from various studies. The estimates are carried out in correspondence with damage as a function of inundation depth and duration. This fragility curve is based on a study of the Philippines, which was also tested in Thailand by Shrestha *et al.* (2019). In addition, this chapter also evaluates agriculture damage based on the fragility curve for Myanmar (Shrestha *et al.*, 2021) and Japan (MLIT, 2005) to ensure an in-depth study based on depth and duration in Thailand using fragility data of different countries. Fig. 6.2 shows the fragility curve for the rice damage at the maturity stage, which is a function of exposed depth and duration based on (a) Philippines, (b) Myanmar, and (c) Japan (MLIT, 2005; Shrestha *et al.*, 2021, 2019). In Fig. 6.2 (a-c), the x-axis shows the duration in days, the y-axis shows the depth in meters and each colored bin represents the yield loss at their respective depth and duration. All three fragility data were tested with the exposure maps for different return periods to calculate the damage in the basin. In addition, Fig. 6.3 shows the modified cropping calendar for Thailand based on recent studies in Thailand (Shrestha *et al.*, 2019; Som-ard *et al.*, 2022). The harvest per unit area in Thailand is 2885 kg/ha, and the farm gate price is 10.18 THB/kg based on SEARCA (2015) and Shrestha *et al.* (2019), respectively.

of the fragility curve.

According to the cropping calendar of Thailand, the rice cultivation months are from May/June to mid-September/November for wet-season rice. The maturing stage of the rice is considered to be from 95 to 135 days from cultivation (Shrestha *et al.*, 2019) until the harvest period. Therefore, utilizing the agricultural calendar and the flood season in Thailand, the evaluation of damage is estimated from the mid-season (September to November) until the harvest season, as shown in Fig. 6.3. The agricultural damage in the 2011 flood is estimated using the fragility curve in the Philippines (Fig. 6.2 (a)) and verified with the results of Shrestha *et al.* (2019), followed by the estimation using the Myanmar (Shrestha *et al.*, 2021) and Japan (MLIT, 2005) fragility values to look into a comprehensive assessment based on various spatial regions. Then the agricultural damage assessment for the d4PDF past and future climate experiments is performed for several return periods using all three fragility curves. The damage maps for 10-year and 100-year return periods are produced in this study based on the Philippines' fragility data. As indicated in Eq. (6.1), this chapter assumes that the farm gate price per harvest P , harvest per area H , and farm area per grid a_i are constants between the past and future climate assessment experiments.

6.4 Results and discussion

This section unravels the agriculture damage assessments for different return periods and depths. The economic damage is analysed for the 2011 flood, d4PDF past and future climate.

6.4.1 2011 agricultural economic damage assessment

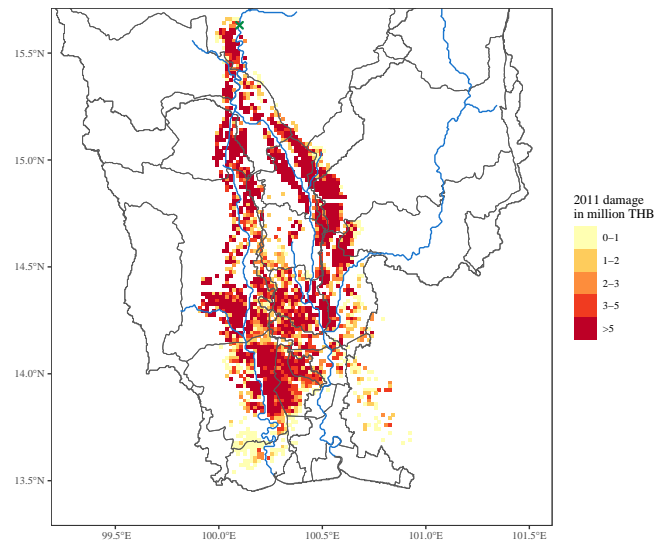


Figure 6.4: Agriculture damage for 2011 flood (the green cross represents the C2 station).

The 2011 rice economic damage is assessed using simulated inundation coupled with the rice cultivation area, which is further converted in terms of loss using the fragility curve for rice crops during the maturity stage. The analysis done for depths greater than 0.5 m shows that the total simulated damage for the whole LCBRB is 10.25 billion THB for rice. The reported damage for the whole CBRB was 26.6 billion THB (Shrestha *et al.*, 2021) in 2011, which is approximately 2.6 times the simulated damage in this study for the LCPRB. Considering only the LCPRB area, this value seems to be justifiable as the LCPRB ($\sim 50,000 \text{ km}^2$) is also 1/3 of the CPRB ($\sim 1,70,000 \text{ km}^2$). For validation, Shrestha *et al.* (2019) also shows that the total rice damage with respect to their simulated results is about 32 billion THB. Fig. 6.4 shows the agricultural damage for rice in the LCPRB based on the inundation simulation results from Chapter 4 and the Philippines fragility curve. In addition, the yield loss for rice is again tested for the other two spatial regions. Using the fragility curve for Myanmar, the 2011 flood damage to agriculture is estimated to be 3.75 billion THB, which is quite low in comparison to the Philippines case. The fragility curve information for Myanmar based on Shrestha *et al.* (2021) mentions this could be due to the wind effect of the typhoons. However, similar to the damage estimation based on the Philippines, Japan also shows

a reasonable damage estimation, which is approximately 10.20 billion THB.

It is also worth noting that the flood depth in the southwest region is shallower than the northeast region in general for the 2011 exposure assessment (Fig. 5.10), while the damage is similar (Fig. 6.4). This may be due to the longer flood duration in both regions.

6.4.2 d4PDF past and future agricultural economic damage assessment

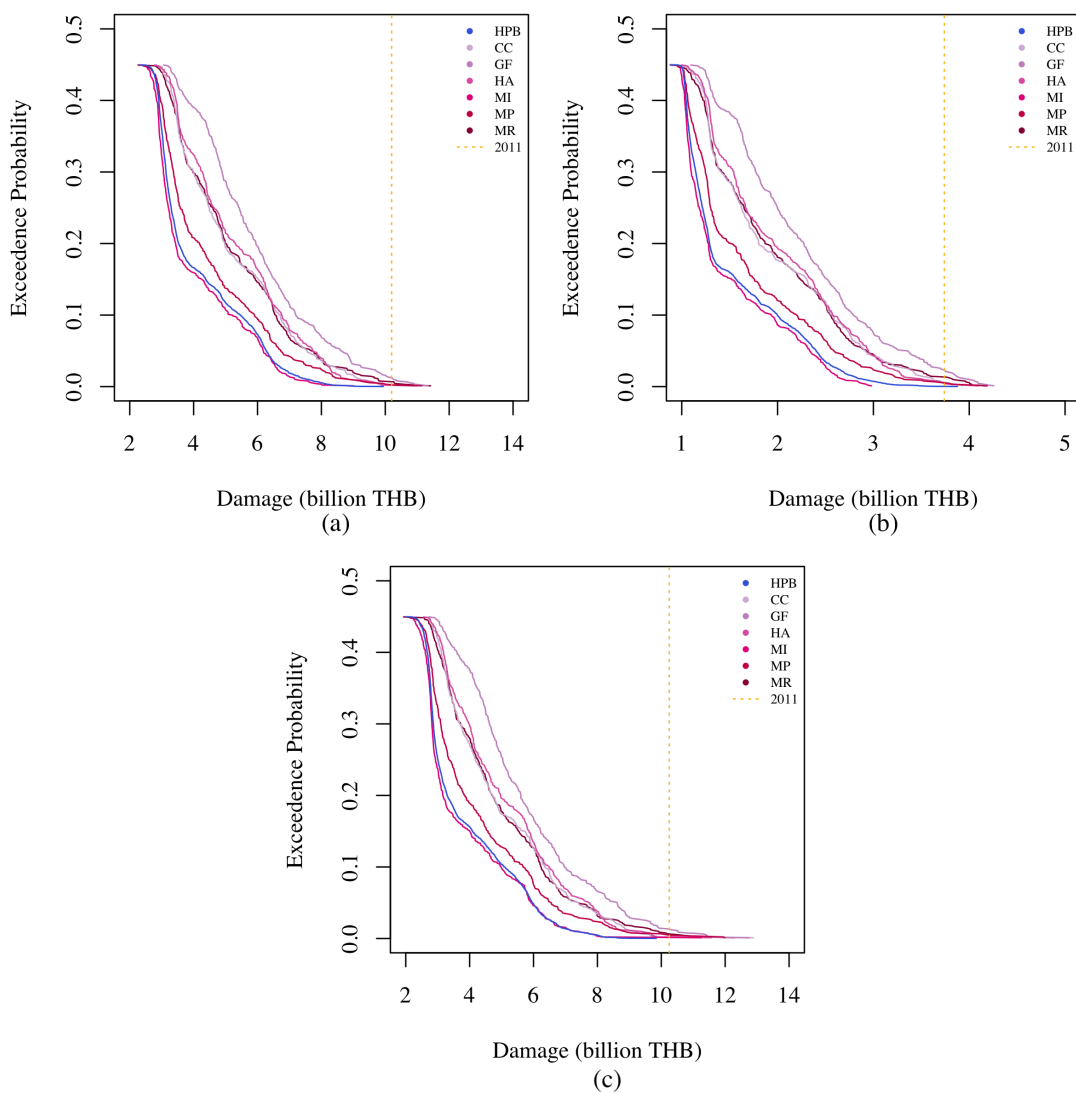


Figure 6.5: Flood risk curve for agriculture damage based on fragility curve for (a) Philippines, (b) Myanmar and (c) Japan.

After the validation of the 2011 rice damage assessment, d4PDF past and future damage was evaluated for flood depth greater than 0.5 m in the LCPRB. Rice damage is likely to increase by about 1-1.7 to 1-1.5 times than the past for high- and low-frequency events, respectively, across all six SST GCMs based on the Philippines fragility curve. For all three spatially different yield loss values, on average, both high and low frequencies are likely to increase by about 1.3 times the past climate, which is huge in terms of monetary value. Similar to the exposure assessment for rice, GF shows the highest increase in economic damage, while MI shows a similar trend to the past climate. The rest of the GCMs lie between MI and GF, as shown in Fig. 6.5. In addition, as mentioned in Chapter 5 the duration in MI is longer than in the past climate; however, the resulting damage is similar to the past climate. This result is because not only is the flood duration crucial but flood area and depth are also important factors. In this case, it is worth noting that flood extent and depth play a significant role in damage estimation.

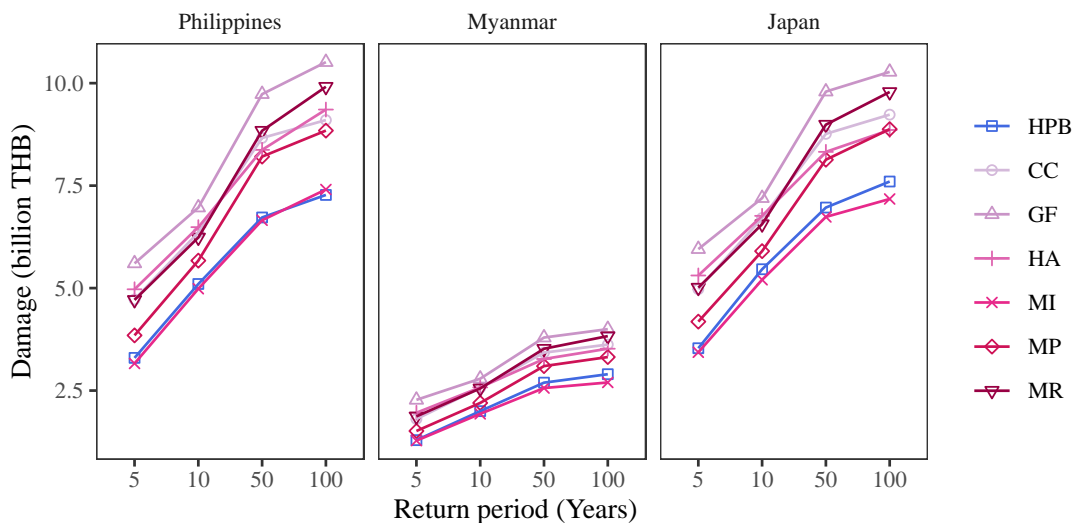


Figure 6.6: Agricultural damage based on three spatial regions (Philippines, Myanmar and Japan) with respect to four return periods (5-year, 10-year, 50-year and 100-year).

Fig. 6.6 and Table 6.1 show the change in damage for d4PDF future climates with respect to the past climate for different high- and low-frequency return periods and different fragility curves based on region. In the 5-year and 10-year return periods, damage shows approximately 3.3 and 5.1 billion THB (Philippines fragility curve), 1.3 and 2 billion THB (Myanmar fragility curve), and 3.5 and 5.5 billion THB (Japan fragility

curve), respectively. Whereas for 50-year and 100-year return periods, as expected, the damage shows a higher value of approximately 6.7 and 7.3 billion THB (Philippines fragility curve), 2.7 and 2.9 billion THB (Myanmar fragility curve), and 7 and 7.6 billion THB (Japan fragility curve), respectively. However, it is interesting to note that even though the damage amount for Myanmar is different than the other two similar (Philippines and Japan) cases, the change in damage is similar. For both high and low frequencies, it is evident that the increase in damage with consideration of climate change scenarios is likely to be between 20 and 30% for the Philippines, Myanmar, and Japan cases.

Table 6.1: Past and future changes in agriculture economic damage based on three fragility curves of the Philippines, Myanmar and Japan. The past columns show the absolute values (billion THB) and the columns for the six GCMs show the change factor.

Fragility Curve	Return Period [years]	Past [Billion THB]	Change in agriculture economic damage					
			CC	GF	HA	MI	MP	MR
Philippines	5	3.3	1.4	1.7	1.5	1.0	1.2	1.4
	10	5.1	1.2	1.4	1.3	1.0	1.1	1.2
	50	6.7	1.3	1.5	1.2	1.0	1.2	1.3
	100	7.3	1.2	1.4	1.3	1.0	1.2	1.4
Myanmar	5	1.3	1.4	1.7	1.5	1.0	1.2	1.4
	10	2.0	1.3	1.4	1.3	1.0	1.1	1.3
	50	2.7	1.3	1.4	1.2	0.9	1.1	1.3
	100	2.9	1.2	1.4	1.2	0.9	1.1	1.3
Japan	5	3.5	1.4	1.7	1.5	1.0	1.2	1.4
	10	5.5	1.2	1.3	1.2	0.9	1.1	1.2
	50	7.0	1.3	1.4	1.2	1.0	1.2	1.3
	100	7.6	1.2	1.4	1.2	0.9	1.2	1.3

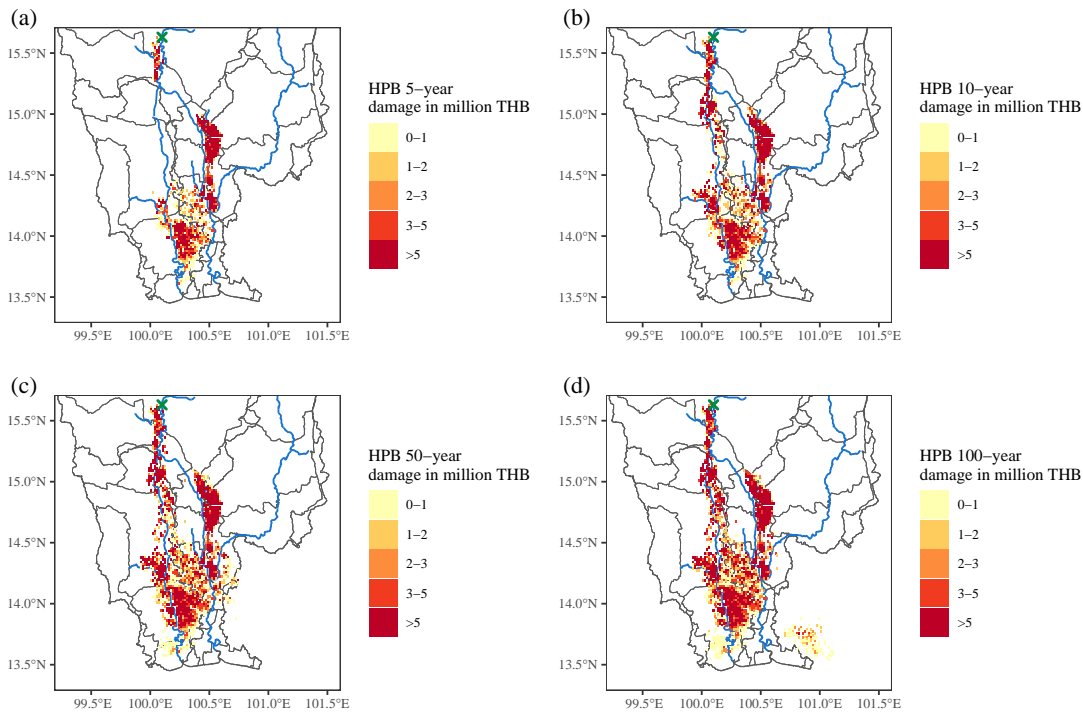


Figure 6.7: Past agriculture damage for the d4PDF (a) 5-year, (b) 10-year, (c) 50-year and (d) 100-year return period with respect to depth > 0 m (the color bar represents the economic damage in million THB and the red cross represents the C2 station).

The past economic damage maps for different return periods (5-year, 10-year, 50-year, and 100-year) are shown in Fig. 6.7 based on the Philippines fragility curve. In the future climate, the southern area will experience extended damage area for some SST ensembles. As expected, the damage amount is increasing with respect to the increase in the return period. This states that the increase in depth and duration affects the damage to the rice crops. The d4PDF results for the future high-frequency 10-year event and low-frequency 100-year event are shown in Fig. 6.8 (a-f) and Fig. 6.9 (a-f), respectively, based on the Philippines fragility curve. The damage maps for rice for 5-year and 50-year are shown in Fig. A.7 (a-f) and Fig. A.8 (a-f), respectively, based on the Philippines fragility curve. As expected, the damage amount increases with respect to the increase in the return period. This states that the increase in depth and duration affects the damage to the rice crops. It is evident that not only is the damage amount more for the higher return periods, but just like the exposure the affected area is also high.

6.4. Results and discussion

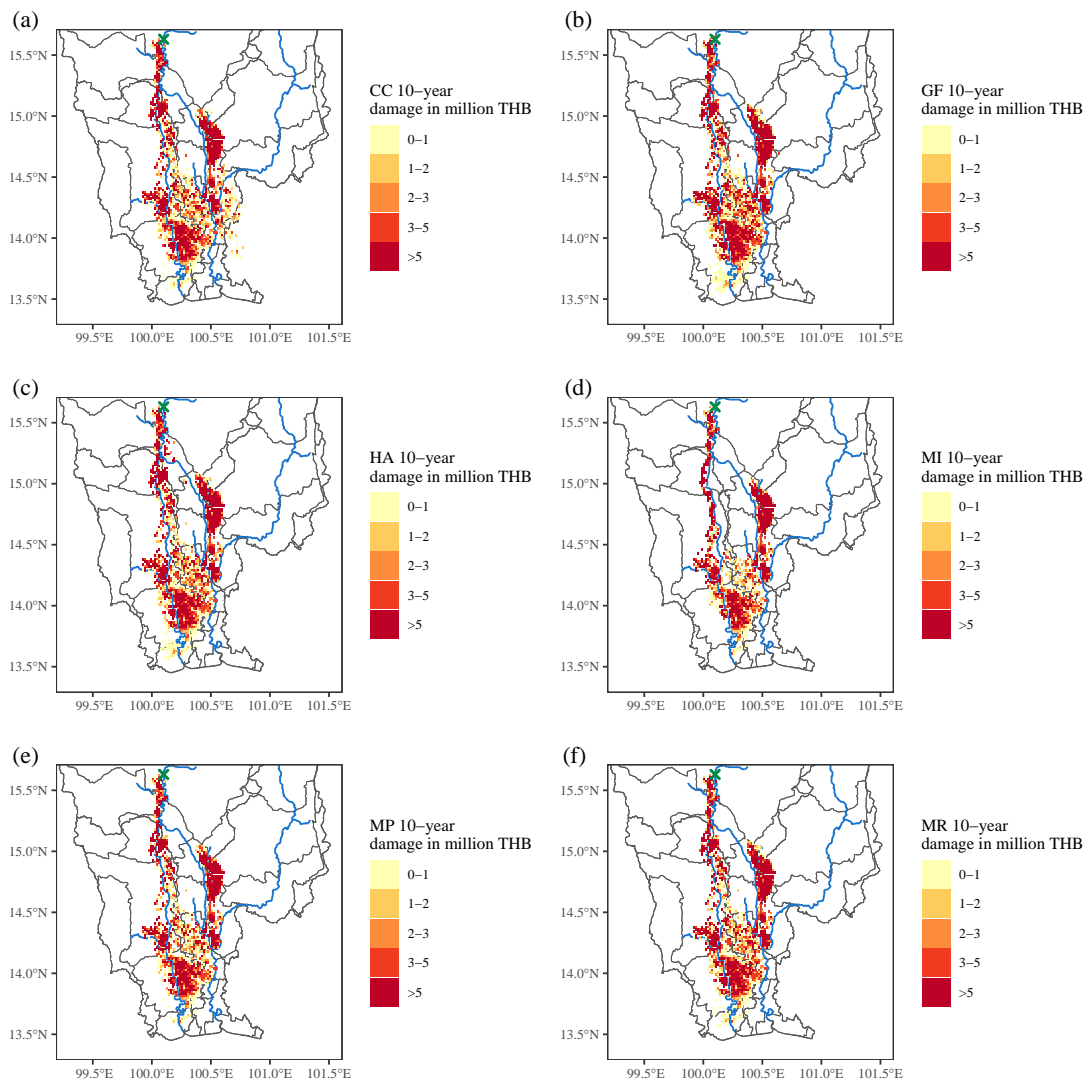


Figure 6.8: Future agriculture damage for six SST GCMs (a) CC, (b) GF, (c) HA, (d) MI, (e) MP and (f) MR with respect to the d4PDF 10-year return period and depth > 0.5 m (the color bar represents the economic damage in million THB and the red cross represents the C2 station).

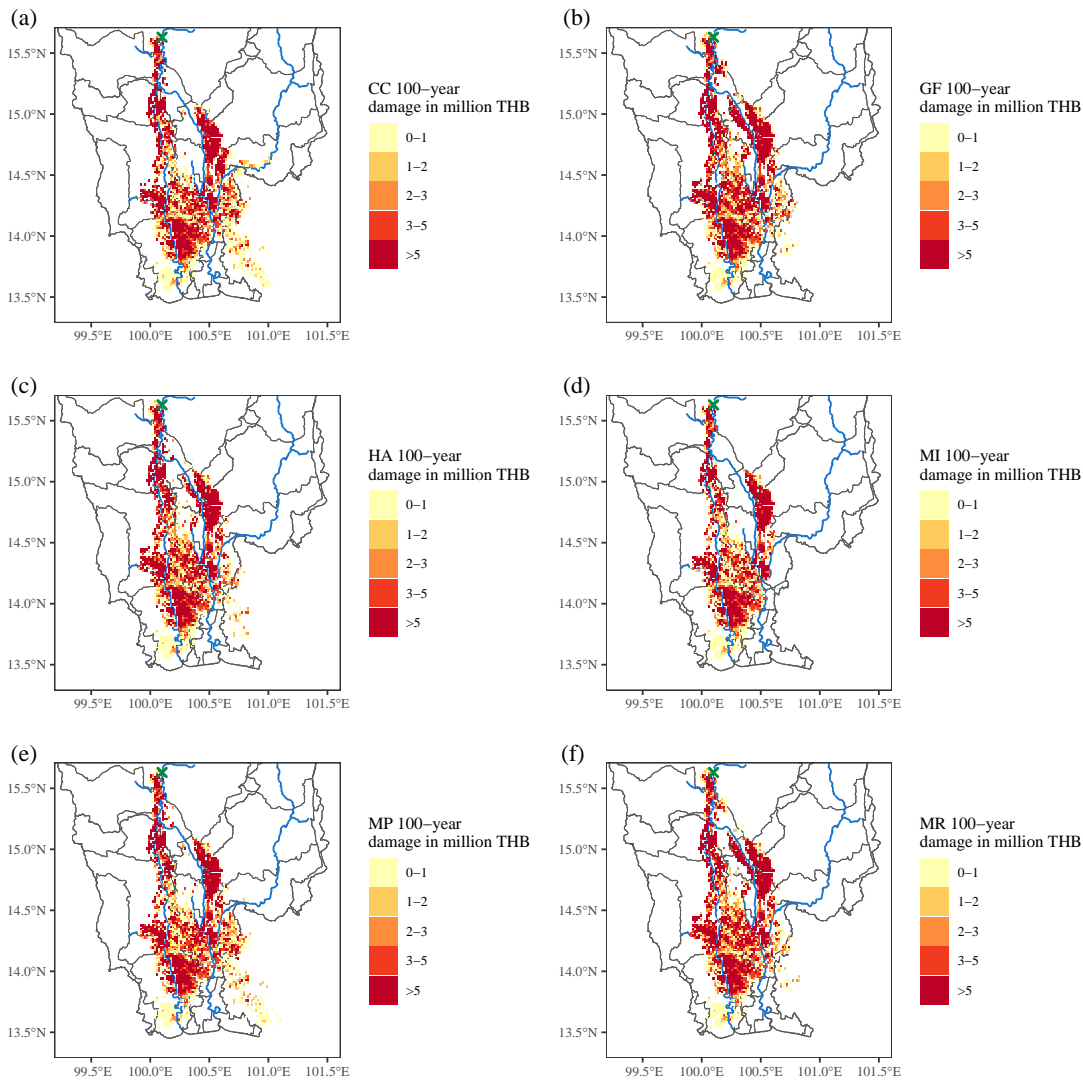


Figure 6.9: Future agriculture damage for six SST GCMs (a) CC, (b) GF, (c) HA, (d) MI, (e) MP and (f) MR with respect to the d4PDF 100-year return period and depth > 0.5 m (the color bar represents the economic damage in million THB and the red cross represents the C2 station).

Similar results in the future climate can be observed in the study by Shrestha *et al.* (2019), which shows that an increase in agricultural damage area by 13% is expected for the whole CPRB for a 100-year return period event. Another study using the d4PDF dataset for the Cambodian floodplain of the Lower Mekong River Basin shows that agricultural damage from extreme flood occurrences with 10-year, 50-year, and 100-year return periods would rise by 32%, 38%, and 39% in the 4K rising scenario (Try *et al.*, 2023). This states that the influence of climate change is likely to be higher for

rice crops for all the low- and high-frequency events in LCPRB and the neighboring regions.

6.5 Conclusions

To plan future development in basins that are prone to flooding, such as LCPRB, it is crucial to identify high-risk areas based on an evaluation of flood damage. Therefore, this chapter assessed the possible effects of future climate change on agriculture, flood risks, and agricultural losses in the LCPRB. This chapter assessed agricultural damage in the LCPRB by utilizing fragility data from the Philippines, Myanmar, and Japan. The goal is to conduct a resilient analysis that considers factors such as yield loss, depth and duration of floods, etc. This approach contributes to a more holistic understanding of the fragility curves of three different spatial regions.

To produce flood risk curves for rice cultivation, this study used large ensemble climate data from the d4PDF dataset. Data on past climate flood risks, damage, and their linkages are important for validating and then identifying future flood risks in economically important areas. The estimated damage from flood occurrences was compared with reported data as well as other studies in the basin in order to verify a flood damage assessment approach. The results show that 2011 flood damage is likely to surpass the d4PDF past climate data. This could be due to higher flood depth and duration in 2011 causing higher damage. On average, agricultural economic damage is likely to increase by 20-30% for both high- and low-frequency flooding events and across fragility data for three spatial regions. The findings indicate that future major flood occurrences will have greater potential damage and magnitude due to the effects of climate change. The extreme flooding events are likely to affect rice cultivation and cause a significant amount of loss in the basin. The three fragility curves employed resulted in largely different estimates as absolute values, while the future change ratio concluded above was consistent over the variability of the fragility curve, implying that climate change signal in the 4-degree warmer world in terms of flood hazard magnification is beyond the uncertainties of rice vulnerability assessment in the LCRB.

Flood mitigation strategies for climate change adaptation may be implemented with the help of the flood damage assessment results of this chapter. In order to reduce the potential damage in the future, further studies on the inclusion of dams in the

basin can be explored for future research. This could lead to a reduction in agricultural damage, particularly rice in the basin. In addition, landuse/cover and other social changes were not incorporated in this chapter, which can also be considered for other future assessments.

Chapter 7

Conclusions

The Chao Phraya River Basin (CPRB) in Thailand is Southeast Asia's heartland and is highly susceptible to climate change impact. This is due to the amplified flooding, especially in the delta of the river basin. However, due to the vast catchment area, diverse climatic conditions, varied terrain, and human interventions due to the construction of dams, there lies a challenge to conduct risk assessments. This complex situation makes it difficult to create precise climate simulations, and model hydrology of the basin accurately. The large ensemble d4PDF dataset, which spans 6000-years of past and 5400-years of future climate (6 Sea Surface Temperature (SST) Global Climate Models (GCMs) with 90 ensembles), is recently gaining popularity in the Southeastern region as it addresses some of the challenges in climate risk assessments. However, bias correction of various hydrological variables such as unmonitored runoff or discharge remains a challenging issue. Therefore, this study makes use of the d4PDF dataset and tries to address the discharge bias correction issue to carry out the climate change risk assessment in the CPRB under the +4K warming scenario in global mean temperature by the late 21st century.

The focus of Chapter 3 is on exploring methods to remove the spatial biases in streamflow within the d4PDF dataset and then understanding its potential implications on future flooding due to the effect of climate change. Therefore, this Chapter 3 utilized d4PDF runoff data, translating it into streamflow in the CPRB using the 1-km Flow Routing Model (1K-FRM) with dam operation modules. Corrections are made to dam inflow biases, aiming to eliminate upstream biases while retaining middle-stream bi-

ases. The study observed that the impact of upstream bias correction was minimal due to significant biases in the midstream catchment. Comparing different bias correction methods for d4PDF shows an expected increase in future flood volumes compared to the past. Results of Chapter 3 suggest that future floods will be more severe than the 2011 Thailand flood and d4PDF past climate, with increased flood volumes, earlier occurrences, and longer duration. The study observed a 1.1–1.6 times increase in 100-year extreme discharge lasting 10–50 days longer than in the past climate.

Further narrowing down the study region, this thesis focuses on an in-depth study of the inundation and its effects on different socio-economic conditions in the Lower Chao Phraya River Basin (LCPRB), as it holds significant importance in the Southeast Asian region. The capital city of Thailand in the LCPRB, plays a crucial role in the nation's economy through various industries and agricultural contributions. However, the basin faces frequent river floods from the Chao Phraya River, impacting both residential and economic zones. The analysis covers both low- and high-frequency flood events, using 2700 years of historical (from a 6000-year dataset) and 2430 years of future climate data (from a 5400-year dataset) under a +4K temperature increase scenario.

When compared to the past climate, low-frequency floods with a +4K rise are anticipated to rise in terms of both maximum volume and inundation area, as mentioned in Chapter 4. However, for all scenarios, the future high-frequency floods with a +4K rise are going to be more severe in terms of both inundation area, maximum volume, and inundation depth. The inundation area is roughly increasing by 1.2–1.3 times across all depths, return periods, and SST GCMs. In addition, the past and future relationships between peak discharge and flood volume show little variation, suggesting that the physical relationships maintained across the d4PDF climates are comparable. Furthermore, the King's Dyke region is represented by the inundation area for each case well, indicating that the Multi-Error-Removed Improved-Terrain Digital Elevation Model (MERIT DEM) in the basin accurately depicts the study area.

In the +4K temperature rise scenario, it is anticipated that future low-frequency flooding, such as 50-year and 100-year events, will exhibit increased severity in terms of exposed area and duration compared to the past climate, as mentioned in Chapter 4. However, Chapter 5 explicates that despite these intensified flooding conditions, the projected future exposed population is expected to decrease by 0.7 to 0.9 times compared to the past climate across all return periods and SST GCMs (depths > 0 m).

Similar patterns are foreseen for flood depths exceeding 0.45 and 3 m. Nonetheless, when the analysis keeps the future population constant regarding flood exposure, it is projected that there will be an increase of approximately 1.2 times for high-frequency floods and 1.5 times for low-frequency floods on average for depths greater than 0 m. This demonstrates the significant impact of climate change in the basin as well as the influence of demographic changes. The study further indicates that the anticipated decrease in the projected population by the year 2100 cancels the effects of climate change on population exposure. Although overall population exposure is not expected to increase due to the combined effects of climate change and decreased population, higher return period flood events are likely to affect a larger population compared to lower return period events.

In addition to population exposure, Chapter 5 conducts an analysis of rice exposure for different return periods, demonstrating a clear increase in the area of rice exposure in the future compared to past climate conditions. On average, Chapter 5 anticipates a 1.3 times increase in the rice exposure area for high-frequency events and a 1.2 times increase for low-frequency events across six SST GCMs. In addition, the average duration of rice exposure is projected to increase by 1.1 times and 1.2 times for high- and low-frequency events, respectively. It is noteworthy that the rise in exposed rice area in the future surpasses the increase in exposed average duration. This outcome could be due to the proximity of the rice fields to the river channel, which allows water to drain more rapidly through the river channel.

Chapter 6 focuses on risk assessment by producing the risk curves and economic damage to rice cultivation in the LCPRB. On average, it is expected that the economic damage in agriculture will increase by 20-30% for both high- and low-frequency flooding events. It is worth noting that the rice yield loss in the future is likely to increase by a similar ratio as per the the analysis based on the rice yield loss for different spatial regions (Philippines, Myanmar, and Japan). However, the actual damage amounts differ from each other for the LCPRB. In addition, the 2011 simulated damage surpasses the historical damage amount indicating that it was one of the most significant economic losses in the past across all three fragility curves. This may be because of severe depth and duration, which causes higher yield loss and damage. Hence, Chapter 6 outcomes highlight that forthcoming severe floods will likely cause significantly higher damages and impacts due to climate change effects. Both high- and low-frequency flood events are anticipated to adversely affect rice production, leading to substantial losses

in the basin. The assessment of flood damage from this study could serve as a basis for implementing flood mitigation strategies to adapt to climate change. To mitigate potential damage in the future, further investigations could explore the potential inclusion of dams within the basin. This measure could notably reduce agricultural losses, particularly in rice cultivation.

Extreme flood effects for agricultural fields and populations living in flood-prone areas present significant issues for the management of water resources. This research suggests that future exposure to both population and rice cultivation is expected to rise, leading to increased hardships and greater losses for local communities. As a result, there is a pressing need for interventions that include both structural and non-structural measures. These approaches are essential for improved adaptation and mitigation strategies to aid the affected residents, necessitating coordinated efforts from relevant agencies and ministries. Urgent climate adaptation is necessary to prevent potentially devastating economic, social, and environmental damage similar to or surpassing the 2011 flood. Moreover, this study did not consider factors like landuse/cover changes and other societal alterations, which could be valuable aspects to explore in future assessments.

References

- Abeysekara, W.C.S.M., Siriwardana, M., Meng, S., 2023. Economic consequences of climate change impacts on the agricultural sector of South Asia: A case study of Sri Lanka. *Economic Analysis and Policy* 77, 435–450. <https://doi.org/10.1016/j.eap.2022.12.003>
- Abhishek, Kinouchi, T., Sayama, T., 2021. A comprehensive assessment of water storage dynamics and hydroclimatic extremes in the Chao Phraya River Basin during 2002–2020. *Journal of Hydrology* 603, 126868. <https://doi.org/10.1016/j.jhydrol.2021.126868>
- Adelodun, B., Odey, G., Lee, S., Choi, K.S., 2023. Investigating the causal impacts relationship between economic flood damage and extreme precipitation indices based on ARDL-ECM framework: A case study of Chungcheong region in South Korea. *Sustainable Cities and Society* 95, 104606. <https://doi.org/10.1016/j.scs.2023.104606>
- Ahmad, D., Kanwal, M., Afzal, M., 2023. Climate change effects on riverbank erosion Bait community flood-prone area of Punjab, Pakistan: An application of livelihood vulnerability index. *Environ Dev Sustain* 25, 9387–9415. <https://doi.org/10.1007/s10668-022-02440-1>
- Ajjur, S.B., Al-Ghamdi, S.G., 2022. Exploring urban growth–climate change–flood risk nexus in fast growing cities. *Sci Rep* 12, 12265. <https://doi.org/10.1038/s41598-022-16475-x>
- Amnuaylojaroen, T., Chanvichit, P., 2019. Projection of near-future climate change and agricultural drought in Mainland Southeast Asia under RCP8.5. *Climatic Change* 155, 175–193. <https://doi.org/10.1007/s10584-019-02442-5>
- Arnell, N.W., Gosling, S.N., 2016. The impacts of climate change on river flood risk at the global scale. *Climatic Change* 134, 387–401. <https://doi.org/10.1007/s10584-014-1084-5>

- Arora, N.K., 2019. Impact of climate change on agriculture production and its sustainable solutions. *Environmental Sustainability* 2, 95–96. <https://doi.org/10.1007/s42398-019-00078-w>
- Bai, Y., Zhang, Z., Zhao, W., 2019. Assessing the Impact of Climate Change on Flood Events Using HEC-HMS and CMIP5. *Water Air Soil Pollut* 230, 119. <https://doi.org/10.1007/s11270-019-4159-0>
- Bennett, J.C., Grose, M.R., Post, D.A., Ling, F.L.N., Corney, S.P., Bindoff, N.L., 2011. Performance of quantile-quantile bias-correction for use in hydroclimatological projections, in: *MODSIM 2011-19th International Congress on Modelling and Simulation-Sustaining Our Future: Understanding and Living with Uncertainty*. pp. 2668–2675. <https://doi.org/http://ecite.utas.edu.au/117161>
- Bertola, M., Viglione, A., Lun, D., Hall, J., Blöschl, G., 2020. Flood trends in Europe: Are changes in small and big floods different? *Hydrol. Earth Syst. Sci.* 24, 1805–1822. <https://doi.org/10.5194/hess-24-1805-2020>
- Bidorn, B., Sok, K., Bidorn, K., Burnett, W.C., 2021. An analysis of the factors responsible for the shoreline retreat of the Chao Phraya Delta (Thailand). *Science of The Total Environment* 769, 145253. <https://doi.org/10.1016/j.scitotenv.2021.145253>
- Boulangé, J., Hanasaki, N., Yamazaki, D., Pokhrel, Y., 2021. Role of dams in reducing global flood exposure under climate change. *Nat Commun* 12, 417. <https://doi.org/10.1038/s41467-020-20704-0>
- Budhathoki, A., Babel, M.S., Shrestha, S., Meon, G., Kamalamma, A.G., 2021. Climate change impact on water balance and hydrological extremes in different physiographic regions of the West Seti River Basin, Nepal. *Ecohydrology & Hydrobiology* 21, 79–95. <https://doi.org/10.1016/j.ecohyd.2020.07.001>
- Budhathoki, A., Tanaka, T., Tachikawa, Y., 2023. Assessing extreme flood inundation and demographic exposure in climate change using large ensemble climate simulation data in the Lower Chao Phraya River Basin of Thailand. *Journal of Hydrology: Regional Studies* 50, 101583. <https://doi.org/10.1016/j.ejrh.2023.101583>
- Budhathoki, A., Tanaka, T., Tachikawa, Y., 2022. Correcting streamflow bias considering its spatial structure for impact assessment of climate change on floods using d4PDF in the Chao Phraya River Basin, Thailand. *Journal of Hydrology: Regional Studies* 42, 101150. <https://doi.org/10.1016/j.ejrh.2022.101150>
- Casale, F., Fuso, F., Giuliani, M., Castelletti, A., Bocchiola, D., 2021. Exploring future vulnerabilities of subalpine Italian regulated lakes under different climate scenar-

-
- ios: Bottom-up vs top-down and CMIP5 vs CMIP6. *Journal of Hydrology: Regional Studies* 38, 100973. <https://doi.org/10.1016/j.ejrh.2021.100973>
- Champathong, A., Komori, D., Kiguchi, M., Sukhapunnaphan, T., Oki, T., Nakaegawa, T., 2013. Future projection of mean river discharge climatology for the Chao Phraya River basin. *Hydrological Research Letters* 7, 36–41. <https://doi.org/10.3178/hrl.7.36>
- Chaowiwat, W., Sarinnapakorn, K., Weesakul, S., 2019. Prediction of Future Agriculture Water Demand in Thailand Using Multi Bias Corrected Climate Models 13. <https://doi.org/https://www.researchgate.net/publication/333835178>
- Chen, A.B., Goodall, J.L., Quinn, J.D., 2023. Exploring the relationship between flood insurance claims, crowdsourced rainfall, and tide levels for coastal urban communities: Case study for the mid-Atlantic United States. *Journal of Hydrology* 625, 130123. <https://doi.org/10.1016/j.jhydrol.2023.130123>
- Chen, C.-A., Hsu, H.-H., Liang, H.-C., Chiu, P.-G., Tu, C.-Y., 2022. Future change in extreme precipitation in East Asian spring and Mei-yu seasons in two high-resolution AGCMs. *Weather and Climate Extremes* 35, 100408. <https://doi.org/10.1016/j.wace.2022.100408>
- Chen, J., Brissette, F.P., Zhang, X.J., Chen, H., Guo, S., Zhao, Y., 2019. Bias correcting climate model multi-member ensembles to assess climate change impacts on hydrology. *Climatic Change* 153, 361–377. <https://doi.org/doi.org/10.1007/s10584-019-02393-x>
- Devitt, L., Neal, J., Coxon, G., Savage, J., Wagener, T., 2023. Flood hazard potential reveals global floodplain settlement patterns. *Nat Commun* 14, 2801. <https://doi.org/10.1038/s41467-023-38297-9>
- Didovets, I., Krysanova, V., Hattermann, F.F., Rocío Rivas López, M. del, Snizhko, S., Müller Schmied, H., 2020. Climate change impact on water availability of main river basins in Ukraine. *Journal of Hydrology: Regional Studies* 32, 100761. <https://doi.org/10.1016/j.ejrh.2020.100761>
- Dottori, F., Szewczyk, W., Ciscar, J.-C., Zhao, F., Alfieri, L., Hirabayashi, Y., Bianchi, A., Mongelli, I., Frieler, K., Betts, R.A., Feyen, L., 2018. Increased human and economic losses from river flooding with anthropogenic warming. *Nature Clim Change* 8, 781–786. <https://doi.org/10.1038/s41558-018-0257-z>
- Duong, D.T., Tachikawa, Y., Shiiba, M., Yorozu, K., 2013. River discharge projection in Indochina Peninsula under a changing climate using the MRI-AGCM3. 2S dataset.

- Journal of Japan Society of Civil Engineers, Ser. B1 (Hydraulic Engineering) 69, I_37–I_42.
- Duong, D.T., Tachikawa, Y., Yorozu, K., 2014. CHANGES IN RIVER DISCHARGE IN THE INDOCHINA PENINSULA REGION PROJECTED USING MRI-AGCM AND MIROC5 DATASETS. *J. JSCE, Ser. B1* 70, I_115–I_120. https://doi.org/10.2208/jscejhe.70.I_115
- Eccles, R., Zhang, H., Hamilton, D., Trancoso, R., Syktus, J., 2021. Impacts of climate change on streamflow and floodplain inundation in a coastal subtropical catchment. *Advances in Water Resources* 147, 103825. <https://doi.org/10.1016/j.advwatres.2020.103825>
- Economou, T., Garry, F., 2022. Probabilistic simulation of big climate data for robust quantification of changes in compound hazard events. *Weather and Climate Extremes* 38, 100522. <https://doi.org/10.1016/j.wace.2022.100522>
- Eka Suranny, L., Gravitiani, E., Rahardjo, M., 2022. Impact of climate change on the agriculture sector and its adaptation strategies. *IOP Conf. Ser.: Earth Environ. Sci.* 1016, 012038. <https://doi.org/10.1088/1755-1315/1016/1/012038>
- Elshamy, M.E., Seierstad, I.A., Sorteberg, A., 2009. Impacts of climate change on Blue Nile flows using bias-corrected GCM scenarios. *Hydrol. Earth Syst. Sci.* 15. <https://doi.org/10.5194/hess-13-551-2009>
- Engeland, K., Hisdal, H., Frigessi, A., 2004. Practical Extreme Value Modelling of Hydrological Floods and Droughts: A Case Study. *Extremes* 7, 5–30. <https://doi.org/10.1007/s10687-004-4727-5>
- Engkagul, S., 1993. Flooding features in Bangkok and vicinity: Geographical approach. *GeoJournal* 31, 335–338. <https://doi.org/10.1007/BF00812783>
- Fabian, P.S., Kwon, H.-H., Vithanage, M., Lee, J.-H., 2023. Modeling, challenges, and strategies for understanding impacts of climate extremes (droughts and floods) on water quality in Asia: A review. *Environmental Research* 225, 115617. <https://doi.org/10.1016/j.envres.2023.115617>
- Farmer, W.H., Over, T.M., Kiang, J.E., 2018. Bias correction of simulated historical daily streamflow at ungauged locations by using independently estimated flow duration curves. *Hydrology and Earth System Sciences* 22, 5741–5758. <https://doi.org/10.5194/hess-22-5741-2018>
- Gao, J., O'Neill, B.C., 2021. Global One-Eighth Degree Urban Land Extent Projection and Base Year Grids by SSP Scenarios, 2000-2100.

-
- Gao, J., O'Neill, B.C., 2020. Mapping Global Urban Land for the 21st Century with Data-driven Simulations and Shared Socioeconomic Pathways. *Nature Communications* 11.
- GFDRR, 2012. Towards a Resilient Future. Global Facility For Disaster Reduction And Recovery ANNUAL REPORT.
- Gu, X., Zhang, Q., Li, J., Chen, D., Singh, V.P., Zhang, Y., Liu, J., Shen, Z., Yu, H., 2020. Impacts of anthropogenic warming and uneven regional socio-economic development on global river flood risk. *Journal of Hydrology* 590, 125262. <https://doi.org/10.1016/j.jhydrol.2020.125262>
- Gunawardana, S.K., Shrestha, S., Mohanasundaram, S., Salin, K.R., Piman, T., 2021. Multiple drivers of hydrological alteration in the transboundary Srepok River Basin of the Lower Mekong Region. *Journal of Environmental Management* 278, 111524. <https://doi.org/10.1016/j.jenvman.2020.111524>
- GWP, 2017. The 2011 Thailand Floods Basin in Bangkok in The Lower Chao Phraya River kok Metropolis.
- Hallegatte, S., Green, C., Nicholls, R.J., Corfee-Morlot, J., 2013. Future flood losses in major coastal cities. *Nature Clim Change* 3, 802–806. <https://doi.org/10.1038/nclimate1979>
- Haraguchi, M., Lall, U., 2015. Flood risks and impacts: A case study of Thailand's floods in 2011 and research questions for supply chain decision making. *International Journal of Disaster Risk Reduction* 14, 256–272. <https://doi.org/10.1016/j.ijdr.2014.09.005>
- Hirai, M., Sakashita, T., Kitagawa, H., Tsuyuki, T., Hosaka, M., OH’IZUMI, M., 2007. Development and Validation of a New Land Surface Model for JMA’s Operational Global Model Using the CEOP Observation Dataset. *Journal of the Meteorological Society of Japan* 85A, 1–24. <https://doi.org/10.2151/jmsj.85A.1>
- Hogendoorn, D., Zegwaard, A., Petersen, A., 2018. Difficult travels: Delta plans don't land in the Chao Phraya delta. *Environmental Science & Policy* 89, 378–384. <https://doi.org/10.1016/j.envsci.2018.09.001>
- Hossain, B., Sohel, Md.S., Ryakitimbo, C.M., 2020. Climate change induced extreme flood disaster in Bangladesh: Implications on people's livelihoods in the Char Village and their coping mechanisms. *Progress in Disaster Science* 6, 100079. <https://doi.org/10.1016/j.pdisas.2020.100079>
- Hu, M., Zhang, X., Li, Y., Yang, H., Tanaka, K., 2019. Flood mitigation performance

- of low impact development technologies under different storms for retrofitting an urbanized area. *Journal of Cleaner Production* 222, 373–380. <https://doi.org/10.1016/j.jclepro.2019.03.044>
- Huang, X., Swain, D.L., 2022. Climate change is increasing the risk of a California megaflood. *Sci. Adv.* 8, eabq0995. <https://doi.org/10.1126/sciadv.abq0995>
- Hughes, D.A., Farinosi, F., 2020. Assessing development and climate variability impacts on water resources in the Zambezi River basin. Simulating future scenarios of climate and development. *Journal of Hydrology: Regional Studies* 32, 100763. <https://doi.org/10.1016/j.ejrh.2020.100763>
- Hunukumbura, P.B., Tachikawa, Y., 2012. River Discharge Projection under Climate Change in the Chao Phraya River Basin, Thailand, Using the MRI-GCM3.1S Dataset. *Journal of the Meteorological Society of Japan* 90A, 137–150. <https://doi.org/10.2151/jmsj.2012-A07>
- Ibarra, D.E., David, C.P.C., Tolentino, P.L.M., 2021. Evaluation and bias correction of an observation-based global runoff dataset using streamflow observations from small tropical catchments in the Philippines. *Hydrology and Earth System Sciences* 25, 2805–2820. <https://doi.org/10.5194/hess-2020-26>
- Ines, A.V.M., Hansen, J.W., 2006. Bias correction of daily GCM rainfall for crop simulation studies. *Agricultural and Forest Meteorology* 138, 44–53. <https://doi.org/10.1016/j.agrformet.2006.03.009>
- IPCC, 2014. Technical Support Unit for the Synthesis Report.
- Ishii, M., Mori, N., 2020. d4PDF: Large-ensemble and high-resolution climate simulations for global warming risk assessment. *Prog Earth Planet Sci* 7, 58. <https://doi.org/10.1186/s40645-020-00367-7>
- Jahandideh Tehrani, M., Helfer, F., Jenkins, G., 2021. Impacts of climate change and sea level rise on catchment management: A multi-model ensemble analysis of the Nerang River catchment, Australia. *Science of The Total Environment* 777, 146223. <https://doi.org/10.1016/j.scitotenv.2021.146223>
- Jamrussri, S., Toda, Y., 2017. Simulating past severe flood events to evaluate the effectiveness of nonstructural flood countermeasures in the upper Chao Phraya River Basin, Thailand. *Journal of Hydrology: Regional Studies* 10, 82–94. <https://doi.org/10.1016/j.ejrh.2017.02.001>
- Jones, B., O'Neill, B.C., 2016. Spatially explicit global population scenarios consistent with the Shared Socioeconomic Pathways. *Environ. Res. Lett.* 11, 084003. <https://doi.org/10.1088/1748-7598/11/8/084003>

//doi.org/10.1088/1748-9326/11/8/084003

- Jular, P., 2011. The 2011 Thailand Floods in The Lower Chao Phraya River Basin in Bangkok Metropolis 25.
- Kc, S., Lutz, W., 2017. The human core of the shared socioeconomic pathways: Population scenarios by age, sex and level of education for all countries to 2100. *Global Environmental Change* 42, 181–192. <https://doi.org/10.1016/j.gloenvcha.2014.06.004>
- Kitpaisalsakul, T., Koontanakulvong, S., Chaowiwat, W., 2016. Impact of climate change on reservoir operation in Central Plain Basin of Thailand 11, 7.
- Kobayashi, K., Takara, K., Sano, H., Tsumori, H., Sekii, K., 2016. A high-resolution large-scale flood hazard and economic risk model for the property loss insurance in Japan: Property loss estimation model in Japan. *J. Flood Risk Manage* 9, 136–153. <https://doi.org/10.1111/jfr3.12117>
- Komori, D., Nakamura, S., Kiguchi, M., Nishijima, A., Yamazaki, D., Suzuki, S., Kawasaki, A., Oki, K., Oki, T., 2012. Characteristics of the 2011 Chao Phraya River flood in Central Thailand. *Hydrological Research Letters* 6, 41–46. <https://doi.org/10.3178/hrl.6.41>
- Kotera, A., Nagano, T., Hanittinan, P., Koontanakulvong, S., 2016. Assessing the degree of flood damage to rice crops in the Chao Phraya delta, Thailand, using MODIS satellite imaging. *Paddy Water Environ* 14, 271–280. <https://doi.org/10.1007/s10333-015-0496-9>
- Kotsuki, S., Tanaka, K., 2013. Impacts of mid-rainy season rainfall on runoff into the Chao Phraya River, Thailand. *Journal of Disaster Research* 8, 397–405. <https://doi.org/doi:10.20965/jdr.2013.p0397>, 2013
- Kotsuki, S., Tanaka, K., Watanabe, S., 2014. Projected hydrological changes and their consistency under future climate in the Chao Phraya River Basin using multi-model and multi-scenario of CMIP5 dataset. *Hydrological Research Letters* 8, 27–32. <https://doi.org/10.3178/hrl.8.27>
- Kumar Mishra, B., Herath, S., 2015. Assessment of Future Floods in the Bagmati River Basin of Nepal Using Bias-Corrected Daily GCM Precipitation Data. *J. Hydrol. Eng.* 20, 05014027. [https://doi.org/10.1061/\(ASCE\)HE.1943-5584.0001090](https://doi.org/10.1061/(ASCE)HE.1943-5584.0001090)
- Kure, S., Tebakari, T., 2012. Hydrological impact of regional climate change in the Chao Phraya River Basin, Thailand. *Hydrological Research Letters* 6, 53–58. <https://doi.org/10.3178/hrl.6.53>

- Lavender, S.L., Walsh, K.J.E., Caron, L.-P., King, M., Monkiewicz, S., Guishard, M., Zhang, Q., Hunt, B., 2018. Estimation of the maximum annual number of North Atlantic tropical cyclones using climate models. *Sci. Adv.* 4, eaat6509. <https://doi.org/10.1126/sciadv.aat6509>
- Lehner, B., 2005. Hydrological Data and Maps Based on SRTM Elevation Derivatives at Multiple Scales, in: AGU Spring Meeting Abstracts. pp. H33A–03.
- Leitold, R., Garschagen, M., Tran, V., Revilla Diez, J., 2021. Flood risk reduction and climate change adaptation of manufacturing firms: Global knowledge gaps and lessons from Ho Chi Minh City. *International Journal of Disaster Risk Reduction* 61, 102351. <https://doi.org/10.1016/j.ijdrr.2021.102351>
- Li, Z., Huang, G., Wang, X., Han, J., Fan, Y., 2016. Impacts of future climate change on river discharge based on hydrological inference: A case study of the Grand River Watershed in Ontario, Canada. *Science of The Total Environment* 548-549, 198–210. <https://doi.org/10.1016/j.scitotenv.2016.01.002>
- Liew, S.C., Gupta, A., Chia, A.S., Ang, W.C., 2016. The flood of 2011 in the lower Chao Phraya valley, Thailand: Study of a long-duration flood through satellite images. *Geomorphology* 262, 112–122. <https://doi.org/10.1016/j.geomorph.2016.03.022>
- Ligaray, M., Kim, H., Sthiannopkao, S., Lee, S., Cho, K., Kim, J., 2015. Assessment on Hydrologic Response by Climate Change in the Chao Phraya River Basin, Thailand. *Water* 7, 6892–6909. <https://doi.org/10.3390/w7126665>
- Liu, S., Yao, Y., Kuang, X., Zheng, C., 2021. A preliminary investigation on the climate-discharge relationship in the upper region of the Yarlung Zangbo River basin. *Journal of Hydrology* 603, 127066. <https://doi.org/10.1016/j.jhydrol.2021.127066>
- Liu, Y., Xu, Y., Zhao, Y., Long, Y., 2022. Using SWAT Model to Assess the Impacts of Land Use and Climate Changes on Flood in the Upper Weihe River, China. *Water* 14, 2098. <https://doi.org/10.3390/w14132098>
- Loc, H.H., Emadzadeh, A., Park, E., Nontikansak, P., Deo, R.C., 2023. The Great 2011 Thailand flood disaster revisited: Could it have been mitigated by different dam operations based on better weather forecasts? *Environmental Research* 216, 114493. <https://doi.org/10.1016/j.envres.2022.114493>
- Loc, H.H., Park, E., Chitwatkulsiri, D., Lim, J., Yun, S.-H., Maneechot, L., Minh Phuong, D., 2020. Local rainfall or river overflow? Re-evaluating the cause of the Great 2011 Thailand flood. *Journal of Hydrology* 589, 125368. <https://doi.org/10.1016/j.jhydrol.2020.125368>

-
- Luo, P., Mu, D., Xue, H., Ngo-Duc, T., Dang-Dinh, K., Takara, K., Nover, D., Schladow, G., 2018. Flood inundation assessment for the Hanoi Central Area, Vietnam under historical and extreme rainfall conditions. *Sci Rep* 8, 12623. <https://doi.org/10.1038/s41598-018-30024-5>
- Manee, D., Tachikawa, Y., Ichikawa, Y., Yorozu, K., 2016. EVALUATION OF BIAS CORRECTION METHODS FOR FUTURE RIVER DISCHARGE PROJECTION. *J. JSCE, Ser. G* 72, I_7–I_12. https://doi.org/10.2208/jscejer.72.I_7
- Maneechot, L., Wong, Y.J., Try, S., Shimizu, Y., Bharambe, K.P., Hanittinan, P., Ram-Indra, T., Usman, M., 2023. Evaluating the necessity of post-processing techniques on d4PDF data for extreme climate assessment. *Environ Sci Pollut Res* 30, 102531–102546. <https://doi.org/10.1007/s11356-023-29572-9>
- Maraun, D., 2016. Bias correcting climate change simulations—a critical review. *Current Climate Change Reports* 2, 211–220. <https://doi.org/doi.org/10.1007/s40641-016-0050-x>
- Mateo, C.M.R., Yamazaki, D., Kim, H., Champathong, A., Vaze, J., Oki, T., 2017. Impacts of spatial resolution and representation of flow connectivity on large-scale simulation of floods. *Hydrol. Earth Syst. Sci.* 21, 5143–5163. <https://doi.org/10.5194/hess-21-5143-2017>
- Meema, T., Tachikawa, Y., Ichikawa, Y., Yorozu, K., 2021. Uncertainty assessment of water resources and long-term hydropower generation using a large ensemble of future climate projections for the Nam Ngum River in the Mekong Basin. *Journal of Hydrology: Regional Studies* 36, 100856. <https://doi.org/10.1016/j.ejrh.2021.100856>
- Meesuk, V., Vojinovic, Z., Mynett, A.E., 2017. Extracting inundation patterns from flood watermarks with remote sensing SfM technique to enhance urban flood simulation: The case of Ayutthaya, Thailand. *Computers, Environment and Urban Systems* 64, 239–253. <https://doi.org/10.1016/j.compenvurbsys.2017.03.004>
- Merz, B., Blöschl, G., Vorogushyn, S., Dottori, F., Aerts, J.C.J.H., Bates, P., Bertola, M., Kemter, M., Kreibich, H., Lall, U., Macdonald, E., 2021. Causes, impacts and patterns of disastrous river floods. *Nat Rev Earth Environ* 2, 592–609. <https://doi.org/10.1038/s43017-021-00195-3>
- Miller, J.D., Hutchins, M., 2017. The impacts of urbanisation and climate change on urban flooding and urban water quality: A review of the evidence concerning the United Kingdom. *Journal of Hydrology: Regional Studies* 12, 345–362. <https://doi.org/10.1016/j.ejrh.2017.03.004>

- doi.org/10.1016/j.ejrh.2017.06.006
- Mishra, B.K., Herath, S., 2011. Climate projections downscaling and impact assessment on precipitation over upper Bagmati River Basin, Nepal, in: Third International Conference on Addressing Climate Change for Sustainable Development Through Up-Scaling Renewable Energy Technologies. RETRUD, pp. 275–281.
- Mishra, B.K., Rafiei Emam, A., Masago, Y., Kumar, P., Regmi, R.K., Fukushi, K., 2018. Assessment of future flood inundations under climate and land use change scenarios in the Ciliwung River Basin, Jakarta: Assessment of future flood inundations under climate and land use change scenarios in the Ciliwung River Basin, Jakarta. *J Flood Risk Management* 11, S1105–S1115. <https://doi.org/10.1111/jfr3.12311>
- Mitchell, D., AchutaRao, K., Allen, M., Bethke, I., Beyerle, U., Ciavarella, A., Forster, P.M., Fuglestedt, J., Gillett, N., Haustein, K., Ingram, W., Iversen, T., Kharin, V., Klingaman, N., Massey, N., Fischer, E., Schleussner, C.-F., Scinocca, J., Seland, Ø., Shiogama, H., Shuckburgh, E., Sparrow, S., Stone, D., Uhe, P., Wallom, D., Wehner, M., Zaaboul, R., 2017. Half a degree additional warming, prognosis and projected impacts (HAPPI): Background and experimental design. *Geosci. Model Dev.* 10, 571–583. <https://doi.org/10.5194/gmd-10-571-2017>
- Mizushima, Y., Yorozu, K., Ichikawa, Y., Tachikawa, Y., 2019. A STUDY ON BIAS CORRECTION METHOD FOR RUNOFF GENERATION DATA BASED ON REFERENCE DATA CREATED BY LAND SURFACE MODEL. Bangkok, Thailand.
- Mizuta, R., Murata, A., Ishii, M., Shiogama, H., Hibino, K., Mori, N., Arakawa, O., Imada, Y., Yoshida, K., Aoyagi, T., Kawase, H., Mori, M., Okada, Y., Shimura, T., Nagatomo, T., Ikeda, M., Endo, H., Nosaka, M., Arai, M., Takahashi, C., Tanaka, K., Takemi, T., Tachikawa, Y., Temur, K., Kamae, Y., Watanabe, M., Sasaki, H., Kitoh, A., Takayabu, I., Nakakita, E., Kimoto, M., 2017. Over 5,000 Years of Ensemble Future Climate Simulations by 60-km Global and 20-km Regional Atmospheric Models. *Bulletin of the American Meteorological Society* 98, 1383–1398. <https://doi.org/10.1175/BAMS-D-16-0099.1>
- MLIT, 2005. Flood control economic survey manual (draft) (free translation).
- Mori, N., Shimura, T., Yoshida, K., Mizuta, R., Okada, Y., Fujita, M., Khujanazarov, T., Nakakita, E., 2019. Future changes in extreme storm surges based on mega-ensemble projection using 60-km resolution atmospheric global circulation model. *Coastal Engineering Journal* 61, 295–307. <https://doi.org/10.1080/21664250.2019.1586290>

-
- Nandi, S., Reddy, M.J., 2022. An integrated approach to streamflow estimation and flood inundation mapping using VIC, RAPID and LISFLOOD-FP. *Journal of Hydrology* 610, 127842. <https://doi.org/10.1016/j.jhydrol.2022.127842>
- Ninomiya, J., Taka, Y., Mori, N., 2021. Projecting changes in explosive cyclones and high waves around Japan using a mega-ensemble projection. *Ocean Engineering* 237, 109634. <https://doi.org/10.1016/j.oceaneng.2021.109634>
- Padiyedath Gopalan, S., Champathong, A., Sukhappunnaphan, T., Nakamura, S., Hanasaki, N., 2022. Potential impact of diversion canals and retention areas as climate change adaptation measures on flood risk reduction: A hydrological modelling case study from the Chao Phraya River Basin, Thailand. *Science of The Total Environment* 841, 156742. <https://doi.org/10.1016/j.scitotenv.2022.156742>
- Padulano, R., Rianna, G., Costabile, P., Costanzo, C., Del Giudice, G., Mercogliano, P., 2021. Propagation of variability in climate projections within urban flood modelling: A multi-purpose impact analysis. *Journal of Hydrology* 602, 126756. <https://doi.org/10.1016/j.jhydrol.2021.126756>
- Park, E., Lim, J., Ho, H.L., Herrin, J., Chitwatkulsiri, D., 2021. Source-to-sink sediment fluxes and budget in the Chao Phraya River, Thailand: A multi-scale analysis based on the national dataset. *Journal of Hydrology* 594, 125643. <https://doi.org/10.1016/j.jhydrol.2020.125643>
- Parker, L., Bourgoin, C., Martinez-Valle, A., Läderach, P., 2019. Vulnerability of the agricultural sector to climate change: The development of a pan-tropical Climate Risk Vulnerability Assessment to inform sub-national decision making. *PLoS ONE* 14, e0213641. <https://doi.org/10.1371/journal.pone.0213641>
- Peel, M.C., Srikanthan, R., McMahon, T.A., Karoly, D.J., 2015. Approximating uncertainty of annual runoff and reservoir yield using stochastic replicates of global climate model data. *Hydrology and Earth System Sciences* 19, 1615–1639. <https://doi.org/doi.org/10.5194/hess-19-1615-2015>
- Piani, C., Weedon, G.P., Best, M., Gomes, S.M., Viterbo, P., Hagemann, S., Haerter, J.O., 2010. Statistical bias correction of global simulated daily precipitation and temperature for the application of hydrological models. *Journal of hydrology* 395, 199–215. <https://doi.org/doi.org/10.1016/j.jhydrol.2010.10.024>
- Pinos, J., Timbe, L., 2019. Performance assessment of two-dimensional hydraulic models for generation of flood inundation maps in mountain river basins. *Water Science and Engineering* 12, 11–18. <https://doi.org/10.1016/j.wse.2019.03.001>

- Ponpang-Nga, P., Techamahasaranont, J., 2016. Effects of climate and land use changes on water balance in upstream in the Chao Phraya River basin, Thailand. *Agriculture and Natural Resources* 50, 310–320. <https://doi.org/10.1016/j.anres.2016.10.005>
- Ram-Indra, T., Tachikawa, Y., Yoroze, K., Ichikawa, Y., 2020a. BIAS CORRECTION OF RUNOFF DATA IN AGCM3.2S FOR UPPER CHAO PHRAYA RIVER BASIN, THAILAND. *Journal of Japan Society of Civil Engineers, Ser. G (Environmental Research)* 76, I_55–I_63. https://doi.org/10.2208/jscejer.76.5_I_55
- Ram-Indra, T., Tachikawa, Y., Yoroze, K., Ichikawa, Y., 2020b. AGCM3.2S RUNOFF DATA BIAS CORRECTION OVER UPPER CHAO PHRAYA RIVER BASIN BASED ON LAND COVER GROUPING. *J. JSCE, Ser. B1* 76, I_91–I_96. https://doi.org/10.2208/jscejhe.76.2_I_91
- Sayama, T., Tatebe, Y., Iwami, Y., Tanaka, S., 2015. Hydrologic sensitivity of flood runoff and inundation: 2011 Thailand floods in the Chao Phraya River basin. *Nat. Hazards Earth Syst. Sci.* 15, 1617–1630. <https://doi.org/10.5194/nhess-15-1617-2015>
- Sayama, T., Tatebe, Y., Tanaka, S., 2017. An emergency response-type rainfall-runoff-inundation simulation for 2011 Thailand floods: Simulation for 2011 Thailand floods. *J Flood Risk Management* 10, 65–78. <https://doi.org/10.1111/jfr3.12147>
- SEARCA, 2015. SEARCA Promotion of Climate Resilience for Food Security in ASEAN Rice. Deutsche Gesellschaft für Internationale Zusammenarbeit (GIZ) GmbH.
- Sebastian, A., Gori, A., Blessing, R.B., Van Der Wiel, K., Bass, B., 2019. Disentangling the impacts of human and environmental change on catchment response during Hurricane Harvey. *Environ. Res. Lett.* 14, 124023. <https://doi.org/10.1088/1748-9326/ab5234>
- Shakti P. C., Miyamoto, M., Kakinuma, D., Misumi, R., Sriariyawat, A., Visessri, S., National Research Institute for Earth Science and Disaster Resilience (NIED) 3-1 Tennodai, Tsukuba, Ibaraki 305-0006, Japan, International Centre for Water Hazard and Risk Management under the auspices of UNESCO (ICHARM), Public Works Research Institute (PWRI), Tsukuba, Japan, Department of Water Resource Engineering, Faculty of Engineering, Chulalongkorn University, Bangkok, Thailand, Disaster and Risk Management Information Systems Research Unit, Faculty of Engineering, Chulalongkorn University, Bangkok, Thailand, 2022. Probable Flood Inundation Depth and Extent in the Chao Phraya River Basin for Different Return

-
- Periods. *JDR* 17, 901–912. <https://doi.org/10.20965/jdr.2022.p0901>
- Shrestha, B.B., Kawasaki, A., Zin, W.W., 2021. Development of flood damage functions for agricultural crops and their applicability in regions of Asia. *Journal of Hydrology: Regional Studies* 36, 100872. <https://doi.org/10.1016/j.ejrh.2021.100872>
- Shrestha, B.B., Perera, E.D.P., Kudo, S., Miyamoto, M., Yamazaki, Y., Kuribayashi, D., Sawano, H., Sayama, T., Magome, J., Hasegawa, A., Ushiyama, T., Iwami, Y., Tokunaga, Y., 2019. Assessing flood disaster impacts in agriculture under climate change in the river basins of Southeast Asia. *Nat Hazards* 97, 157–192. <https://doi.org/10.1007/s11069-019-03632-1>
- Smith, A., Bates, P.D., Wing, O., Sampson, C., Quinn, N., Neal, J., 2019. New estimates of flood exposure in developing countries using high-resolution population data. *Nat Commun* 10, 1814. <https://doi.org/10.1038/s41467-019-09282-y>
- Som-ard, J., Immitzer, M., Vuolo, F., Ninsawat, S., Atzberger, C., 2022. Mapping of crop types in 1989, 1999, 2009 and 2019 to assess major land cover trends of the Udon Thani Province, Thailand. *Computers and Electronics in Agriculture* 198, 107083. <https://doi.org/10.1016/j.compag.2022.107083>
- Sriariyawat, A., Kimmany, B., Miyamoto, M., Kakinuma, D., Shakti P. C., Visessri, S., Department of Water Resource Engineering, Faculty of Engineering, Chulalongkorn University, Phayathai Road, Patumwan, Bangkok 10330, Thailand, International Centre for Water Hazard and Risk Management under the auspices of UNESCO (ICHARM), Public Works Research Institute (PWRI), Ibaraki, Japan, National Research Institute for Earth Science and Disaster Resilience (NIED), Tsukuba, Japan, Disaster and Risk Management Information Systems (DRMIS) Research Unit, Chulalongkorn University, Bangkok, Thailand, 2022. An Approach to Flood Hazard Mapping for the Chao Phraya River Basin Using Rainfall-Runoff-Inundation Model. *JDR* 17, 864–876. <https://doi.org/10.20965/jdr.2022.p0864>
- Stevanović, M., Popp, A., Lotze-Campen, H., Dietrich, J.P., Müller, C., Bonsch, M., Schmitz, C., Bodirsky, B.L., Humpenöder, F., Weindl, I., 2016. The impact of high-end climate change on agricultural welfare. *Sci. Adv.* 2, e1501452. <https://doi.org/10.1126/sciadv.1501452>
- Tachikawa, Y., Takino, S., Fujioka, Y., Yorozu, K., Kim, S., Shiiba, M., 2011. Projection of river discharge of Japanese river basins under a climate change scenario. *J. Japan Soc. of Civil Eng. B* 1, 1–15. <https://doi.org/10.2208/jscejhe.67.1>
- Tanaka, T., Kiyohara, K., Tachikawa, Y., 2020. Comparison of fluvial and pluvial flood

- risk curves in urban cities derived from a large ensemble climate simulation dataset: A case study in Nagoya, Japan. *Journal of Hydrology* 584, 124706. <https://doi.org/10.1016/j.jhydrol.2020.124706>
- Tanaka, T., Kobayashi, K., Tachikawa, Y., 2021. Simultaneous flood risk analysis and its future change among all the 109 class-A river basins in Japan using a large ensemble climate simulation database d4PDF. *Environmental Research Letters* 16, 074059. <https://doi.org/10.1088/1748-9326/abfb2b>
- Tanaka, T., Tachikawa, Y., Ichikawa, Y., Yorozu, K., 2019a. An automatic domain updating method for fast 2-dimensional flood-inundation modelling. *Environmental Modelling & Software* 116, 110–118. <https://doi.org/10.1016/j.envsoft.2019.02.018>
- Tanaka, T., Tachikawa, Y., Ichikawa, Y., Yorozu, K., 2018. Flood risk curve development with probabilistic rainfall modelling and large ensemble climate simulation data: A case study for the Yodo River basin. *Hydrological Research Letters* 12, 28–33. <https://doi.org/10.3178/hrl.12.28>
- Tanaka, T., Tachikawa, Y., Ichikawa, Y., Yorozu, K., 2017. Impact assessment of upstream flooding on extreme flood frequency analysis by incorporating a flood-inundation model for flood risk assessment. *Journal of Hydrology* 554, 370–382. <https://doi.org/10.1016/j.jhydrol.2017.09.012>
- Tanaka, T., Tachikawa, Y., Yorozu, K., 2015. A flood risk curve development for inundation disaster considering spatio-temporal rainfall distribution. *Proceedings of the International Association of Hydrological Sciences* 370, 57–62. <https://doi.org/10.5194/piahs-370-57-2015>
- Tanaka, T., Yuki, K., Tachikawa, Y., 2019b. Reproducibility evaluation of annual maximum basin average rainfall in national first-class river basins using d4PDF. *JSCE Proceedings B1 (Hydraulic Engineering)* 75. https://doi.org/10.2208/jscejhe.75.2_I_1135
- Tanoue, M., Taguchi, R., Nakata, S., Watanabe, S., Fujimori, S., Hirabayashi, Y., 2020. Estimation of Direct and Indirect Economic Losses Caused by a Flood With Long-Lasting Inundation: Application to the 2011 Thailand Flood. *Water Resour. Res.* 56. <https://doi.org/10.1029/2019WR026092>
- Tebaldi, C., Knutti, R., 2007. The use of the multi-model ensemble in probabilistic climate projections. *Phil. Trans. R. Soc. A.* 365, 2053–2075. <https://doi.org/10.1098/rsta.2007.2076>
- Tellman, B., Sullivan, J.A., Kuhn, C., Kettner, A.J., Doyle, C.S., Brakenridge, G.R., Er-

-
- ickson, T.A., Slayback, D.A., 2021. Satellite imaging reveals increased proportion of population exposed to floods. *Nature* 596, 80–86. <https://doi.org/10.1038/s41586-021-03695-w>
- The World Bank, 2012. *Thai Flood 2011: Rapid Assessment for Resilient Recovery and Reconstruction Planning*.
- Tierolf, L., Moel, H. de, Vliet, J. van, 2021. Modeling urban development and its exposure to river flood risk in Southeast Asia. *Computers, Environment and Urban Systems* 87, 101620. <https://doi.org/10.1016/j.compenvurbsys.2021.101620>
- Tingting, L., Chuang, L., 2010. Study on extraction of crop information using time-series MODIS data in the Chao Phraya Basin of Thailand. *Advances in Space Research* 45, 775–784. <https://doi.org/10.1016/j.asr.2009.11.013>
- Tong, K., Zhao, Y., Wei, Y., Hu, B., Lu, Y., 2018. Evaluation and Hydrological Validation of GPM Precipitation Products over the Nanliu River Basin, Beibu Gulf. *Water* 10, 1777. <https://doi.org/10.3390/w10121777>
- Try, S., Sayama, T., Phy, S.R., Sok, T., Ly, S., Oeurng, C., 2023. Assessing the impacts of climate change and dam development on potential flood hazard and damages in the Cambodian floodplain of the lower mekong basin. *Journal of Hydrology: Regional Studies* 49, 101508. <https://doi.org/10.1016/j.ejrh.2023.101508>
- Try, S., Tanaka, S., Tanaka, K., Sayama, T., Hu, M., Sok, T., Oeurng, C., 2020. Projection of extreme flood inundation in the Mekong River basin under 4K increasing scenario using large ensemble climate data. *Hydrological Processes* 34, 4350–4364. <https://doi.org/10.1002/hyp.13859>
- Tuitjer, L., 2023. Unruly waters: Exploring the embodied dimension of an urban flood in Bangkok through materiality, affect and emotions. *Geogr. Helv.* 78, 281–290. <https://doi.org/10.5194/gh-78-281-2023>
- UNDRR, 2021. UNITED NATIONS OFFICE FOR DISASTER RISK REDUCTION- Annual report 2021.pdf.
- Van Der Wiel, K., Wanders, N., Selten, F.M., Bierkens, M.F.P., 2019. Added Value of Large Ensemble Simulations for Assessing Extreme River Discharge in a 2 °C Warmer World. *Geophysical Research Letters* 46, 2093–2102. <https://doi.org/10.1029/2019GL081967>
- Wang, X., Liu, Z., Chen, H., 2022. Investigating Flood Impact on Crop Production under a Comprehensive and Spatially Explicit Risk Evaluation Framework. *Agriculture* 12, 484. <https://doi.org/10.3390/agriculture12040484>

- Wannasin, C., Brauer, C.C., Uijlenhoet, R., Verseveld, W.J. van, Weerts, A.H., 2021. Daily flow simulation in Thailand Part II: Unraveling effects of reservoir operation. *Journal of Hydrology: Regional Studies* 34, 100792. <https://doi.org/10.1016/j.ejrh.2021.100792>
- Ward, P.J., Jongman, B., Salamon, P., Simpson, A., Bates, P., De Groeve, T., Muis, S., De Perez, E.C., Rudari, R., Trigg, M.A., Winsemius, H.C., 2015. Usefulness and limitations of global flood risk models. *Nature Clim Change* 5, 712–715. <https://doi.org/10.1038/nclimate2742>
- Wassmann, R., Phong, N.D., Tho, T.Q., Hoanh, C.T., Khoi, N.H., Hien, N.X., Vo, T.B.T., Tuong, T.P., 2019. High-resolution mapping of flood and salinity risks for rice production in the Vietnamese Mekong Delta. *Field Crops Research* 236, 111–120. <https://doi.org/10.1016/j.fcr.2019.03.007>
- Watanabe, S., Yamada, M., Abe, S., Hatono, M., 2020. Bias correction of d4PDF using a moving window method and their uncertainty analysis in estimation and projection of design rainfall depth. *Hydrological Research Letters* 14, 117–122. <https://doi.org/doi.org/10.3178/hr1.14.117>
- Wichakul, S., Tachikawa, Y., Shiiba, M., Yorozu, K., 2015. River discharge assessment under a changing climate in the Chao Phraya River, Thailand by using MRI-AGCM3. 2S. *Hydrological Research Letters* 9, 84–89.
- Wichakul, S., Tachikawa, Y., Shiiba, M., Yorozu, K., 2013. DEVELOPING A REGIONAL DISTRIBUTED HYDROLOGICAL MODEL FOR WATER RESOURCES ASSESSMENT AND ITS APPLICATION TO THE CHAO PHRAYA RIVER BASIN. *J. JSCE* 69, I_43–I_48. https://doi.org/10.2208/jscejhe.69.I_43
- Yamamoto, K., Sayama, T., Apip, 2021. Impact of climate change on flood inundation in a tropical river basin in Indonesia. *Prog Earth Planet Sci* 8, 5. <https://doi.org/10.1186/s40645-020-00386-4>
- Yamazaki, D., Ikeshima, D., Neal, J.C., O’Loughlin, F., Sampson, C.C., Kanae, S., Bates, P.D., 2017. MERIT DEM: A new high-accuracy global digital elevation model and its merit to global hydrodynamic modeling, in: *AGU Fall Meeting Abstracts*. pp. H12C–04.
- Yang, J.-A., Kim, S., Mori, N., Mase, H., 2018. Assessment of long-term impact of storm surges around the Korean Peninsula based on a large ensemble of climate projections. *Coastal Engineering* 142, 1–8. <https://doi.org/10.1016/j.coastaleng.2018.09.008>

-
- Yang, S., Zhao, B., Yang, D., Wang, T., Yang, Y., Ma, T., Santisirisomboon, J., 2023. Future changes in water resources, floods and droughts under the joint impact of climate and land-use changes in the Chao Phraya basin, Thailand. *Journal of Hydrology* 129454. <https://doi.org/10.1016/j.jhydrol.2023.129454>
- Yuan, S., Stuart, A.M., Laborte, A.G., Rattalino Edreira, J.I., Dobermann, A., Kien, L.V.N., Thúy, L.T., Paothong, K., Traesang, P., Tint, K.M., San, S.S., Villafuerte, M.Q., Quicho, E.D., Pame, A.R.P., Then, R., Flor, R.J., Thon, N., Agus, F., Agustiani, N., Deng, N., Li, T., Grassini, P., 2022. Southeast Asia must narrow down the yield gap to continue to be a major rice bowl. *Nat Food* 3, 217–226. <https://doi.org/10.1038/s43016-022-00477-z>
- Zhang, Y., Wang, Y., Chen, Y., Liang, F., Liu, H., 2019. Assessment of future flash flood inundations in coastal regions under climate change scenarios—A case study of Hadahe River basin in northeastern China. *Science of The Total Environment* 693, 133550. <https://doi.org/10.1016/j.scitotenv.2019.07.356>
- Zhao, B., Lei, H., Yang, D., Yang, S., Santisirisomboon, J., 2022. Runoff and sediment response to deforestation in a large Southeast Asian monsoon watershed. *Journal of Hydrology* 606, 127432. <https://doi.org/10.1016/j.jhydrol.2022.127432>

Appendix A

Supplementary materials

A.1 Appendix for Chapter 4

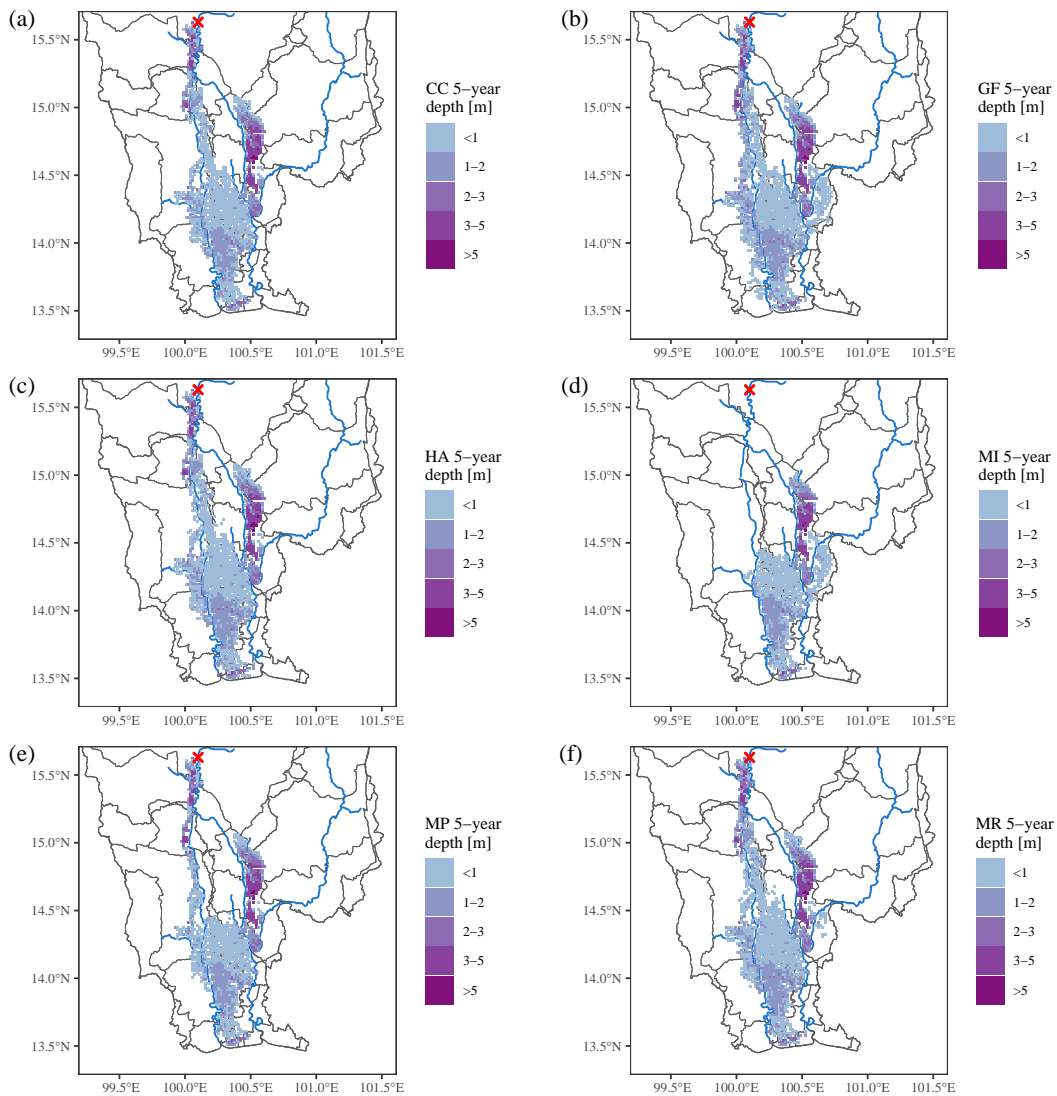


Figure A.1: Simulated future flood inundation extent and depth for 6SST GCMs (a) CC, (b) GF, (c) HA, (d) MI, (e) MP and (f) MR with respect to the d4PDF 5-year return period and depth > 0 m (the color bar represents the inundation depth in meters and the red cross represents the C2 station).

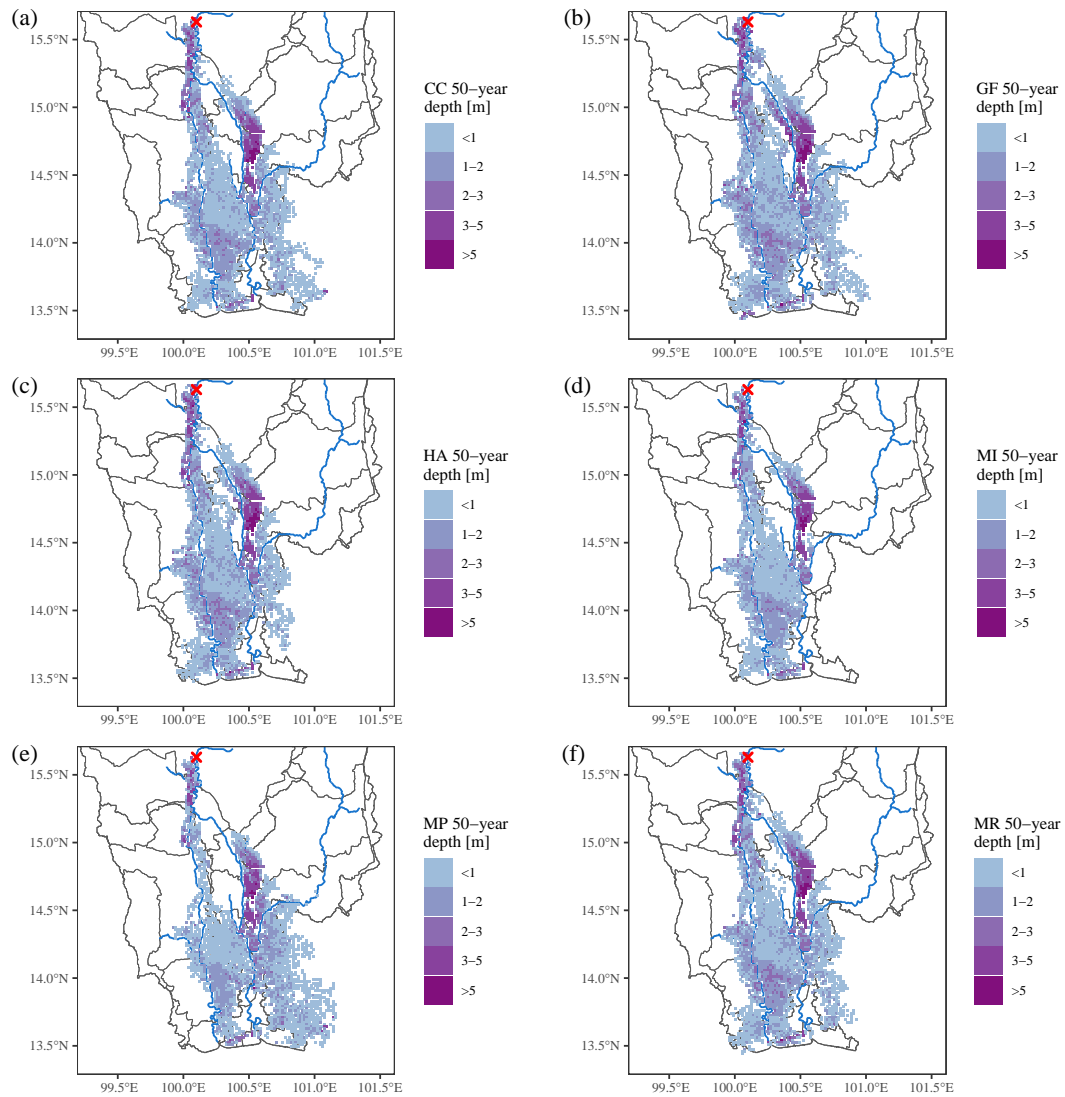


Figure A.2: Simulated future flood inundation extent and depth for 6SST GCMs (a) CC, (b) GF, (c) HA, (d) MI, (e) MP and (f) MR with respect to the d4PDF 50-year return period and depth > 0 m (the color bar represents the inundation depth in meters and the red cross represents the C2 station).

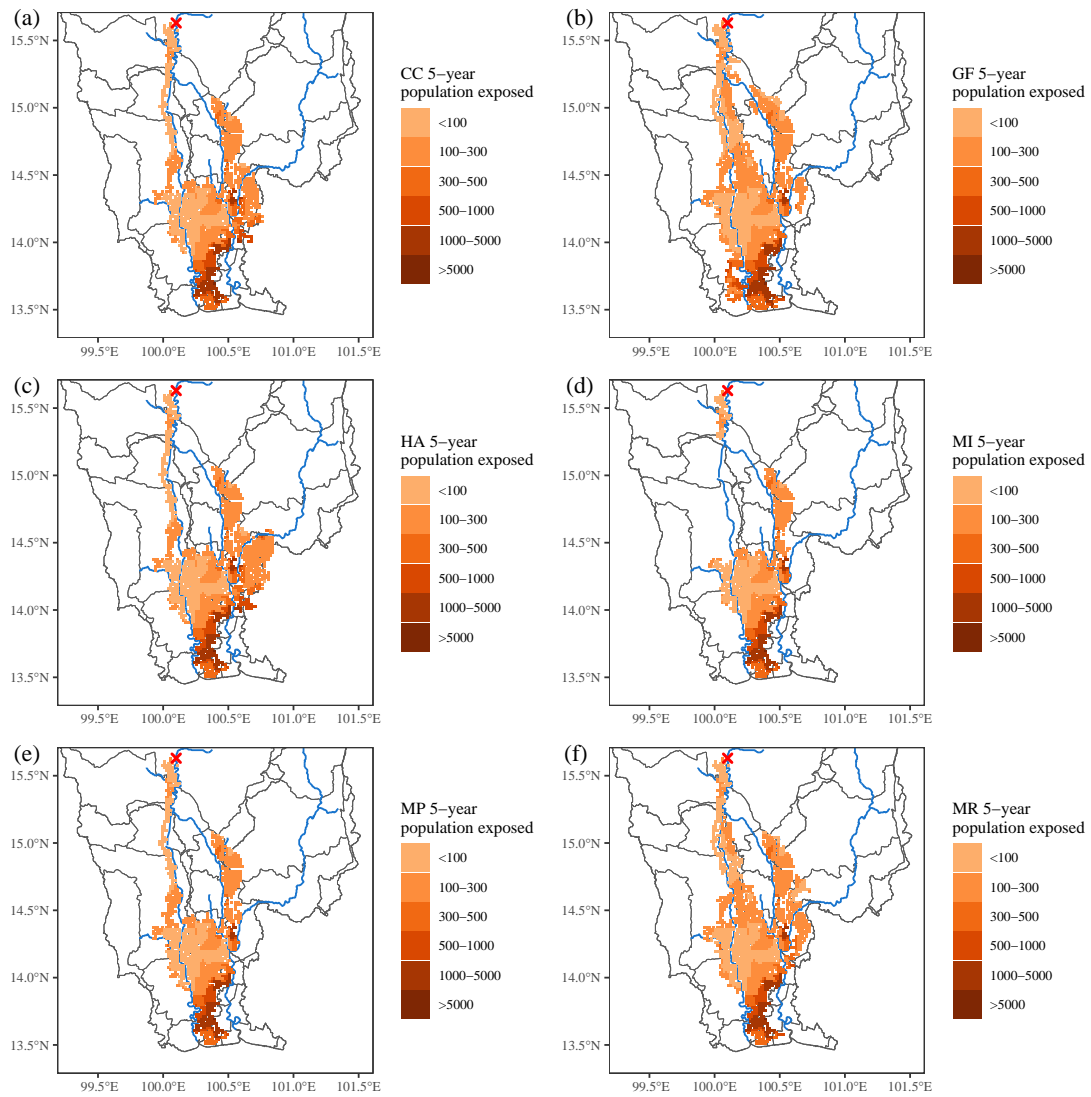


Figure A.3: Population exposure to future floods for 6SST GCMs (a) CC, (b) GF, (c) HA, (d) MI, (e) MP and (f) MR with respect to the d4PDF 5-year return period and depth > 0 m (the color bar represents the population in nos. and the red cross represents the C2 station).

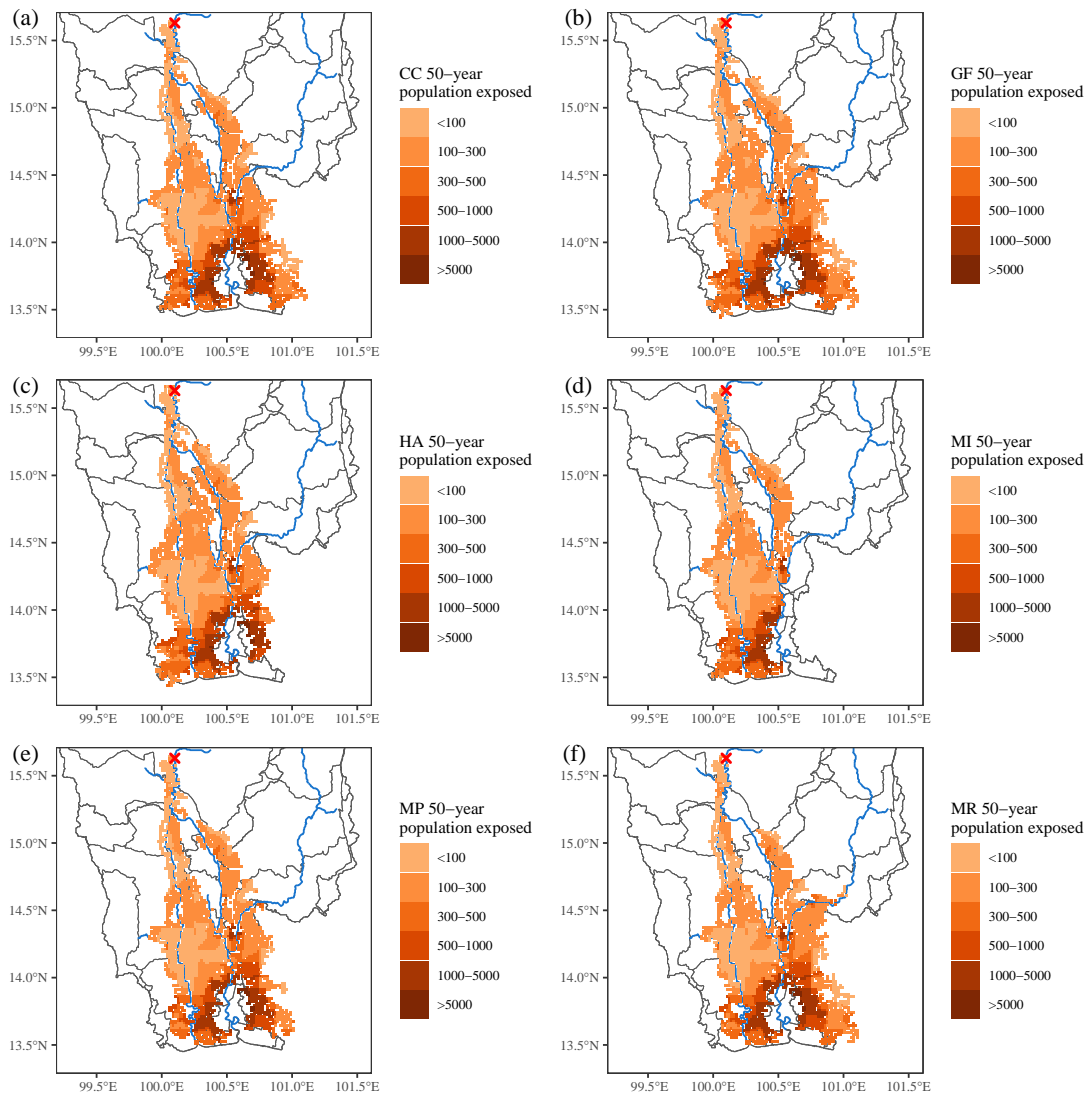


Figure A.4: Population exposure to future floods for 6SST GCMs (a) CC, (b) GF, (c) HA, (d) MI, (e) MP and (f) MR with respect to the d4PDF 50-year return period and depth > 0 m (the color bar represents the population in nos. and the red cross represents the C2 station).

A.2 Appendix for Chapter 5

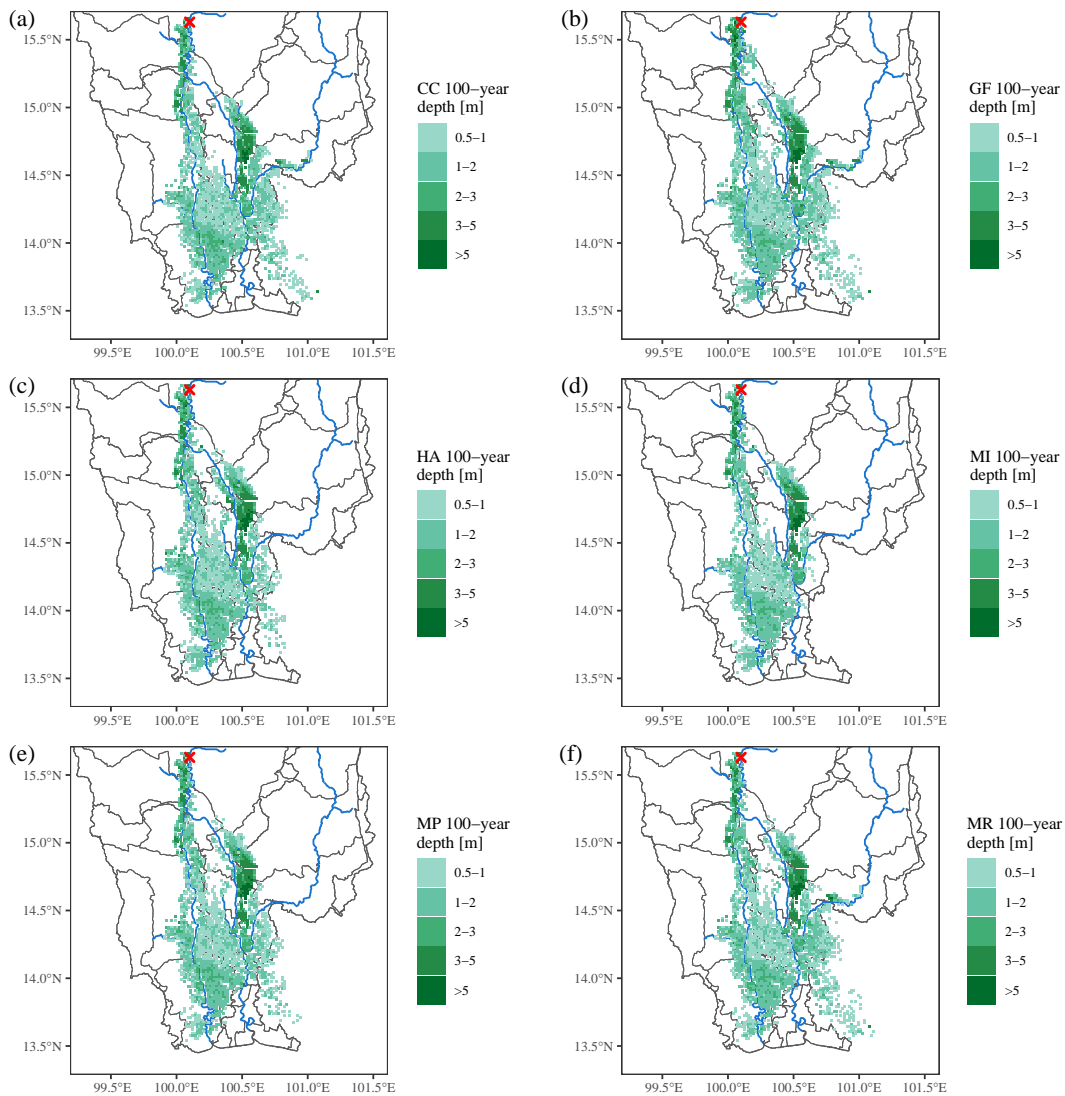


Figure A.5: Rice exposure to future floods for 6SST GCMs (a) CC, (b) GF, (c) HA, (d) MI, (e) MP and (f) MR with respect to the d4PDF 5-year return period and depth > 0.5 m (the color bar represents the exposed inundation depth in meters and the red cross represents the C2 station).

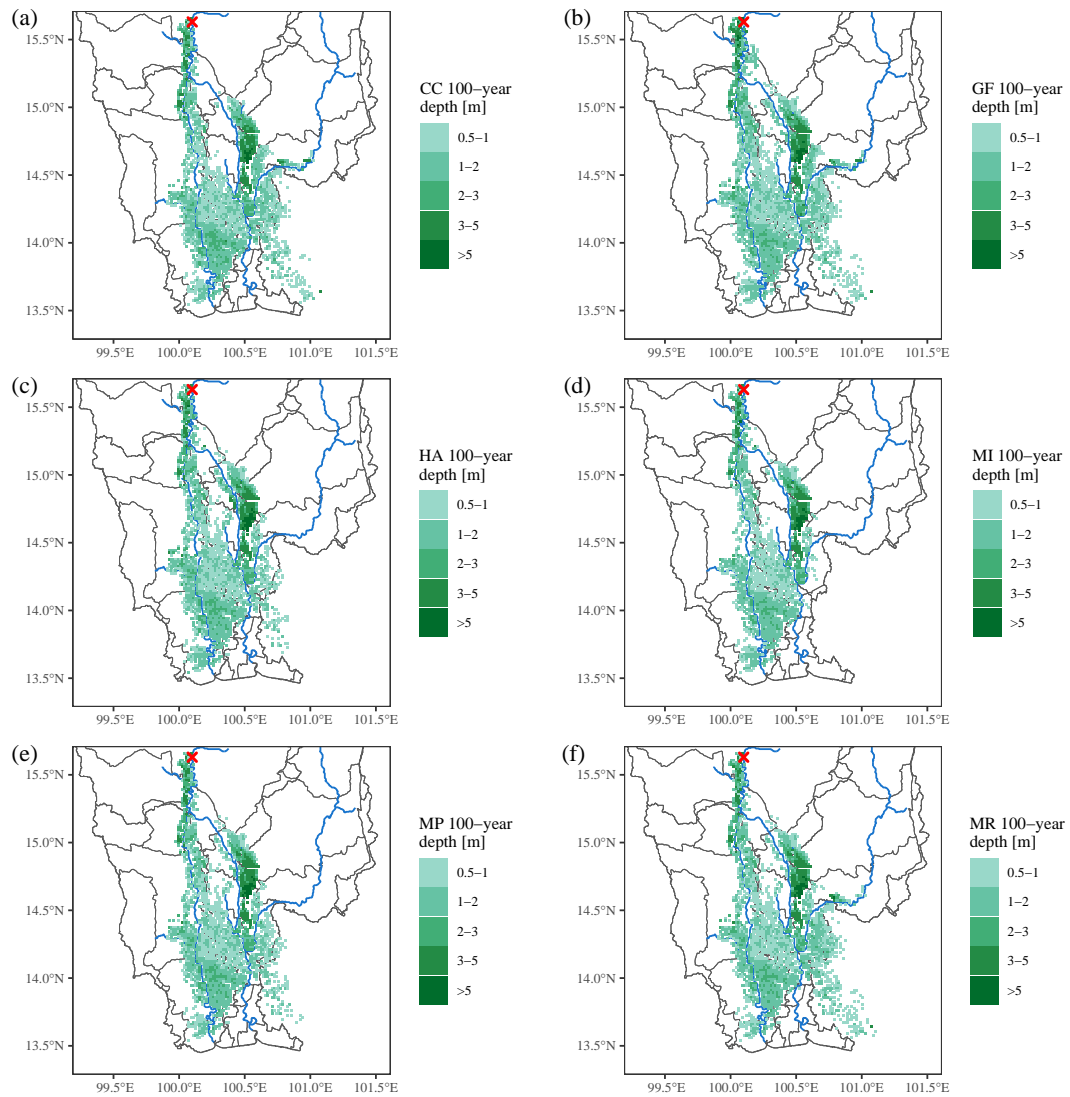


Figure A.6: Rice exposure to future floods for 6SST GCMs (a) CC, (b) GF, (c) HA, (d) MI, (e) MP and (f) MR with respect to the d4PDF 50-year return period and depth > 0.5 m (the color bar represents the exposed inundation depth in meters and the red cross represents the C2 station).

A.3 Appendix for Chapter 6

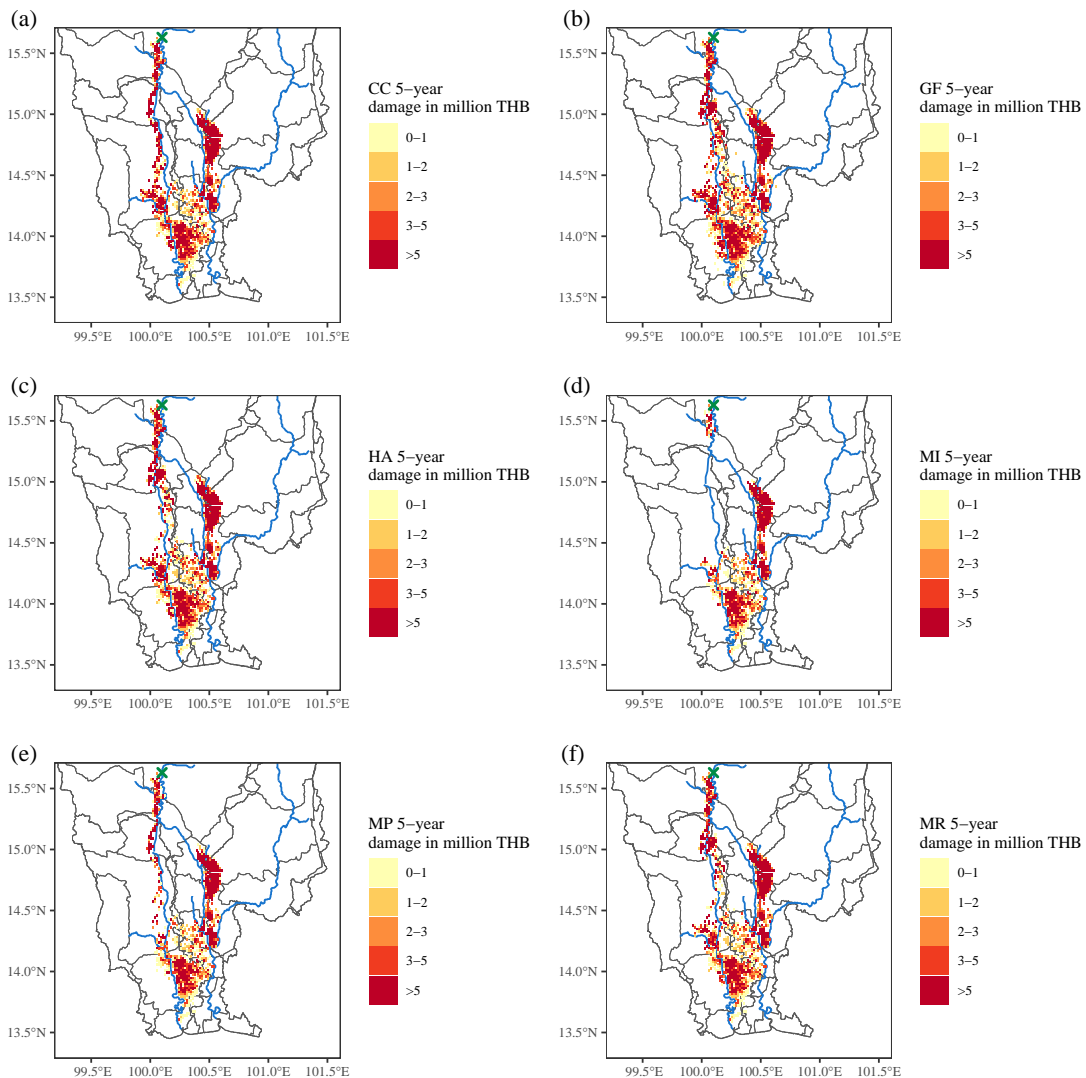


Figure A.7: Future agriculture damage for 6SST GCMs (a) CC, (b) GF, (c) HA, (d) MI, (e) MP and (f) MR with respect to the d4PDF 5-year return period and depth > 0.5 m (the color bar represents the economic damage in million THB and the red cross represents the C2 station).

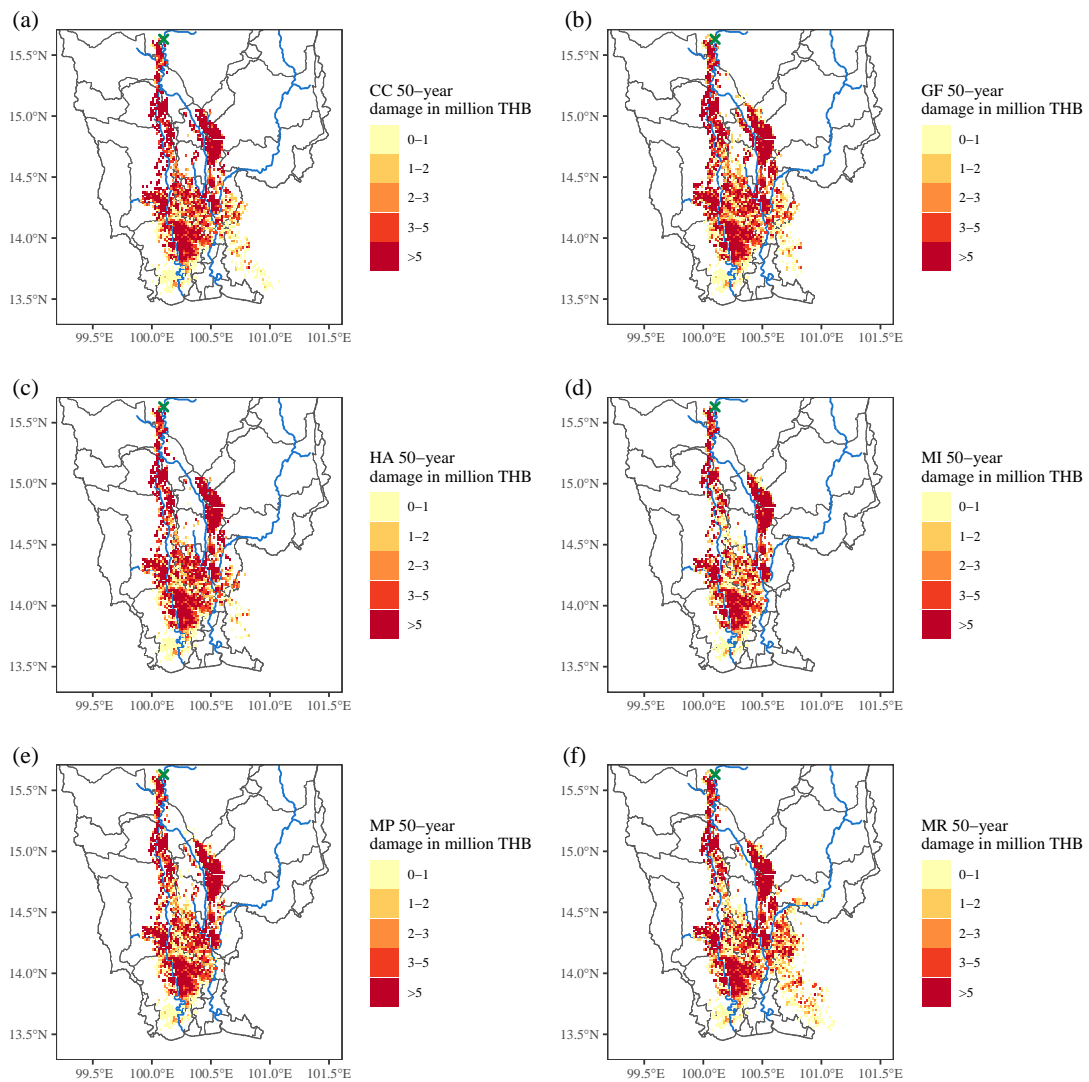


Figure A.8: Future agriculture damage for 6SST GCMs (a) CC, (b) GF, (c) HA, (d) MI, (e) MP and (f) MR with respect to the d4PDF 50-year return period and depth > 0.5 m (the color bar represents the economic damage in million THB and the red cross represents the C2 station).